Carbone, L. & Cozzoli, P. D. Colloidal heterostructured nanocrystals: Synthesis and growth mechanisms. Nano Today 5, 449–493

ARTICLE *in* NANO TODAY · JANUARY 2010

Impact Factor: 15 · DOI: 10.1016/j.nantod.2010.08.006

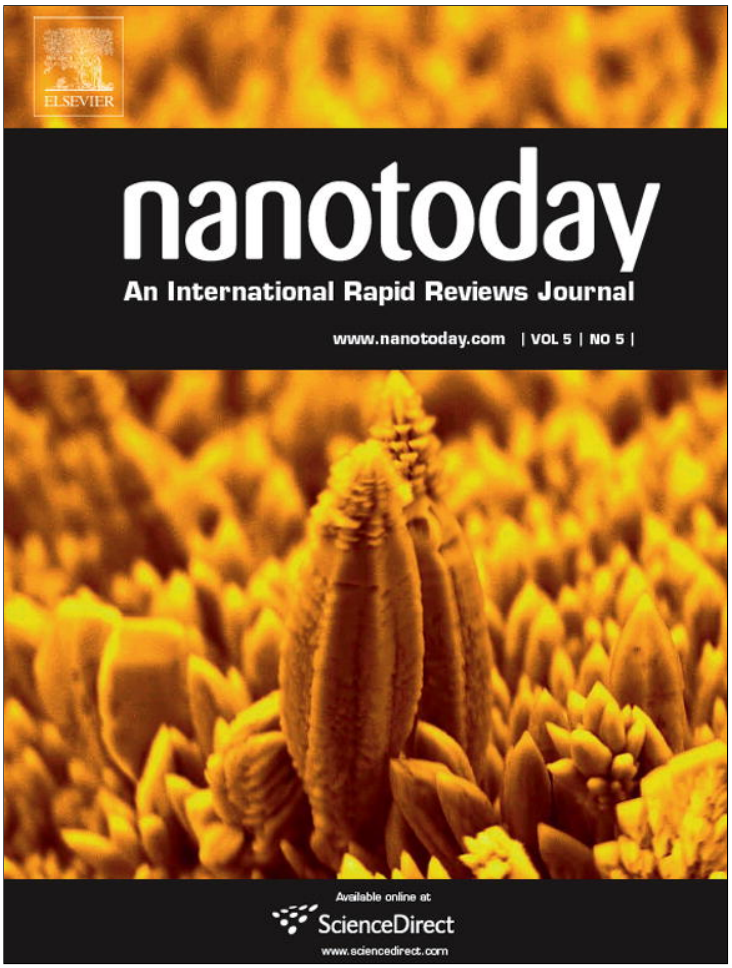

Nano Today (2010) 5, 449—493

available at www.sciencedirect.com

ScienceDirect

journal homepage: www.elsevier.com/locate/nanotoday

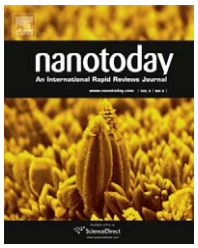

REVIEW

Colloidal heterostructured nanocrystals: Synthesis and growth mechanisms

Luigi Carbone[a], P. Davide Cozzoli[a,b,*]

[a] National Nanotechnology Laboratory (NNL) — Nanoscience Institute of CNR, Via per Arnesano Km 5, 73100 Lecce, Italy
[b] Department of Innovation Engineering, University of Salento, Via per Arnesano, 73100 Lecce, Italy

Received 9 June 2010; received in revised form 19 August 2010; accepted 25 August 2010

KEYWORDS
Colloidal synthesis;
Surfactants;
Nanocrystals;
Heterostructures;
Heteroepitaxy;
Seeded growth;
Topological control;
Surface energy;
Interfacial strain

Summary One frontier approach of colloidal chemistry to nanoscale entities capable to exhibit enhanced or even unconventional physical—chemical properties as well as diversified capabilities for multitask applications envisages fabrication of breed-new hybrid nanocrystals (HNCs) with a spatially controlled distribution of their chemical composition. These are all-inorganic multicomponent nanoheterostructures in which domains of distinct materials are arranged via permanent bonding interfaces in elaborate concentric/eccentric onion-like or oligomer-type architectures. This review covers recent progress achieved in the wet-chemical development of HNCs based on functional associations of semiconductors, metals and magnetic compounds. Within the frame of seeded-growth techniques to heteroepitaxial deposition in solution media, relevant synthetic strategies are illustrated, along with systematic examination of the mechanisms by which heterostructures can be selectively accessed in nonequivalent topological configurations. The peculiar properties and technological perspectives offered by such novel generations of complex nanomaterials are also succinctly highlighted.

Introduction

The recognition of the unique dimensionality dependence of the chemical—physical properties of nanoscale matter has propelled efforts toward controllable fabrication and in-depth characterization of inorganic nanostructures with programmable compositional and geometric features. At the forefront of the current scientific revolution of nanoscience colloidal nanocrystals (NCs), crystalline particles grown in liquid media, stand out over other classes of inorganic nanomaterials due to the high degree of control with which their crystal structure, size, shape, and surface functionalities can be engineered in the synthesis stage and to the versatility with which they can be processed and implemented into a large spectrum of mesoscopic materials, devices, and processes [1—5]. Valuable technological applications have already been envisaged in disparate fields, including optoelectronics, catalysis, energy conversion and production, sensing, environmental remediation, and biomedicine [4—7].

Wet-chemistry approaches have especially been acknowledged for their capability to produce a variety of semiconductor, metal and oxide NCs systematically tailored

* Corresponding author. Tel.: +39 0832 298231; fax: +39 0832 298230.
E-mail address: davide.cozzoli@unile.it (P.D. Cozzoli).

1748-0132/$ — see front matter © 2010 Elsevier Ltd. All rights reserved.
doi:10.1016/j.nantod.2010.08.006

with sub-nanometer level accuracy over a broad range of dimensional-morphological regimes by careful regulation of thermodynamic parameters and growth kinetics in liquid media under assistance of selected solvents, ligands, surfactants or catalyst additives [1–5,8–10]. While this synthetic expertise is yet susceptible to be refined, new challenges are presently being imposed on nanochemistry research to meet the rising demand for advanced breeds of colloidal nanostructures entities that should not only exhibit reinforced properties, but also demonstrate diversified capabilities to be simultaneously exploitable in multiple applications. In this regard, nanochemistry research has recently made tremendous advances with the solution-phase synthesis of generation-new heterostructured NCs with a topologically defined distribution of their composition, broadly referred to as hybrid nanocrystals (HNCs). HNCs are elaborated multicomponent NCs, consisting of two or more different material sections that are permanently joint through chemical bonding interfaces (i.e., without any molecular bridges), eventually attaining heteroepitaxial junctions. Available examples include elaborate concentric or eccentric core@shell and yolk@shell geometries, as well as intricate phase-segregated hetero-oligomer architectures made of discrete shaped sections fused via small connecting areas at selected locations [2,4,5,11–16].

Development of HNCs represents a new generic paradigm in synthetic nanochemistry, whereby an increased level of structural-architectural sophistication is pursued as a means of boosting the technological potential of conventional nanoparticles beyond the limitations imposed by their inherent compositional and geometric features. Elaboration of multicomponent heterostructured NC-based entities allows enhanced and/or diversified capabilities to be achieved through controlling the size, morphology and crystal-phase of the constituent building units, on one side, and through engineering their relative spatial arrangement and relevant interface structure, on the other side.

The technological scenarios that HNCs promise to open up are extraordinarily wide. Primarily, individually processable HNCs made of coexisting inorganic portions, each characterized by peculiar optical, electric, magnetic, and/or chemical properties, hold potential as key multifunctional nanostructured elements over which new transition pathways to unprecedented applications can be founded. These include, for example, the possibility to assemble ''superstructures'' made of nanoscale building blocks, to implement cooperative catalytic conversions, to create anisotropic surface distribution of selected molecules, to devise multimodal techniques for biomedical diagnostics/therapeutics [2,4,5,11–16]. Additionally, HNCs represent artificial platforms on which electronic communication establishing across neighbouring material sections can generate synergistically enhanced and/or tunable chemical–physical responses, or even lead to emergence of unusual phenomena, not otherwise accessible by any of the single components alone, or their physical mixture counterparts. For example, the peculiar optical and/or conduction behaviour observable for HNCs based on semiconductors and/or noble metals can result from altered quantum confinement degree, modified charge-carrier recombination or separation dynamics, and/or plasmon-to-exciton coupling effects. In the case of HNCs incorporating magnetic phases anomalously modified hysteresis parameters can reflect establishment of magnetic exchange-coupling mechanisms and/or induced extra anisotropy [2,4,5,11–13]. These findings have preliminary suggested that creating effective bonding junctions among dissimilar nanoscale domains may be utilizable as a new tool to engineer the performances of complex HNCs thereof, as well as a source of novel magneto-optical or spintronic phenomena that may originate from interaction of nonhomologous properties across suitably devised nanoheterostructured material platforms [11–13].

Research on HNCs has expanded tremendously in the past five years. Following previous efforts to categorize and explain reaction pathways to heterostructures that had been discovered to date [4], a few review articles have later addressed the field of HNCs, either focusing on particular classes of materials [11,13,16] and selected configurations [16], or addressing specific applications [4,13–15], patents [11], and technology perspectives [4,5]. However, a comprehensive classification and in-depth mechanistic examination of synthetic routes by which structure-tailored HNCs can be created so as to meet specific functional requirements is still lacking.

The synthesis of colloidal HNCs requires developing a higher degree of synthetic ingenuity and creativity. Indeed, the formation of multimaterial architectures occurs at a critical thermodynamic-kinetic crossover, whereby the delicate balance that governs the size and shape evolution of individual component portions is further complicated by the interplay of atomic diffusion and/or exchange, facet-specific reactivity, and/or insurgence of interfacial strain. Control over such a complex dynamics is inherently difficult to achieve, since pathways underlying HNC formation and topology selection are not fully understood and may be broadly varying, depending on the specific material association concerned and the particular reaction conditions adopted.

This review will examine recent progress made in the development of colloidal strategies for the tailored synthesis of breed-new HNCs with a topologically controlled distribution of their chemical composition, spanning from concentric/eccentric core@shell and yolk-shell geometries to more spatially elaborate hetero-oligomer architectures. The mechanisms by which heterostructures can be accessed in nonequivalent configurations will be systematically illustrated and discussed for a rich selection of material associations within the frame of general seeded-growth techniques to heteroepitaxial deposition in solution media. The main properties and technological advantages offered by such generations of complex nanomaterials will also be succinctly highlighted.

Basic concepts in wet-chemical synthesis of heterostructured nanocrystals

Synthesis of single-material nanocrystals

Colloidal NCs are generated upon reaction of molecular precursors (that carry the atomic species necessary to build up the targeted material) in a liquid solution that may contain coordinating solvents and some stabilizing agents,

such as ligands, polymers, surfactants, or soft templates (e.g., micelles). Once the synthesis is activated at a suitable temperature, the highly reactive species that are generated, commonly referred to as the ''monomers'', induce the nucleation of NCs and sustain their subsequent enlargement. The organic ligands, surfactants or coordinating agents play several key roles along the course of NC formation. They can regulate the solution supersaturation degree upon forming complexes with the monomers, and participate in an adsorption–desorption equilibrium at the surface of the growing clusters, preventing irreversible aggregation and ensuring steady growth advancement [5,8,11,17,18].

Judicious adjustment of a few experimental parameters, such as the temperature, the type and the relative concentrations of precursors and organic stabilizers affects a number of complex processes and chemical–physical variables underlying crystal formation in liquid media, among which solution supersaturation, reactant diffusion, relative polymorph stability, and crystallographic-direction-dependent lattice development [5,8]. Mechanistic insights have suggested that the key to producing monodisperse NCs relies on realizing a short burst of nucleation, which should be associated with a temporally separated diffusion-controlled growth [11,17]. Systematic size tuning along with size-distribution narrowing can be achieved by balancing the relative consumption of monomers between the nucleation and the growth stages. The most common strategies to achieve this goal are based on application of appropriate reactant delivery techniques (e.g., a primary ''hot-injection'' combined with delayed secondary additions of precursors at slow rate), exploitation of the unique reactivity of the system (e.g., a ''delayed'' nucleation event followed by fast ''autocatalytic'' growth), or deliberate promotion of digestive ripening to induce dissolution of the smallest unstable nanoparticles [11,17,18]. In addition, it has to be recalled that the adhesion of organic stabilizers can severely modify the relative stability of surface facets exposed on the growing NCs, leading to evolution of nonspherically shaped nanostructures (e.g., cubes, polyhedrons, rods, wires, polypods). In particular anistropic lattice development may be promoted under kinetically overdriven growth conditions propelled by high monomer fluxes, as well as by other conditions breaking growth symmetry (e.g., formation of soft surfactant or polymer templates, occurrence of crystal-oriented attachment, presence of foreign particle catalysts, or the application of external electric/magnetic fields) [5,8,11].

Energy balance underlying heterostructure formation

The formation HNCs requires creation of one or multiple inorganic interfaces between chemically and structurally dissimilar materials. The way in which this is attained may be understood within the frame of simple thermodynamic arguments, analogous to those traditionally used for accounting the formation of multilayered thin-film heterostructures onto crystallographically oriented substrates performed by classical vapour-phase techniques. This is illustrated thorough the sketches in Scheme 1. When a secondary material (referred to as ''2'' in the sketch) has to be deposited over a

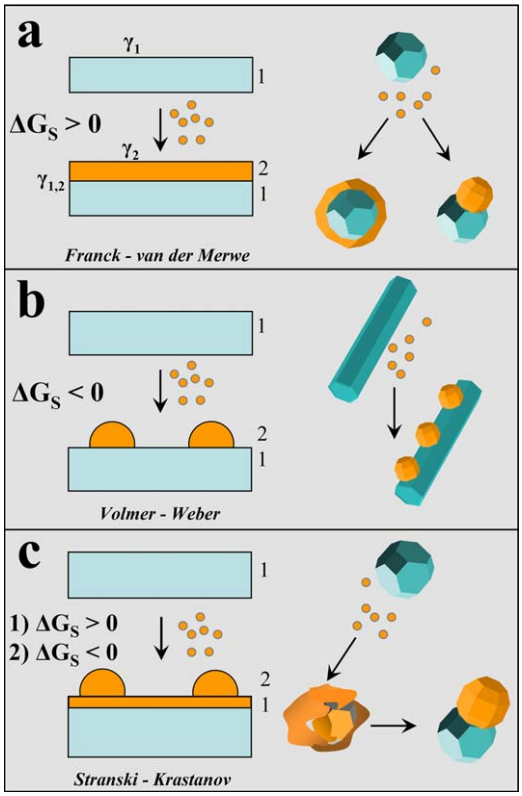

Scheme 1 Comparative sketches illustrating possible heterogeneous deposition modes for a secondary material (referred to as ''2'') that is deposited from the respective molecular precursors onto a preformed seed substrate of a different material (referred to as ''1''): (a) *Franck – van der Merwe*; (b) *Volmer – Weber*; and (c) *Stranski – Krastanov* regimes (adapted from Ref. [12] with permission, copyright Wiley-VCH Verlag GmbH & Co. KGaA).

pre-existing seed substrate of a different material (denoted as ''1''), the sign of total Gibbs free surface energy change function, ΔG_S, that accompanies the heterogeneous deposition process, will dictate the tendency of the system to adopt a given growth mode [19]:

$$\Delta G_S = \gamma_1 - \gamma_2 + \gamma_{1,2} \quad (1)$$

where γ_1 and γ_2 are the surface energies associated with the respective materials (the solid/solution interfacial energies in the case of colloidal nanostructure in a liquid medium) and $\gamma_{1,2}$ is the solid/solid interfacial energy. The former two terms can be expected to be influenced by adhesion of foreign species (e.g., surfactants, ligands, monomers), while the latter depends on the bonding strength and degree of crystallographic compatibility of the concerned lattices.

If the secondary material exposes lower energy surfaces ($\gamma_2 < \gamma_1$) and/or attains good crystallographic matching with the substrate ($\gamma_{1,2}$ is small), then its deposition will likely take place layer-by-layer, resulting in a continuous and uniform coverage ($\Delta G_S > 0$: *Frank–van der Merwe* mode in Scheme 1a). As opposed, if the secondary material is featured by higher energy surfaces ($\gamma_2 > \gamma_1$) and/or is significantly lattice-mismatched ($\gamma_{1,2}$ is high), then it will tend to deposit adopting the habit of a discontinuous island-like domain array as a means of minimizing of the overall

interfacial area shared with the seed substrate underneath ($\Delta G_S < 0$: *Volmer–Weber* mode in Scheme 1b). Another possibility may involve a progressive two-mode deposition regime (*Stranski–Krastinov* mode in Scheme 1c). In the early stages, the secondary material forms according to a layer-by-layer growth ($\Delta G_S > 0$). Subsequently, as the deposited layer exceeds a critical thickness, segregation into discrete islands can be observed ($\Delta G_S < 0$) in response to the significant intensification of interfacial strain fields.

Seeded growth

The most widely exploited class of strategies to synthesize HNCs relies on the so-called ''*seeded growth*'' approach, which represents the solution-phase analogue of classical vapour-phase heteropitaxial deposition. According to this scheme, the HNC-generating environment contains preformed NCs of a target material, referred to as the ''seeds'', which serve as primary substrate centres for accommodating secondary inorganic portions of different materials upon reaction of the respective molecular precursors. This approach is founded on a key principle of the Classical Nucleation Theory (CNT) [2,5,8,9,12], according to which the energy barrier, ΔG^*_{het}, that has to be surpassed for a given material to nucleate heterogeneously onto a pre-existing condensed phase (the seeds) is lower than the activation energy, ΔG^*_{hom}, required to induce corresponding homogeneous nucleation of separate crystal embryos:

$$\Delta G^*_{het} = f(\theta)\Delta G^*_{hom} \quad (2)$$

where the ''wetting'' function, $0 < f(\theta) < 1$, depends on the particular system geometry (e.g., size/shape of the substrate seed and of the material domain ''droplet'' deposited thereon) and on the tension equilibrium attained at the three-boundary seed/''droplet''/solution region [2]. Note that the barrier for the growth of the heterogeneously nucleated domain, ΔG^*_{growth}, is far smaller than both ΔG^*_{hom} and ΔG^*_{het} and corresponds to the limiting case of complete wetting ($f(\theta) \to 0$ for $\theta \to 0$). In an equivalent way heterogeneous nucleation can be understood as requiring a much lower chemical potential of solution monomers (proportional to their concentration) to be triggered, relative to homogenous nucleation:

$$\Delta\mu_{het} < \Delta\mu_{hom} \quad (3)$$

The deposition regimes predicable on the basis of the evolution of the ΔG_S function sign (Eq. (1)) can be equally translated to the context of a seeded-growth synthesis, whereby the energy gain justifying the preference for a given topological configuration arises from a compensation mechanism by which the surface and interfacial energy terms (Eq. (1)) conveniently offset with each other. For instance, following heterogeneous deposition on a highly faceted NC seed, a secondary material can either attain continuous shell (hence, leading to a HNC with an onion-like geometry) or develop into a discrete section (hence, giving rise to a heterodimer HNC), if complete ''wetting'' is either realized for any of the facets exposed, or selectively for just a few of them, respectively (Scheme 1a). On the other hand, under conditions favouring only partial ''wetting'' regime, one or more sufficiently extended facets of the original seeds can accommodate multiple domains of the foreign material (Scheme 1b). As an intermediate evolutionary case, a transformation from a metastable onion-like architecture (e.g., due to formation of an amorphous shell) to a phase-segregated heterodimer heterostructure could be expected as a convenient pathway toward lowering of interfacial strain as crystallization proceeds (Scheme 1c).

At this point, it is important to remark that the creation of nanoscale heterointerfaces in solution can greatly profit from binding of organic stabilizers or other solution species, which can significantly impact on the surface energy terms (i.e., γ_1 and γ_2 terms) and therefore alter the ultimate Gibbs free energy balance. This potentially transcribes into a unique flexibility in the synthesis of HNCs made of structurally dissimilar materials arranged in nonequivalent topologies, provided that properly engineered seeds are combined with heterogeneous deposition routes characterized by suitable ΔG^*_{hom} and ΔG^*_{het} parameters. However, the interplay of kinetic processes associated, for example, with solution supersaturation, reactant diffusion, and/or the inherent chemical reactivity of the seeds and/or the particular molecular precursor selected, as well as operation of unusual mechanisms by which misfit strain may be relieved can greatly complicate mechanistic interpretation.

Heterostructures with core/shell geometries

The topological configuration in which HNCs have most commonly been engineered is the so-called core@shell geometry. In such systems an inner NC ''core'' is evenly embedded within a ''shell'' composed of one or more layers of other materials, which governs or mediates the heterostructure interactions with the external environment. Semiconductors, metals and oxides arranged in onion-like configurations share large bonding heterointerfaces, across which strong electronic communication may be established, leading to chemical–physical properties distinct from those inherent to the individual components, such as enhanced or tunable plasmon absorption or photoluminescence, modified magnetic behavior, and improved (photo) catalytic and photoelectrochemical responses, depending on the specific combination.

HNCs with coherently grown epitaxial interfaces may be attained when the core and shell materials are characterized by similar crystal structure and closely matching lattice parameters (usually within 1–3%), which permits minimization of misfit strain and retards the generation of dislocations or other defects until the coating thickness is kept sufficiently small. However, various circumstances may occur under which the requirements of lattice compatibility can be fairly less prohibitive [2,5,12,13]. For example, pathways for plastic strain relaxation may be available when the secondary material deposition proceeds non-epitaxially, developing a polycrystalline or even partially amorphous shell. Misfit strain constraints could easily be bypassed under kinetically overdriven deposition conditions leading to fast incorporation of a large density of crystal defects at some reaction stages. In such cases, the core/shell interface can ultimately involve a number

of small-extension coherent heterojunctions at which dissimilar crystallographic relationships locally hold between the relevant lattices. Alternatively, the ligand environment may allow the interfacial energy to be efficiently counterbalanced by a proportional decrease in surface energy associated with the outermost exposed shell surfaces (see Eq. (1)). Obviously, the quality features of the shell as well as the structure of the connecting interfaces may have a profound impact on the ultimate chemical–physical properties of the heterostructures.

Over the past decade colloidal strategies to core@shell HNCs have reached an unprecedented level of synthetic ingenuity. Most of the most successful ones transcribe or take advantage of the basic seeded-growth principle. A convenient classification of preparation schemes may be made according to the relevant mechanisms leading to shell formation, as sketched in Scheme 2: (a–c) direct heterogeneous deposition on geometry- and crystal-phase-controlled seeds; (d) sequential heterogeneous deposition steps, involving growth of an amorphous shell onto preformed seeds and its conversion to crystalline upon cation exchange; (e) silica shell growth upon priming of the seed surface and subsequent polymerization; (f) sacrificial redox replacement of the outer seed surface layers, eventually followed by hollowing; (g) self-regulated nucleation-growth dynamics; (h) thermally driven crystal-phase segregation; (i) solid-state diffusion and coalescence.

Direct heterogeneous deposition

A broad family of core@shell heterostructures has been obtained by accomplishing direct heterogeneous nucleation and growth of one or more secondary material layers onto preformed NC seeds serving as starting ''cores'' (Scheme 2a–c). Synthetic strategies aim, on one side, at inhibiting parasitic homogeneous nucleation of isolated NCs made of the shell material, and, on the other side, at achieving selective size- and shape-controlled deposition of the shell section beyond limitations imposed by the inevitable insurgence of misfit strain at the core/shell interface. Practical techniques to realize these objectives rely on devising accurately programmed reactant mixing sequences, depending on the inherent chemical accessibility of the seeds as well on the reactivity of the shell molecular precursors in liquid (generally nonaqueous) media. Regulation of temperature and selection of suitable surface-adhering organic ligands or surfactants, in association with an appropriate reactant injection rate, critically influence on the temporal evolution of the solution supersaturation degree, in turn deciding whether shell formation will take place under thermodynamically or kinetically controlled growth regimes.

To date, disparate combinations of metals, semiconductors and oxides have been addressed by manipulating direct heterogeneous deposition pathways. In the following, we will critically review most recent achievement in the field, analyzing the issues concerned with the colloidal fabrication of core@shell HNC systems based of main functional material associations. Representative transmission electron microscopy (TEM) and high-resolution TEM examples of core@shell HNCs can be found in Figs. 1–3, respectively.

Non-oxide semiconductors

A broad class of core@shell HNCs has been based on associations of fluorescent II-IV and III-V semiconductors, such as transition-metal chalcogenides, phosphides, and arsenides, which feature various cases of quantum-confinement prototypes. In general, to enable the detailed study of their electronic structure or to allow their exploitation as efficient emitters in any application, it is required that NCs of such materials can produce light with high efficiency from band-edge states. Unfortunately, the band-edge emission from colloidal ''quantum dots'' has to compete with both radiative and nonradiative decay channels involving midgap electronic states, often associated with structural imperfections and/or dangling bonds at the surface. Coating the surface of the NCs with suitable organic molecules can minimize this problem, while preserving the solubility and processability of the particles. However, such type of passivation is often incomplete or reversible, exposing some regions of the surface to inevitable degradation effects (e.g., photo-oxidation) [4,16,20]. In the case of anisotropically shaped NCs, such as nanorods or branched objects, two additional factors could further reduce the band-edge luminescence, when compared to their spherical counterparts: first, the relatively higher surface-to-volume ratio, implying a higher occurrence of surface trap states; second, the increased delocalization of carriers, which can reduce the overlap of the electron and hole wavefunctions, thereby lowering the probability of radiative recombination.

The realization of core@shell HNCs, in which one or more layers of different inorganic materials are grown onto the surface of a starting NC core represents a widely exploited means of efficiently and permanently removing most of the deleterious surface states which would otherwise trigger undesired charge carrier decay pathways. Such systems are usually built of materials characterized by a close structural similarity, which favours good epitaxial deposition of the outer protecting shell and consequent healing of structural defects and/or dangling bonds on the pristine loosely organic-passivated core surface. The enhanced chemical robustness and improved optical properties of such heterostructures, relative to those of their single-component nanocrystal counterparts, has already proven to be beneficial to several optoelectronic and biomedical applications [4,20,21–35].

In the ''straddling'' (or type-I) configuration (e.g., in CdS@ZnS, CdSe@ZnSe, InAs@CdSe), the edge energy levels of both the valence and the conduction bands of the core material are located within the band gap of the shell material. The size-morphological and crystal-structure parameters of the core and shell sections, on one side, and the absolute values of the relevant band-edge offsets, on the other side, dictate the extent to which both excited charge carriers can be confined in the core region, ultimately affording enhanced photoluminescence quantum yields [16,20,30,36–55]. In addition, band engineering through appropriate structural-compositional design (e.g., via coupling core and shell domains with mixed dimensionality) of HNCs may be used to determine unusual alteration in their intrinsic opto-electronic properties or even emergence of unconventional behavior [4,30,44,45,52–54,56–64].

In the ''staggered'' (or type-II) configuration (e.g., in ZnSe@CdS, CdTe@CdS; CdTe@CdSe; Cu_2S@CuS), either of

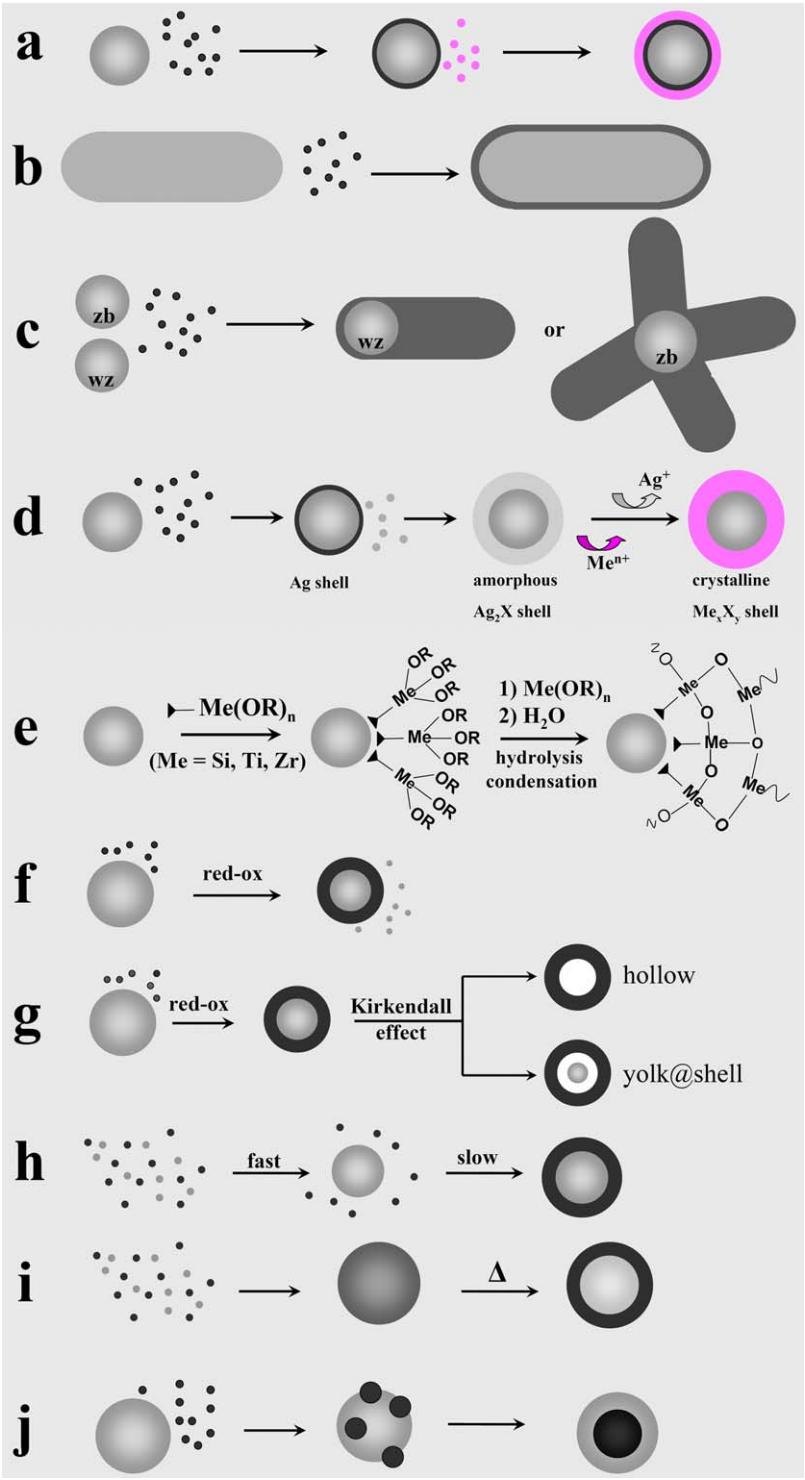

Scheme 2 Sketch of mechanisms leading to the formation of core@shell HNCs: (a—c) direct heterogeneous nucleation and growth of the shell material onto preformed nanocrystal seeds with controlled shape and crystal structure; (d) sequential heterogeneous nucleation and growth steps onto preformed seeds, involving deposition of an amorphous shell and its conversion to crystalline upon cation exchange; (e) silica shell growth by priming of the seed surface and subsequent polymerization; (f) sacrificial red-ox replacement of the outer seed layer; (g) surface-confined red-ox reaction followed by hollowing via the Kirkendall effect; (h) self-controlled nucleation-growth; (i) thermally driven crystal-phase segregation; (j) solid-state diffusion and coalescence (adapted from Ref. [12] with permission, copyright Wiley-VCH Verlag GmbH & Co. KGaA).

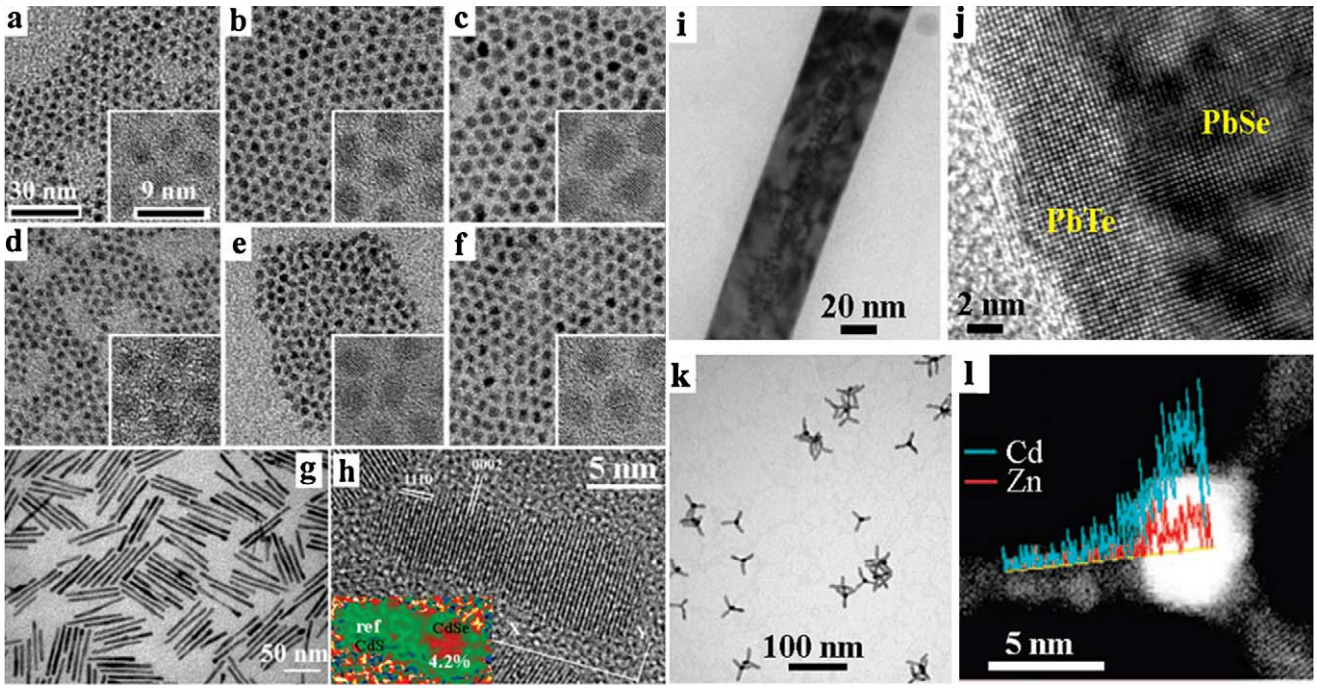

Figure 1 Gallery of TEM and high-resolution TEM (HRTEM) images showing examples of core@shell HNCs, composed of combinations of semiconductor materials, that have been synthesized by direct heterogeneous nucleation of the shell material onto preformed NC seeds (cf. Scheme 2a—c). (a—c) CdSe, CdSe@CdS, and CdSe@CdS@ZnS spherical HNCs prepared by consecutive deposition of CdS and ZnS shells around the same CdSe cores, respectively. (d—f) TEM and HRTEM images of CdSe, CdSe@ZnSe, and CdSe@ZnSe@ZnS HNCs prepared by consecutive deposition of ZnSe and ZnS shells around the same CdSe cores, respectively (reproduced in part from Ref. [82] with permission, copyright American Chemical Society). (g and h) Eccentric rod-shaped CdSe@CdS HNCs obtained by growing a rod-like CdS shell onto spherical CdSe seeds (cf. Scheme 2c). The inset in panel *h* reports a ''mean dilatation'' strain map, obtained from the Geometric Phase Analysis (GPA) of the corresponding HRTEM image, which shows an area within the rod where lattice parameters are altered by 4.2% with respect to the reference area, due to the presence of the CdSe core (adapted from Ref. [44] with permission, copyright American Chemical Society). (i and j) PbSe@PbTe nanowires (adapted from Ref. [88] with permission, copyright Wiley-VCH Verlag GmbH & Co. KGaA). (k and l) ZnTe@CdTe tetrapods made of a central spherical *zb* ZnTe core onto which *wz* CdTe arms have been grown (cf. Scheme 2c). Panel (l) shows a high-angle annular dark-field (HAADF) image of a single tetrapod, along with traces of spatially resolved energy dispersive X-ray spectra (EDS) spectra showing the presence of Zn and Cd in the core and arm sections, respectively (adapted from Ref. [46] with permission, copyright American Chemical Society).

the band edges of core material is located in the gap of the shell material, which promotes spatial separation of the charge carriers to the core and shell regions, respectively, or their recombination at the core/shell interface [16,46,47,65—75]. While the former circumstances are considered to benefit the fabrication of photovoltaic devices [76], the latter occurrence can lead to fluorescence in a wavelength range that would otherwise be inaccessible to their isolated components (e.g., infrared emission from a NC made of a large band-gap material) [20,74,77]. Also for this type of HNCs, the confinement regime can be adjusted by proper engineering of heterostructure composition and geometry [20,46,54,60,65,66,71—75,78].

Typically, the synthesis of semiconductor core@shell HNCs involves suitable manipulation of the same key ingredients used to synthesize high-quality NCs of individual materials (Scheme 2a). The most successful routes have been based on nonaqueous approaches, whereby the reaction of organometallic precursors and/or metal complexes (e.g., $Cd(CH_3)_2$, $Zn(C_2H_5)_2$, metal oxides and carboxylates, elemental S, Se or Te, $S[Si(CH_3)_3]_2$) is carried out in high-boiling solvents and/or surfactants, such as dioctyl ether (DOE), n-octadecene (ODE), alkyl phosphines (tri-n-butylphosphine, TBP; tri-n-octylphosphine, TOP), tri-n-octylphosphine oxide (TOPO), alkyl amines (hexadecylamine, HDA; dodecylamine, DDA; octadecylamine, ODA; oleyl amine, OLAM), oleic acid (OLAC), alkyl phosponic acids (hexylphosphonic acid, HPA; tetradecylphosphonic acid, TDPA; octadecylphosphonic acid, ODPA), or their mixtures at moderate to high temperatures (200—380 °C) [4,16]. On the other hand, the synthesis in aqueous environments, where various metal salts and molecular chalcogenide sources (thioacetamide, thiourea, hydrogen chalcogenides) are allowed to react at $\leq$100 °C under ambient pressure or at higher temperatures under solvothermal conditions (in tightly sealed vessels) in the presence of water-stabilizing polyfunctional ligands (e.g., equipped with one or more amino, carboxylic and/or thiol moieties), has received less success, due to the lower structural quality with which HNCs thereof can be obtained [16,48,49,79,80]. In most cases, to circumvent homogeneous nucleation of the shell material, the solution supersaturation is kept controllably low upon performing judiciously slow additions of dilute solutions containing all of the necessary shell precursors or

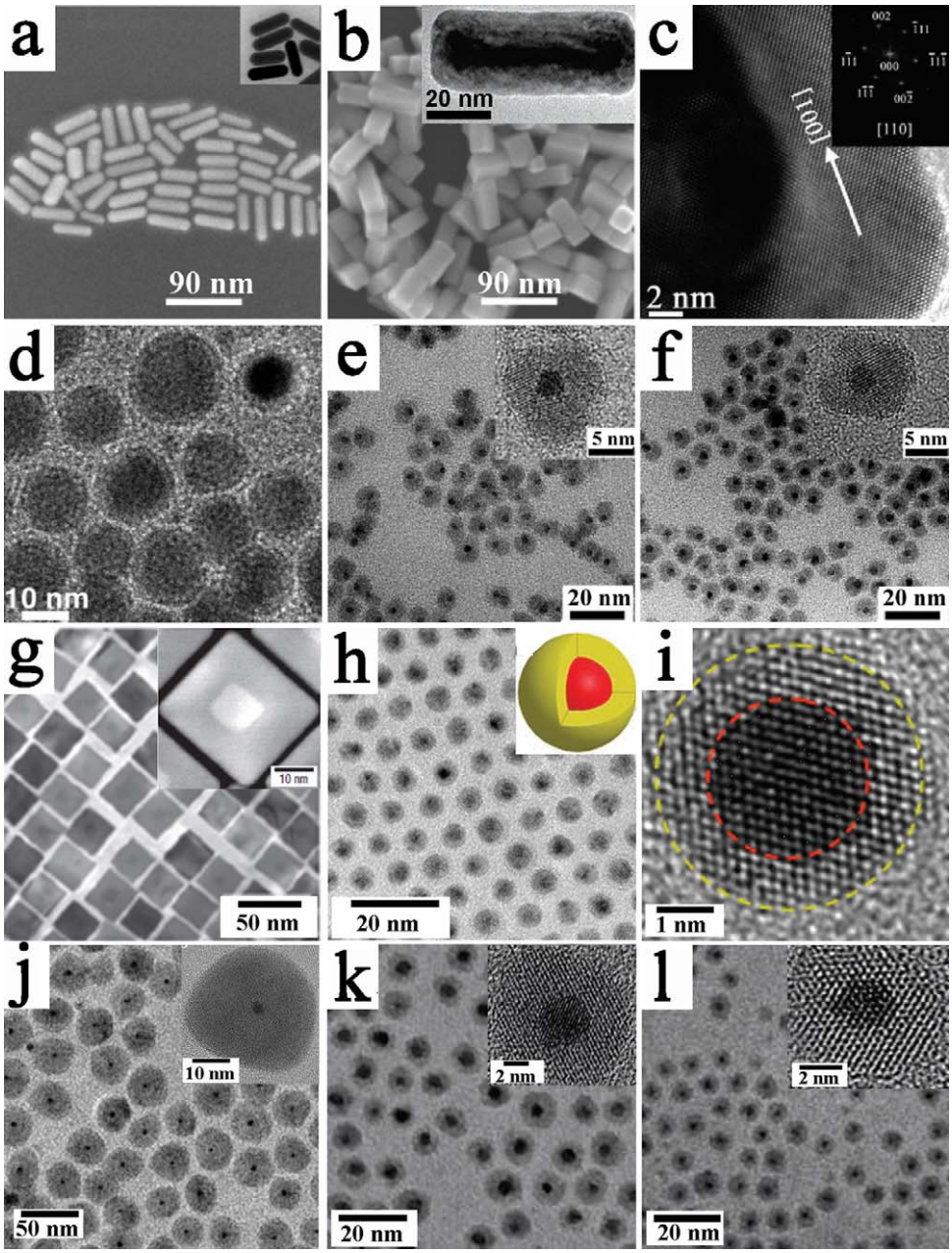

Figure 2 Gallery of representative scanning electron microscopy (SEM), TEM and HRTEM images illustrating examples of core@shell HNCs made of metal and semiconductor associations, which have been synthesized by direct heterogeneous nucleation and growth of the shell material onto preformed seeds (cf. Scheme 2a—d). (a) Au nanorod seeds and (b and c) Au@Pd HNCs prepared by growing a Pd shell onto the Au cores (reproduced from Ref. [105] with permission, copyright American Chemical Society). (d) Co@CdSe (reproduced from Ref. [114] with permission, copyright American Chemical Society). (e and f) FePt@CdS and FePt@CdSe HNCs (reproduced from Ref. [115] with permission, copyright American Chemical Society). (g) Cubic-shaped Pt@Pd HNCs (reprinted from Ref. [93] with permission, copyright Nature Publishing Group). (h and i) Au@Ag HNCs synthesized by a three-phase boundary approach (reproduced with permission from Ref. [113] with permission, copyright American Chemical Society). (j—l) Au@CdS, Au@PbS and Pt@CdS HNCs synthesized according to the general protocol sketched in Scheme 2d (reproduced with permission from Ref. [122], copyright AAAS).

alternated injections of individual anionic and cationic precursor species (the so-called SILAR, i.e., ''successive ion adsorption and reaction method'') to a seed-loaded surfactant mixture at moderate temperature (usually much lower than that at which the cores are synthesized or NCs of the shell materials can rapidly grow). Post-deposition treatments (e.g., light irradiation, heating) may also be applied to improve the crystalline quality of the shell and/or anneal interfacial defects [16,79,81]. By exploiting these general synthetic criteria, a rich library of type-I and type-II core@shell HNCs with concentric distribution of their component materials were accessed, in which the

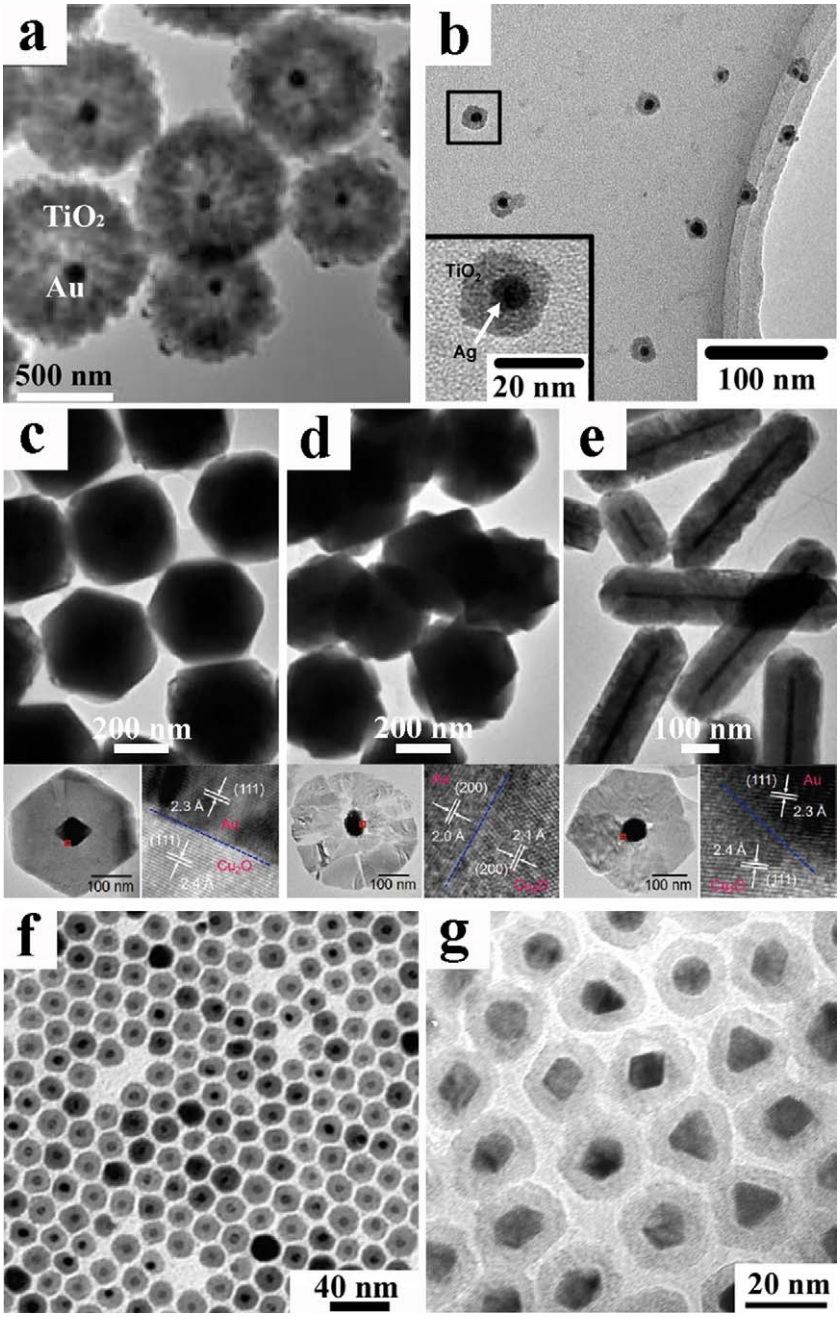

Figure 3 Gallery of TEM and HRTEM images showing examples of core@shell HNCs based on oxide materials, which have been synthesized by direct heterogeneous nucleation and growth of the shell material onto preformed nanocrystal cores (cf. Scheme 2a—c). (a) Au@TiO_2 nanoreactors with inner vacant space (adapted from Ref. [127] with permission, copyright Wiley-VCH Verlag GmbH & Co. KGaA). (b) Ag@TiO_2 HNCs (adapted from Ref. [128] with permission, copyright American Chemical Society); (c—e) Au@Cu_2O HNCs with different core and shell shapes. The smaller bottom panels report cross-sectional views of the relevant interfacial regions (reproduced from Ref. [129] with permission, copyright American Chemical Society). (f) Au@Fe_3O_4 HNCs (reproduced from Ref. [57] with permission, copyright American Chemical Society); (g) Pt@Fe_2O_3 HNCs (reproduced from Ref. [161] with permission, copyright IOP Publishing).

shell habit conformed to the spherical symmetry of the underlying NC cores. These heterostructures offer optical absorption and fluorescence properties that can be tuned over the whole visible to near-infrared wavelength interval by suitable compositional and structural design [16].

Increasingly sophisticated onion-like architectures have been synthesized in order to circumvent the dramatic photoluminescence deterioration that normally takes place as the shell thickness exceeds a critical value. This abatement is correlated with the almost inevitable generation of structural defects (e.g., misfit dislocations, stacking

faults) in proximity of the intervening interfacial regions or in the shell, whereby strain fields arising from lattice-mismatched heterojunction conditions can intensify to a point at which they can no longer be relieved through elastic crystal deformation mechanisms. To remedy this drawback, core@shell HNCs with a more elaborate sandwiched configuration were devised, in which the core was buried by a shell made of consecutive layers of two or three semiconductors featured by gradually diverging lattice parameters (e.g., in CdSe@CdS@ZnS or InAs@CdSe@ZnSe) [30,81–83]. Such double- or triple-composition shell possessed a graded structure that guaranteed smooth relaxation of the interfacial strain, ultimately leading to robust heterostructures with greatly improved and stable photoluminescence (Fig. 1a–f). Other HNCs featured quantum confinement prototypes of ''quantum well''–in–''quantum dot'' systems, such as CdS@HgS@CdS onion-like structures, in which a thin layer of small band-gap semiconductor (HgS) was buried between a spherical core and an outer shell, both made of a higher band-gap material (CdS) [84–86]. In the latter cases, carriers are confined within the intermediate HgS domain where they may recombine radiatively. More recently, increasingly elaborated chemistry protocols have permitted access to core@shell semiconductor HNCs equipped with ultra-thick shells capable to induce noticeable alteration in optical properties to significant extra strain being exerted onto the core underneath [52–55].

Compared with the huge progress so far achieved in the development of their symmetric analogues, the current selection of core@shell HNCs with nonspherical (e.g., rod-like, branched) shapes has reached limited success. Major synthetic challenges in the fabrication of anisotropic core@shell HNCs starting, for example, from nanorod/wire or tetrapod seeds, are related to the fact that the coherent growth of an epitaxial shell over such shaped cores requires ''wetting'' a rather extended surface exhibiting a generally high average curvature (intermediate between the curvature of spherical NC and that of flat surface) with abrupt discontinuities at edges, tips and branch regions. This implies that existence of surface sites with varying degrees of reactivity, on one side, and location-dependent interfacial strain, on the other side, can eventually pose more severe constraints against uniform shell deposition, relative to those encountered when accomplishing the coating of dots [16,47,81]. Frequent occurrence of structural defects at the shell or interface region, and/or attainment of coverage with variable thickness and/or polycrystalline structure may therefore be expected to pose additional issues to overcome [43,47–49,81].

One family of anisotropic core@shell HNCs includes core-conformal architectures, in which the shell habit adapts to the symmetry as well as the shape of the starting core (Scheme 2b). One-dimensionally elongated heterostructures were fabricated by different approaches, depending on the core size and the coordinating reaction media. It was reported that rod-like CdSe@CdS@ZnS HNCs could be synthesized in a single shell-growth step, whereby hexagonal wurtzite (*wz*) CdSe nanorod seeds dissolved in TOPO were reacted at 160 °C with a TBP solution co-loaded with $Zn(C_2H_5)_2$ and $S[Si(CH_3)_3]_2$ and minute $Cd(CH_3)_2$ amounts [30,81]. The attained shell possessed a graded CdS@ZnS composition as a result of a strain-driven interfacial segregation mechanism, according to which the spontaneous nucleation of CdS layer anticipated the ZnS deposition due to the more favourable CdSe/CdS lattice matching. The intermediate CdS naturally served as a buffer alleviating the otherwise intolerably high strain that would be experienced by a ZnS layer deposited on the CdSe cores. The pristine shell that possessed a defective character as a consequence of the mild temperature conditions, was subsequently annealed out and irreversibly restructured via photochemical pathways triggered by prolonged laser irradiation, which benefited photoemission yield and confers elevate stability against photocorrosion [30,81]. By using an alternative approach, direct ZnS overcoating of CdSe nanorods was achieved without the need for any post-synthesis annealing treatment by adding a TOP-diluted $Zn(C_2H_5)_2/S[Si(CH_3)_3]_2$ precursor to a different ligand environment composed of TOPO/HDA mixture and unpurified seeds at 190 °C, where both accessibility of the cores and their stability against dissolution or ripening were guaranteed during the shell synthesis course [43]. CdTe@CdX (X = S, Se) embodying a CdTe tetrapod core were also claimed, although no support of structural and compositional analyses at the single-particle level was provided [74,78].

Core@shell nanowires of CdS@CdSe, CdSe@CdS and CdSe@ZnTe were produced by exploiting purposely modified organometallic schemes that relied on the addition of TOP-diluted shell precursors to a noncoordinating ODE solution containing CdS or CdSe nanowire seeds at 210–250 °C, respectively [47]. Such particular conditions were considered to be a critical prerequisite to chemically activating the nanowire seeds, which were, in fact, assumed to be provided with a low surface density of ledges serving as low-energy sites for the shell material nucleation, compared to their nanorod counterparts. The difficulty to realize overcoating of CdSe and CdS nanowires clearly emerged from the observation that the shell tended to develop into island-like polycrystalline features (*Volmer–Weber* growth mode) rather than evenly conforming to the cores underneath, which reflected the interplay of strain limitations and spatial inhomogeneity in surface reactivity of the seeds [47]. In another study focusing on the formation of coaxial PbSe@PbS heterostructures by an organometallic approach, PbS shell growth was observed to switch from *Stranski–Krastanov* to a *Franck–van der Merve* regime on increasing the temperature from 150 °C to 180 °C [87]. Similar findings were documented for one-dimensional CdS@ZnS systems for which the shell was generated under either short reflux at 70 °C or prolonged solvothermal treatment at 180 °C in aqueous media [48,49]. On the other hand, a SILAR-based technique, relying on the sequential addition of each shell Pb and X (X = S, Te) precursors to the seed solution at 130 °C [88], was proven to be viable to prepare PbSe@PbX nanowires with highly epitaxial and conformal PbX shells (Fig. 1i and j), while circumventing parasitic homogeneous nucleation and undesired alloying.

Remarkable deviations from the core-conformal shell growth mode were achieved by elegant manipulation of the heterostructure formation kinetics. An interesting class of binary architectures has been realized through synthetic strategies inspired by the mechanism of formation of rod-like and branched metal chalcogenide NCs with a polytypic structure. Such shaped NCs frequently incorporate stacked

domains of structurally similar cubic zinc blende (*zb*) and hexagonal wurtzite (*wz*) crystal phases (e.g., at the central branch point and at the arm sections, respectively, in polypod-shaped NCs), as they can indeed switch between the two polymorphs at the nucleation and/or growth stages under appropriate reaction conditions (polytypism) [5]. These pathways have been translated into powerful seeded-growth schemes that enable the synthesis of HNCs with shape-tailored core@shell architectures starting from isotropically shaped size- and crystal-phase-controlled metal-chalcogenide NCs as nucleation seeds. The latter can be driven to evolve into heterostructured nanorods upon overgrowth and anisotropic development of a second foreign material, or act as branch points from which multiple linear arms of a different compound can depart (Scheme 2c). For example, high aspect-ratio type-I CdSe@CdS core@shell HNCs were synthesized by a technique involving the rapid injection of a TOP/S solution containing preformed wurtzite CdSe seeds into a hot bath of Cd-surfactant complexes obtained by decomposing CdO in a TOPO/ODPA/HPA mixture at 350—380 °C [44,45]. Under such kinetically overdriven growth conditions assisted by facet-selective surfactants adhesion, all-*wz* noncentrosymmetric CdSe@CdS nanorod heterostructures were produced that embodied one of the original *wz* CdSe seed in an eccentric position across a [001]-elongated rod-like *wz* CdS shell section (in a region between 1/3 and 1/4 of their overall longitudinal length) as a consequence of the dissimilar growth rate of the wurtzite lattice along the *c*-axis (Fig. 1g and h) [44,58]. In a modified protocol, CdSe@CdS nanorods, albeit with low aspect-ratio, were accessed at temperatures as low as 120—180 °C in *wz* CdSe-seed-loaded HDA/TOPO/TOP mixture by performing a slow injection of a S-rich $TOP(CH_3)_2Cd/S[Si(CH_3)_3]_2$ solution [58]. The S excess was considered to be beneficial to propel fast unidirectional development of the CdS section out of the most (00—1) chemically active facets [58]. The seed/precursor co-injection approach was extended to the preparation of type-II asymmetric ZnSe@CdS nanorods [71,72]. In all cases, the relative seed to shell precursor proportion, in conjunction with temperature, were the most influential parameters that regulated the balance of monomer consumption between heterogeneous nucleation and growth stages [44,58,71,72]. Bicomponent heterostructured core@shell nanorods were prepared with excellent size and shape monodispersity, which represented a favourable prerequisite to promoting their lateral or vertical organization in close-packed assemblies over large-area substrates upon application of controlled-solvent-evaporation or additive-induced destabilization techniques or under assistance of electric-fields [31,44,45,58,89].

Alternatively, within the frame of the same aforementioned synthesis schemes, multipod heterostructures belonging to the same semiconductor material class were generated by exploiting CdX or ZnX (X = Se, Te) seeds with a *zb* structure. In such circumstances, two or more [001]-oriented *wz* rod CdX or ZnX sections could nucleate and develop out of the equivalent (1 1 1)-type seed facets that structurally match with the fastest-growing (0 0 1) facets of the wurtzite lattice (Fig. 1k and l) [45,46,68,73,90]. The size and faceting of the seeds appeared to be decisive in dictating the ultimate degree of branching achievable [73].

These anisotropically rod- and branched-shaped HNCs with nonconformal core@shell arrangements were found to exhibit synergistically reinforced optoelectronic properties that are indeed characteristic of one-dimensional systems, including tunable Stokes shifts, huge extinction coefficient, giant Stark effect, linearly polarized emission, optical nonlinearity, and/or tunable charge carrier confinement or separation, depending on their composition, geometry and electronic structure [4,44—46,58—64,68,73,78,90]. Applications of such nanostructures in photocatalysis [48,91], biolabeling and cell studies [30,33—35], and prototypical light-emitting and photovoltaic devices [28,29,92] are currently being explored.

Transition-metals

The impact of shell deposition on the resulting physical—chemical properties is particularly evident for core@shell HNCs based on coinage metals (such as Ag, Au, Cu, Pd, Pt) and other transition-metal elements (e.g., Co, Ni), in which a significant degree of interfacial alloying may lead to strong exchange coupling or electric-field enhancement effects. Depending on the specific material association, remarkably altered surface plasmon oscillations, modified magnetic parameters, improved Raman scattering responses, or extreme catalytic activity have been observed, with respect to those offered by the individual components [93—95]. Especially, HNCs composed of coinage and magnetic metals behave as bifunctional platforms, whereby interesting magnetic and optical properties are simultaneously available and/or synergistically altered, which hold promise in NC-based diagnostics and therapeutics [96—103].

In most cases, bimetallic core@shell HNCs have been synthesized in aqueous media, in which preformed core NCs of the desired material are allowed to react with secondary metal ion precursors and a mild reducing agent (e.g., ascorbic acid, hydroxyl amine) (Scheme 2a and b). The seeds act as powerful red-ox catalysts, selectively enhancing heterogeneous nucleation by fast ion reduction at their surface and eventually inducing anisotropic growth continuation under the assistance of facet-preferential adhesion of surfactants (e.g., tetraalkylammonium bromide salts) or other additives (e.g., gaseous NO_2) [93—99,101—110]. A refined level of simultaneous topological and shape control was reached in the synthesis of Me@Pd (Me = Au, Pt) [93—95,105,111], Au@Me (Me = Pt, Ni, Ag) [104,107,110,112], and Pd@Au [109] heteronanostructures that consisted of faceted or anisotropically shaped cores embedded within relatively thick and uniform shells (Fig. 2g and h). In these systems, the evolution of the overall HNCs toward a rod-, cubic-, or polyhedral-like morphology was explained in terms of competing overgrowth along the different crystal facets that the nascent shell exposed to the solution [105]. As an example, in the case of the Pt@Pd system, where negligible lattice misfit is experienced by the two materials interfaced, the Pd shell could either be achieved epitaxially conformal to the morphology of Pt seeds or be shaped independently, as desired [93—95]. On the other hand, whenever metal deposition occured over lattice-mismatched seed facets, phase-segregated heterostructures, made of sections sharing only small interfaces at which misfit strain could better be accommodated, were

likely to form [93]. However, several studies have evidenced that kinetic factors involved in the ion reduction dynamics may also be responsible for the observation of otherwise unexpected site-preferential or continuous polycrystalline shell deposition over anisotropic seeds [104,107—112].

More recently, seeding routes accomplished in organic phase have been also proposed, which, for example, involve high-temperature OLAM-driven reduction of selected metal acetylacetonates [94], or more generally applicable self-reduction of metal-ion-DDA complexes (obtained by a phase-transfer procedure) at the surface of preformed seeds of various materials [106]. An original and powerful mixed aqueous/organic protocol was reported [113], which relied on ascorbic-acid driven reduction of any desired metal ion species at three-phase boundaries obtained by mixing OLAC-dispersed hydrophobic-capped seeds, an aqueous metal ion solution, a metal-ion phase-transfer molecule catalyst (a fatty acid salt), and an intermediate-polarity phase. The latter served to facilitate transport of the in-situ forming metal complex across the various liquid/liquid interfaces involved, permitting controllable formation of Ag, Pd, Pt shells on Au cores (Fig. 2h and i) as well as on semiconductor PdSe, Ag_2Se with single-layer coverage accuracy [113].

Non-oxide semiconductors/transition-metals

Examples of nanoheterostructures incorporating both transition-metals and fluorescent non-oxide semiconductors are worth mentioning. These include Co@CdSe (Fig. 2d) [114], and FePt@CdX (X = S, Se) HNCs with either single- or poly-crystalline shell [115,116] (Fig. 2e and f), which were produced by one-pot, two-step reaction schemes, whereby metal seeds were first nucleated in-situ and subsequently allowed to sequentially react with the metal chalcogenide precursors in conventional coordinating mixtures at 120—180 °C [115,116]. Notably, higher reaction temperatures (280—300 °C) could promote conversion to dimer-like heterostructures by shell coalescence into a separate domain attached aside (see next paragraphs and Scheme 3) [115,117,118]. These core@shell HNCs still retained the superparamagnetic properties of their magnetic core components, whereas substantial quenching of the shell luminescence due to metal-driven charge carrier separation was observed [114—116,118,119].

Monodisperse spherical or cubic-shaped FePt@PbS HNCs were generated by bis(trimethylsilyl)sulfide injection into a FePt-seed-loaded DOE/lead oleate environment at 100 °C and 150 °C, respectively. Accurate seed washing with labile OLAM was claimed to be critical to guarantee the formation of an ubiquitous PbS shell via multiple domain recrystallization, instead of a discrete PbS particle attached aside [120]. Interestingly, these magnet-in-semiconductor heterostructures exhibited semiconductor-type transport properties with magnetoresistance characteristic of magnetic tunnel junctions [120]. A similar approach was used to produce Au@PbX HNCs (X = S, Se) that were investigated in field-effect transistor devices [119].

Recently, some general strategies to nearly spherical noble-metal@Me_xX_y HNCs (Me = Zn, Cd, Ag, Ni or Cu and X = S, Se) have been devised [106,121,122]. One protocol involved hydrothermal decomposition of metal tiobenzoates as single-source Me/S precursors in cetyltrimethylammonium bromide (CTAB) solution containing shape-controlled Au seeds [121]. The latter were previously provided with a ''wetting'' layer of Ag_2S or CuS, which facilitated heterogeneous deposition of Me_xX_y via an initial cation-exchange reaction, while also preventing the cores from being etched out. Other authors synthesized Au@Ag_2S and various Ag@Me_xS_y by exploiting the mild co-reaction of elemental S and organic-soluble metal-DDA complexes (obtained by a phase-transfer procedure) in the presence of Au or Ag seeds, respectively [106]. It was remarkable that exchanging the nature of the seed and shell materials led to metal—Me_xS_y heterodimers rather than to inverted Me_xS_y@metal core@shell structures. This fact could be presumed to reflect an altered interplay of the respective surface energies [106,123].

Another more elaborate strategy was demonstrated to pave the way to a broad family of metal@metal-chalchogenide HNCs of the type Me@X_xY_y (Me = Au, Pt, Pd, FePt; X = Cd, Pb, Zn; Y = S, Se), which could attain monocrystalline shells with thickness tunable over an extremely broad size range, regardless of the lattice mismatch holding between the concerned materials [122]. The procedure (Scheme 2d) involved a three-step shell growth process in organic media: (i) the initial deposition of a Ag layer with precisely tailored thickness onto the target Me cores [113]; (ii) the conversion of the latter to an amorphous Ag_xS shell upon sulfidation under suitable thermal conditions; (iii) a cation-exchange reaction leading to Ag^+ replacement by X^{n+} metal ions (favoured by the strong acid softness of Ag^+), which ultimately resulted in a single-crystalline X_xY_y coverage. Indeed, the key for succeeding in the deposition of a high-quality ultrathick semiconductor X_xY_y shell standed within the ability to create a precursor Ag_xS shell with amorphous character in the intermediate step. This conveniently allowed bypassing strain fields that would inevitably arise if direct heteroepitaxial growth of shell layers were attempted on structurally dissimilar material cores, as done in traditional approaches (Fig. 2j—l).

To date, anisotropically shaped semiconductor@metal systems are limited to Ag_2S@Au nanorods that have been exploited as optical biosensors [124,125].

Transition-metal oxides

A variety of core@shell HNCs incorporating at least one transition-metal oxide component have been made available by direct heterogeneous nucleation approaches (Scheme 2a and b). They can be roughly classified as follows. Examples are shown in Fig. 3.

(i) *Plasmonic metals/nonmagnetic oxides*. Noble-metal@transition-metal-oxide HNCs made of a Au or Ag core surrounded by either a continuous or flower-like shell of TiO_2, ZrO_2 or SnO_2, were generated by performing hydrolysis-condensation of transition-metal alkoxides in the presence of surfactant-capped Au or Ag NC seeds in mixed organic/aqueous media or in microemulsions (Fig. 3a and b) [12,126—128]. These routes typically yielded amorphous and/or nanoporous oxide coatings, which could severely modify the plasmonic properties of the noble-metal core (e.g., upon electron uptake from the photoexcited oxide), while guaranteeing chemical accessibility to the latter. These features stimulated exploration of the potential of

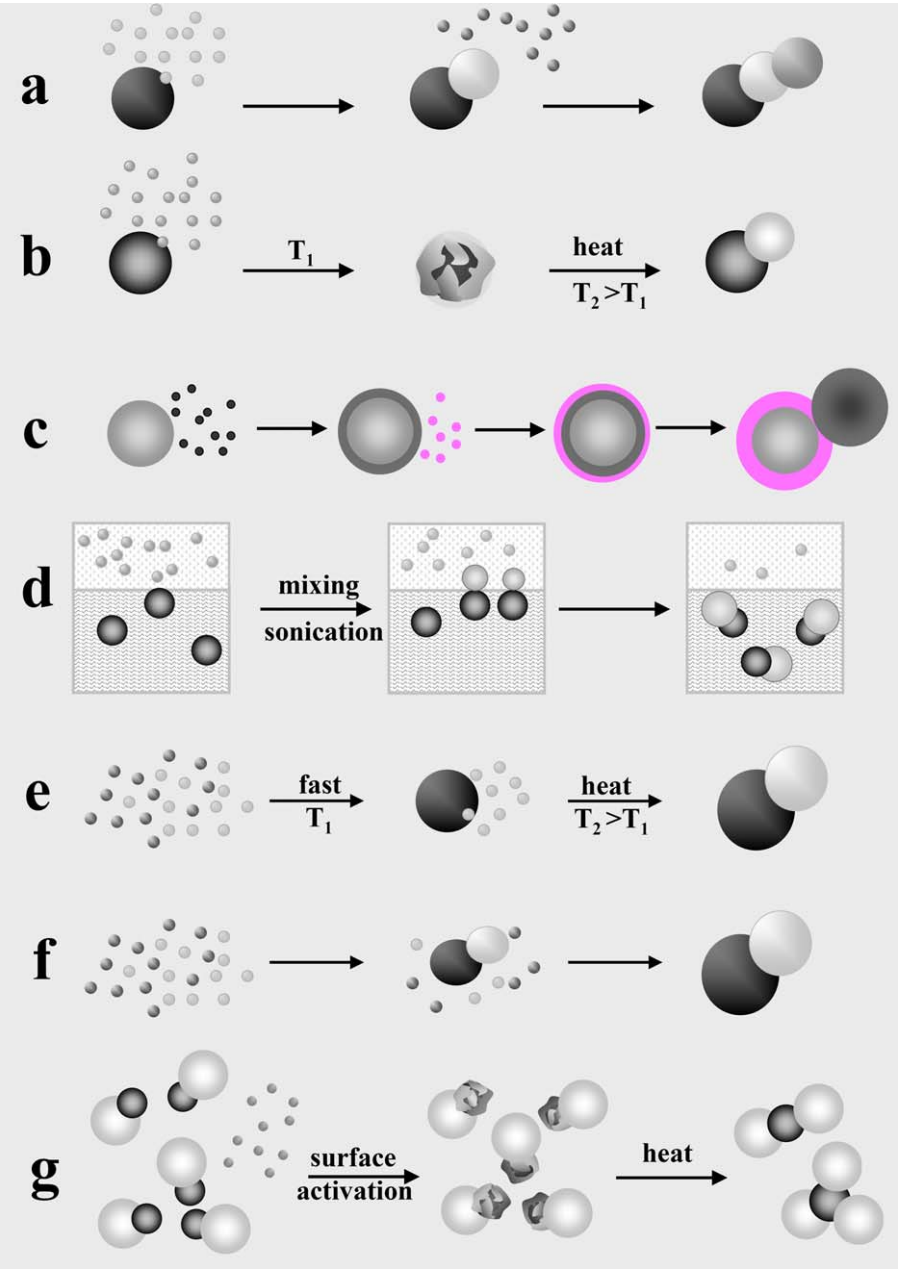

Scheme 3 Sketch of mechanisms underlying formation of oligomer-type HNCs: (a) direct heterogeneous nucleation; (b and c) nonepitaxial deposition followed by thermally driven coalescence/crystallization and/or solid-state atomic diffusion; (d) reactions at liquid/liquid interfaces; (e and f) self-regulated homogeneous—heterogeneous nucleation; and (g) induced attachment of preformed heterodimers (adapted from Ref. [12] with permission, copyright Wiley-VCH Verlag GmbH & Co. KGaA).

such core@shell HNCs as catalytically active nanoreactors, capacitors, and templates for the creation of hollow oxide capsules upon selective metal core etching [12]. Recently, a broad set of all-crystalline variable-shape Au@Cu_2O HNCs have been fabricated by a room-temperature aqueous route involving delicate adjustment of alkaline $CuCl_2$ reduction with NH_2OH in sodium dodecylsulfate surfactant environment loaded with shape-tailored Au seeds [129]. Despite of the relatively large differences in lattice parameters of the two materials, core@shell heterostructures with epitaxial interfaces were achieved, in which the shell could be either grown conformal to the morphology of the Au core underneath or be almost independently shaped over a wide size interval (Fig. 3c—e).

Chemical [12,130—133] or oxide-photocatalyzed reduction [12,134—137] of metal ion precursors on weakly organic-protected transition-metal-oxide NCs in alcoholic media was used to prepare a rich library of core@shell HNCs, embodying a ZnO or TiO_2 core decorated with either discontinuous patch-like or even layer of Au, Ag, Pt, or Cu. These architectures represent interesting platforms for solar energy conversion processes, as relative metal to semiconductor band alignment facilitates separation of electron-hole pairs under band-gap photoexcitation of the

oxide section. Examples of practical exploitation of such dynamics include light-driven modulation of the surface plasmon oscillation of the metal, enhancement of photocatalytic activity of the oxide, and/or control of electron storage capabilities of both heterostructure components [137].

(ii) *Non-oxide semiconductors/oxides*. Despite the proliferation of reports on their micro- and nano-composite counterparts (e.g., in thin-film form), oxide-semiconductor core@shell associations, based on the coupling of metal chalcogenides and large band-gap metal oxides, have been addressed sparsely [138—146]. In these systems, a type-II band alignment is met, whereby the metal chalcogenide essentially acts as visible-light sensitizer while the oxide may help preventing photocorrosion. These features are highly desirable for photovoltaic and/or photocatalytic applications [142—145]. One example is represented by ZnO nanorods and SnO_2 nanosheets unevenly decorated with shaped crystalline CdS domains deposited upon ultrasonication of aqueous suspensions containing oxide seeds, $CdCl_2$ and thiourea [138,140]. Slightly modified recipes (e.g., introducing citrate functionalization of the seeds) were applied to produce highly seed-shape-conformal polycrystalline CdS coatings of large thickness on rod- and wire-like TiO_2 nanostructures at close to room temperature [141,142]. The improved electron transport and gas-sensing ability of ZnO@CdS HNCs and the altered carrier lifetimes in TiO_2@CdS HNCs, compared to those of their respective oxide component alone, suggested existence of electronic communication exploitable in the design of new optoelectronic functional devices [138,142].

Onion-like HNCs with inverted semiconductor@metal-oxide configuration have also been pursued. CdSe@ZnO and CdTe@CdS@ZnO HNCs were obtained by alkaline hydrolysis of zinc acetate at the surface of CdSe NCs depleted of their original surfactants under sonication in alcohols [139] or on top of core@shell CdTe@CdS cores stabilized by 3-mercaptopropionic acid in water, respectively [145]. The emitted fluorescence could be tuned in between the green and red regions of the visible spectrum by adjusting the size of the core or the thickness of the ZnO shell. In addition, it was shown that thermal annealing and crystallization of a shell of Eu^{3+}—doped $LaPO_4$ deposited on citric-acid-functionalized CdS nanorods yielded CdS@$LaPO_4$:Eu heterostructures that produced increased Eu^{3+}—related luminescence due to energy transfer from the CdS core to Eu^{3+} ions in the $LaPO_4$ shell [146].

Another smart functional configuration was realized by depositing a TiO_2 layer (via hydrolysis-condensation followed by calcination) onto upconverting Yb^{3+}/Tm^{3+}—codoped YF_3 spherical seeds [144]. In these HNCs, the YF_3:Yb:Tm cores absorbed infrared light and convert edit into ultraviolet emission that could, in turn, stimulate the photocatalytic activity of the TiO_2 shell. This study demonstrated that photocatalysis could be indirectly activated in large band-gap semiconductors also by infrared light in properly engineered multimaterial heterostructures.

(iii) *Metals/magnetic oxides*. Another interesting family includes bifunctional core@shell HNCs, in which an optically active and biocompatible noble metal, such as Au or Ag, covers a ferro- or ferri-magnetic (FM, FiM) material domain, such as of Fe, FePt, or iron oxide (Fe_xO_y), utilizable as magnetic resonance imaging (MRI) contrast agent [147—153].

In organic-phase synthetic approaches, surfactant-capped Fe_3O_4 or FePt NCs were used as templates for the reduction of Au(III)- or Ag(I)-salts in the presence of oleic acid (OLAC) and/or oleyl amine (OLAM) at ~170—180 °C [148—150,153]. Such high temperature was needed to weaken surfactant binding to the surface of the seeds so as to render the latter accessible to the reactive metal species. Other authors demonstrated that OLAC/OLAM-capped Fe_3O_4 and unstable thiol-capped Au NCs in toluene in the presence of an ammonium bromide salt at 150 °C could be thermally driven to coalesce to Fe_3O_4@Au HNCs, thereby decreasing the overall surface energy of the system [148].

There have been reports dealing with aqueous syntheses under mild conditions, which however afford modest control over the size distribution and the aggregation degree of the heterostructures. Starting from suspensions or water-in-oil microemulsions containing weakly organic-stabilized Fe_xO_y seeds, it was possible to grow thick Au or Ag shells by reducing Au(III) salts with hydroxylamine [149] or $AgNO_3$ with borohydride, respectively [148]. These Fe_xO_y@noble-metal HNCs exhibited shell-thickness-dependent surface plasmon absorption and altered magnetic properties (e.g., lower blocking temperature, higher coercitivity), relative to those of their bare magnetic components, which was explained by invoking attainment of different interparticle coupling degrees as a consequence of the metal shell screening [150,153]. Prototypical bio-applications of these heterostructures in bioassays, magnetic-field-assisted separation, and in bacteria killing have been tackled [147,150].

HNCs based on reverse metal@magnetic oxide configuration were accessed by coupling metal seeds with high-temperature nonhydrolytic routes to transition-metal oxides, which were inherently characterized by a high activation barrier for homogeneous nucleation [11,154—160]. For example, monodisperse spherical or cube-shaped Au@Fe_3O_4 HNCs (Fig. 3f) with epitaxial interfaces were synthesized by decomposing $Fe(CO)_5$ at 200—300 °C in the presence of small Au seeds and OLAC/OLAM/DOE media [57]. Uniform Pt@Fe_2O_3 HNCs were obtained in similar mixtures in a one-pot approach, whereby Pt NCs were first nucleated in situ by alkyldiol reduction of platinum acetylacetonate and then combined with the iron precursor for shell deposition (Fig. 3g) [158,161]. In another report, $CoFe_2O_4$ NCs were used to seed Fe_3O_4 overgrowth, unexpectedly leading to CoFe@Fe_3O_4 HNCs with different degrees of interfacial coherence [155]. Bi-magnetic FePt@MFe_2O_4 HNCs (where M = Fe, Co) with a coherent core/shell interface were accessed directly by surfactant-assisted two-step solution synthesis [155,159,160]. In the reported procedure, Fe_xPt_{1-x} seeds, obtained by simultaneous platinum acetylacetonate reduction and iron carbonyl decomposition, were covered with a MFe_2O_4 upon co-decomposition of cobalt and iron acetylacetonate in suitable proportion in the presence of OLAC and OLAM stabilizers. In most of the aforementioned cases, the relative geometric parameters of the HNCs were easily engineered by adjusting the relative reactant concentration ratio, with the seeds dictating the relative balance of shell precursor consumption in the heterogeneous nucleation and growth stages. The relevant magnetic data indicated that effective exchange interactions were

established between the relevant magnetic phases, whose relative proportions dictated the overall coercitivity value.

By using a slight modification of the above reported procedures to shell growth, other material combinations were successfully combined, such as biocompatible $Me@Fe_2O_3$ HNCs (Me = Co, $SmCo_{5.2}$) that were applied in the selective separation histidine-tagged proteins after surface functionalization [154,156]. A technologically appealing approach to hard nanomagnets was devised, which combined solution-phase processing with a solid-state reaction. The proposed methodology relied on subjecting colloidal $Co@Sm_2O_3$ HNCs to high-temperature reductive annealing, which yielded hexagonal close-packed nanocrystalline $SmCo_5$ exhibiting large magnetic coercitivity [156].

FePt@ZnO HNCs with large shell-to-core volume ratio were synthesized by OLAM-driven aminolysis of zinc acetate in FePt seed/DOE mixtures at 260 °C [162]. These core@shell heterostructures, which offered both superparamagnetic behaviour and the typical fluorescence of ZnO, a valuable piezoelectric material, were envisioned to provide a basis for realizing future magnetically controlled electromechanical devices.

(iv) *All-oxides*. A few prototypes of *all-oxide* HNCs deserve to be mentioned. OLAC-assisted thermal decomposition of metal acetate in DOE and tri-n-octylamine mixtures at 320 °C was used to deposit a shell of antiferromagnetic (AFM) MnO onto monodisperse FiM cores of spinel-phase $MeFe_2O_4$ (Me = Zn, Co) [163]. The resulting bi-magnetic $MeFe_2O_4@MnO$ HNCs exhibited the signature of magnetic exchange coupling between interfacial spins of the FM (or FiM) and AFM sections, which produced enhanced unidirectional anisotropy with consequent distinctive alterations in the hysteresis cycles (e.g., horizontal loop shift by an ''exchange bias'' field) and coercitivity of the FM (or FiM) phase [12,164—166]. These nanoheterostructures, for which exchange bias effects can underlie enhancement of the thermal stability of the magnetization, are appealing candidates for high-density magnetic recording media [167,168].

Several Fe_3O_4-based heterostructures have been pursued. A synthesis of spherical $Fe_3O_4@ZnO$ HNCs has recently been reported, which relies on pyrolysis of calibrated amounts of zinc acetate in the presence of Fe_3O_4 seeds that have previously been de-capped from their original oleate ligands by a pyridine treatment [162]. These HNCs showed to be magnetically responsive, however no fluorescence from the ZnO shell was detected. Other protocols were proposed by which magnetically recordable, aggregated $Fe_3O_4@ZnO$ heterostructures showing photocatalytic activity were obtained [169].

More interesting properties were found to be associated with porous $Fe_3O_4@SnO_2$ and $Fe_3O_4@ZnO$ nanorods, which were fabricated upon reductive annealing of the cores of their α-$Fe_2O_3@SnO_2$ and α-$Fe_2O_3@ZnO$ parent heterostructures with shells grown by hydrothermal treatment of potassium stannate and zinc acetate at 120—170 °C, respectively [170—172]. These HNCs exhibited multi-nonlinear dielectric loss behavior and excellent electromagnetic wave absorption capability, which were ascertained to result from favorably complementary dielectric and magnetic losses associated with the respective materials [170—172]. Other heterostructures were realized by more elaborate seeded-growth techniques combining vapor- and solution-phase processing and selective thermally induced phase-transformation steps, among which type-II TiO_2-covered-ZnO tetrapods [173], coaxial anatase/B-phase TiO_2 nanofibers with excellent photocatalytic performances [174,175], and $CdPO_4@LaPO_4$ nanorod heterostructures achieved by a hydrothermally assisted seeded route [176].

Silica coating

Procedures to enwrap NCs of a variety of materials within a biocompatible and hydrophilic SiO_2 shell have proliferated over the past years. Such techniques generally rely on a ''priming'' step, which consists of creating a primary polymerization layer of alkoxide groups at the surface of the NC seeds via attaching bifunctional coupling agents, such as silicon or zirconium organometallic molecules, polymers or gelatine [177—190]. Controlled hydrolysis and condensation reactions in organic media by judicious supply of the desired metal alkoxide and water molecules results in the built-up of metal oxide network covering the starting seeds (Scheme 2e) [177—180,191—198]. The outer shell surface can further serve as platform for implanting other chemical functionalities that would be otherwise difficult to anchor onto the original NCs. These types of metal oxide shells can be grown to large thicknesses, since they are usually characterized by an amorphous and porous structure that does not induce significant strain to the core underneath. Examples of core@shell HNCs prepared by means of this aforementioned technique are reported in Fig. 4.

A variety of materials has been enwrapped within a SiO_2 shell. For example, SiO_2 coating of magnetic NCs, such as of Fe_xO_y, Co, and FePt (Fig. 4c and d) was used to transfer such nanomaterials to biological environments for specific cell targeting/sorting or MRI imaging purposes, while minimizing release of toxic heavy metals to aurous media [177,179,184,185,195,196,199—203]. Organic-coated hydrophobic semiconductor NCs (e.g., CdSe@ZnS, InP@ZnS PbSe) were made water-soluble and stabilized in high ionic-strength media with appreciable retention of their native fluorescence and reduced susceptibility toward photodegradation [178—180,186,197,198,204—206]. SiO_2 coating of noble-metal NCs was investigated as a tool for modifying their surface plasmon absorption responses (Fig. 4a and b) [191—193,195,198,206—208]. These achievements stimulated biological studies along with the development of various optical detection techniques [180,195,198]. Three-component magnetic/luminescent@SiO_2, magnetic/metal@SiO_2 or double-shell metal@$SiO_2@M_xO_y$ (Me_xO_y = TiO_2, ZrO_2, Y_2O_3) systems were also reported by combined multi-step approaches [184,187—189,209—211]. Among others, transition-metal@SiO_2 HNCs have attracted considerable interest as valuable functional nanostructures exploitable in the fabrication of space-filling superstructures (e.g., inverse lattices, opals, and photonic crystals) or serving plasmon-based sensing platforms and/or nanoreactors due to molecules being able to diffuse through the porous shell directly to the inner metal domain [177,186,198,206,212]. Selective etching of the core and/or partial leaching of the SiO_2 interlayer in metal@$SiO_2@Me_xO_y$ was exploited to generate thermally stable yolk@shell nanostructures

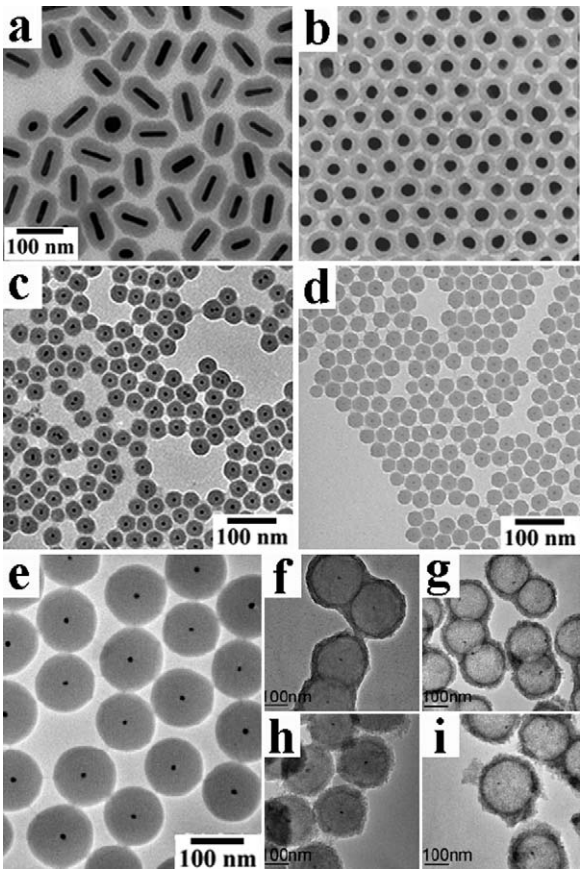

Figure 4 Gallery of TEM images showing core@shell HNCs synthesized by activating the surface of seed cores for silica shell growth (cf. Scheme 2e). (a and b) $Au@SiO_2$ HNCs with different shapes (reproduced with permission from Ref. [193], copyright American Chemical Society, and from ref. [191], copyright American Chemical Society, respectively). (c) $FePt@SiO_2$ HNCs (reproduced from Ref. [196] with permission, copyright American Chemical Society); (d) $CoFe_2O_4@SiO_2$ HNCs (adapted from Ref. [203], copyright American Chemical Society). (e) $Au@SiO_2$ core@shell HNCs and (f and g) $Au@SiO_2@ZrO_2$ core@shell@shell and $Au@ZrO_2$ yolk@shell HNCs thereof, respectively. (h and i) $Au@SiO_2@TiO_2$ core@shell@shell HNCs and $Au@TiO_2$ yolk-shell HNCs thereof (adapted from Ref. [188], copyright Wiley-VCH Verlag GmbH & Co. KGaA).

(Fig. 4e—i), which possessed a highly catalytically active metal core with virtually ''clean'' surface separated by a void space from the surrounding thermally stable shell walls [186—189,211]. Recently, it has been demonstrated that SiO_2 capsules can serve as confining nanoscale reactors in which chemical and structural transformation (e.g., reductive annealing) can take place in an environment preserved against irreversible thermal coalescence, leading to nanostructures with otherwise inaccessible crystal-phase composition [170,211,213,214].

Shell formation by red-ox reactions

Another commonly pursued strategy towards core@shell HNCs relies on the sacrificial conversion of the outermost exposed layers of a starting NC core into a different material by a galvanic replacement reaction (Scheme 2f) [164,215—224]. In this respect, many transition-metal NCs are potentially useful substrates, since they are easily oxidized when exposed to air, solvated oxygen species, or other oxidizing reagents (e.g., metal ions). In addition, such red-ox conversions permit the creation of oxide core@shell HNCs where the mean oxidation state of metal atoms located in the core is different from that in the shell section. Examples of as-synthesized HNCs are assembled in Fig. 5.

A set of magnetic-metal-based core@shell bimetallic HNCs was prepared through performing transmetalation reactions in organic media [80,215—217]. Metal ion (such as Au^{3+}, Pt^{2+}, Pd^{2+}, Cu^{2+}) precursors were reduced at 140—180 °C at the surface of surfactant-capped Co (or Fe) NCs to their corresponding zero-valence state at the expense of the topmost exposed Co^0 atomic layers, which were, in turn, released as Co^{2+}—ligand (or Fe^{3+}—ligand) complexes to the solution (Fig. 5a—d). Providing a magnetic NCs with a noble metal shell could switch its response from superparamagnetic to ferromagnetic, while a labile core, protected against oxidative corrosion, was equipped with a foreign surface to which selected molecules could be better attached (e.g., to enable HNC transfer into water and biofunctionalization). Exploitation of dual magnetic-catalytic functionality has been proven to be viable [80]. By conceptually similar synthesis approaches, Ag@Au and Ag@Pt HNCs with tuneable plasmonic properties were prepared [106,218], as well as a number of mono- and bi-metallic nanostructures with hollow interior or partial voids under extreme replacement reaction conditions [225].

Metal@metal-oxide systems achieved by calibrated oxidation of their respective metal cores deserve more extensive discussion. For example, monodisperse Ni@NiO HNCs [220] and $Fe@Fe_xO_y$ nanoparticles with amorphous cores [222] were generated upon room-temperature air exposure of TOPO-capped Ni seeds and OLAM-capped Fe seeds, respectively, and used for biomolecule tagging and magnetic separation purposes [220]. By an analogous route, Co@CoO HNCs were synthesized by subjecting preformed ferromagnetic (FM) Co NCs to controlled O_2 supply, which led to deposition of an antiferromagnetic (AFM) CoO shell or to full particle oxidation, depending on the conditions [164,219]. Inverted AFM/ferrimagnetic(FiM) $MnO@Mn_3O_4$ HNCs were derived from particle surface-confined oxidation of MnO NCs prepared by surfactant-assisted pyrolysis of manganese acetylacetonate in the presence of oleyl amine and 1,2-hexadecandiol [221] or by thermal decomposition of manganese oleate. All these types of HNCs were found to be technologically valuable as they indeed showed FM (or FiM)-AFM exchange bias effects [164—166,219,221,226,227]. The latter could be modulated by proper topological design and size tailoring of the core and shell domains to meet requirements for device implementation [167,168].

Unprecedented progress toward simultaneous morphological and compositional control have been made with the synthesis of complex yolk@shell HNCs via a mechanism known in metallurgy as the ''Kirkendall effect'', an atomic diffusion process that takes place through vacancy exchange rather than by direct interchange of atoms [225]. It is indeed established that, in a nanoscale object, where the inner core region hosts fast-diffusing species and the outer region acts as reservoir of slower diffusing species (e.g., metal cations

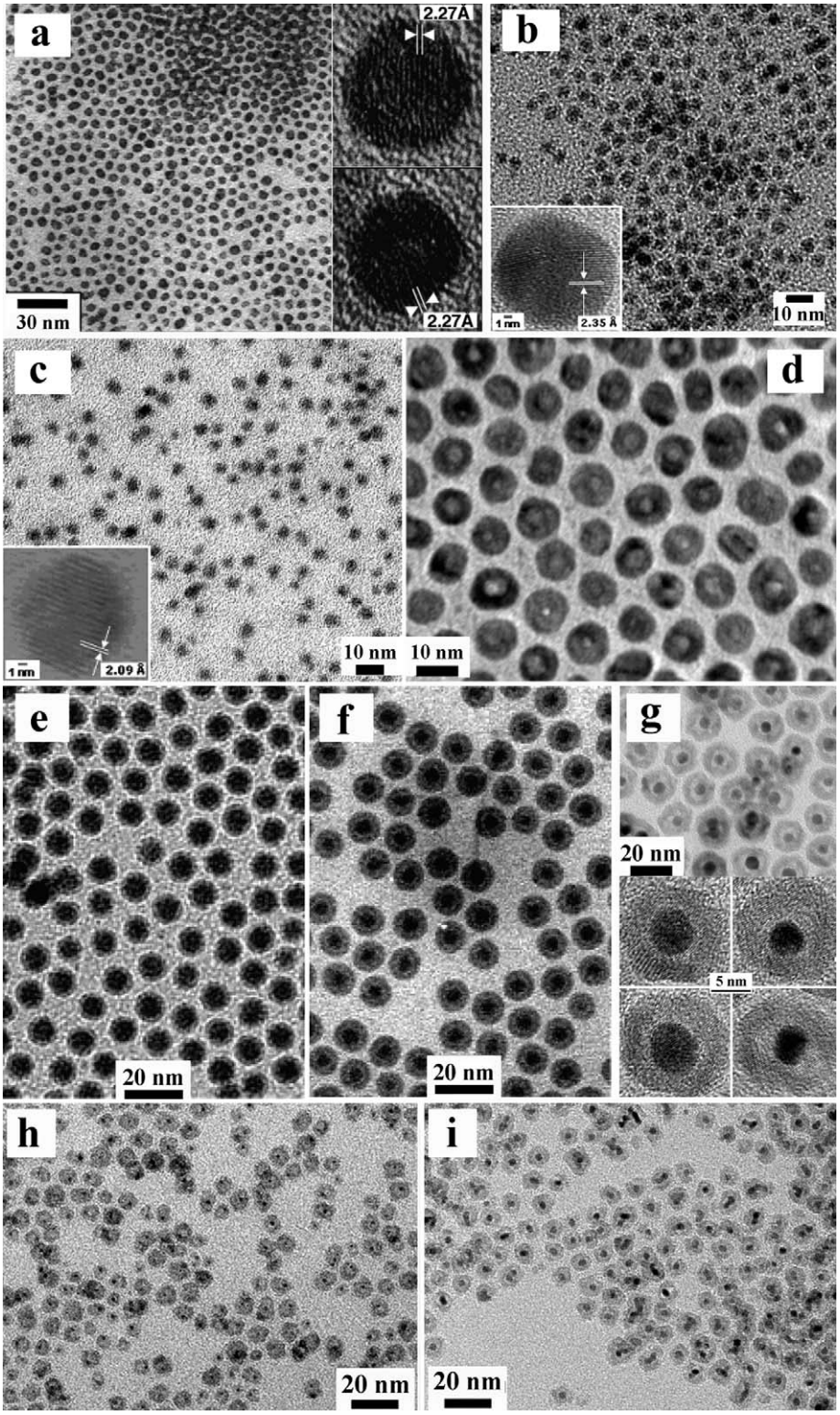

Figure 5 Gallery of TEM an HRTEM images showing examples of core@shell and yolk@shell HNCs synthesized by performing red-ox replacement reactions on metal seed cores (cf. Scheme 2f and g). (a) Co@Pt HNCs (reproduced from Ref. [215] with permission, copyright American Chemical Society). (b and c) Co@Au HNCs and Co@Cu HNCs (reproduced from Ref. [216] with permission, copyright American Chemical Society). (d) Au@Ag HNCs (reproduced from Ref. [218] with permission, copyright American Chemical Society). (e and f) Core@shell Fe@Fe_3O_4 and corresponding yolk@shell Fe@Fe_3O_4 HNCs thereof, respectively (adapted from Ref. [224] with permission, copyright American Chemical Society). (g) Au@Fe_3O_4 yolk@shell HNCs (adapted from Ref. [231] with permission, copyright Wiley-VCH Verlag GmbH & Co. KGaA). (h and i) FePt@Fe_3O_4 and Pt@Fe_3O_4 yolk@shell HNCs (adapted from Ref. [228] with permission, copyright American Chemical Society).

and oxygen anions in oxide-passivated metallic nanoparticle, respectively), a net transport of matter from the core outwards can take place along with coalescence of the generated vacancies into a single large void (Scheme 2g) [225]. For example, during the temperature-controlled oxidation of amorphous Fe nanoparticles with either O_2/Ar flow or trimethylamine N-oxide in octadecene/OLAM solution, the entire evolution from amorphous Fe@Fe_xO_y core@shell to Fe@Fe_3O_4 yolk@shell nanostructures (Fig. 5e and f), and finally to hollow Fe_3O_4 NCs was traced [223,224]. These findings suggested further smart routes to achieve increasingly sophisticated heterostructure design. Actually, selective application of the Kirkendall mechanism to the shell section of preformed core@shell HNCs has opened access to more topologically complex yolk@shell architectures, in which a void space intervenes between core and shell portions of different chemical composition. Relevant demonstrations include Au@Fe_3O_4, Pt@CoO, FePt@Fe_3O_4 and FePt@CoS_2 HNCs, obtained upon reacting Au@Fe, Pt@Co, FePt@Fe or FePt@Co core@shell HNCs with O_2 or sulfur, respectively (Fig. 5g—i) [228—231]. The internal void structure of the yolk@shell heterostructures has been assessed by further interesting probe experiments. For instance, Pt@CoO yolk@shell HNCs were found to be catalytically active in ethylene hydrogenation, thus confirming that small molecular reactants and products could permeate through grain boundaries of the CoO shell and reach the surface of the inner Pt core [229,232]. In a set of biological tests, FePt@CoS_2 yolk-shell HNCs, dispersed in aqueous medium, were observed to behave as powerful killing agents for HeLa cells [230]. Indeed, after cellular uptake and exposure to the intracellular acidic environment, the highly reactive FePt cores were oxidized, releasing toxic Pt^{2+} ions that diffused out of CoS_2 porous barrier and then entered the nucleus and mitochondria, ultimately leading to cell apoptosis [230]. Along this research direction, FePt@Fe_3O_4 yolk-shell HNCs were proposed to serve both as an MRI contrast agent and as a potent anticancer drug [228]. These achievements are expected to propel future development of new nanomedicine tools for cancer detection and therapy.

Unconventional pathways: self-controlled nucleation-growth, thermally induced phase segregation and solid-state atomic diffusion

There have been successful efforts to devise one-pot single-step approaches to core@shell HNCs, in which all necessary material precursors can simultaneously be present in the same growing solution, and the nucleation-growth of core and the shell coating stage may be self-regulated due to operation of less conventional mechanistic pathways. The search for such ''smart'' colloidal systems, for which the overall preparation procedure is obviously simplified, represents an extremely challenging task, which in fact explains why only a few cases have so far been documented. HNC systems accessed by such routes will be here briefly reviewed on the basis of the representative examples reported in Fig. 6.

(i) *Self-controlled nucleation-growth*. Under appropriate conditions, the inherent reactivities of the molecular precursors chosen to generate the core and shell materials, or, equally, the energy activation barriers for the homogeneous nucleation of the individual compounds may diverge to such an extent that: (i) two different materials form at distinct times or temperatures; and (ii) the shell material is produced most exclusively by heterogeneous nucleation on the in-situ formed seeds (Scheme 2h). Such dynamics permits bypassing the use of the classical ''hot-injection'' technique of precursor delivery, which is frequently exploited to temporally separate the nucleation and growth processes [17]. As an additional practical advantage, these routes do not require performing additional slow precursor injections at later synthesis stages to facilitate focusing of the size distribution [17,20,233].

Metal@metal-oxide HNCs (where Me = Ag, Au, and metal-oxide = TiO_2, ZrO_2) were derived by refluxing metal alkoxides with the desired Ag(I)- or Au(III)-salt in dimetylformamide (DMF)/H_2O mixtures [234—238]. At a suitable temperature DMF acted as reducing agent for the metal ions, inducing fast nucleation of metallic seeds. The latter were subsequently covered with a thin amorphous oxide shell upon slower hydrolysis-condensation reactions of the alkoxide in the presence of chelating/stabilizing agent. Ag@TiO_2 HNCs behaved as electron-storing platforms upon TiO_2 photoexcitation, which could utilize such charges to affect either the metal surface plasmon resonance of the core or to accomplish post-irradiation dark reductions [236,237].

Additional examples that illustrate the concept of self-controlled nucleation/growth mechanism are provided by the circumstances under which Ag@Co [239], Cu@Ni [240], Au@Co [238], and Cr@γ-Fe_2O_3 [241] HNCs were formed. For example, Ag@Co HNCs were accessed by combining $Co_2(CO)_8$ thermolysis with a trasmetalation reaction, namely Co(0)-driven $AgClO_4$ reduction in OLAC/tridodecylamine mixtures at 140 °C, during which a selective nucleation of Ag NCs was followed by the deposition of Co on top of the formed nuclei (Fig. 6a—c) [239]. A similar sequence underlied the formation of Au@Co upon heating $HAuCl_4$ and $Co(NO_3)_2$ in ODA at 120 °C, which led to initial nucleation of Au NCs that catalyzed the otherwise kinetically prohibited reduction of Co^{2+}—ODA complexes at their surface [238]. Spherical Cu@Ni HNCs were derived by switching a mixture of hydrate $CuCl_2$, $NiCl_2$ salts and NaOH dissolved in ethylene glycol (EG) reducing solvent between reflux (175 °C) and distillation conditions (165 °C), along which temporal separation of Cu core formation and Ni shell deposition was naturally realized [240]. Analogously, the different decomposition rates of the relevant precursors were assumed to be responsible for the formation of Cr@γ-Fe_2O_3 systems in mesitylene [241].

More recently, a few protocols to all-semiconductor core@shell heterostructures have been reported by manipulation established chemistry known for the individual materials. For example, the reaction of zinc stearate, indium myristate, tris(trimethylsilyl)phosphine, and dodecanthiol at 300 °C yielded highly fluorescent InP@ZnS core@shell NCs, in which the initially formed InP cores possessed a radial In:P composition gradient that allowed relieving strain caused by ZnS shell deposition at later reaction stages [174]. Bi_2Te_3@Bi_2S_3 nanorods assembled in branched topologies via penetration twins were synthesized on heating of $BiCl_3$, H_2TeO_4 and L-glutathionic acid (LGTA) in polyethylene glycole (PEG) at 140—195 °C [242]. In such mixtures, Bi_2Te_3 was first formed by faster PEG-driven reduc-

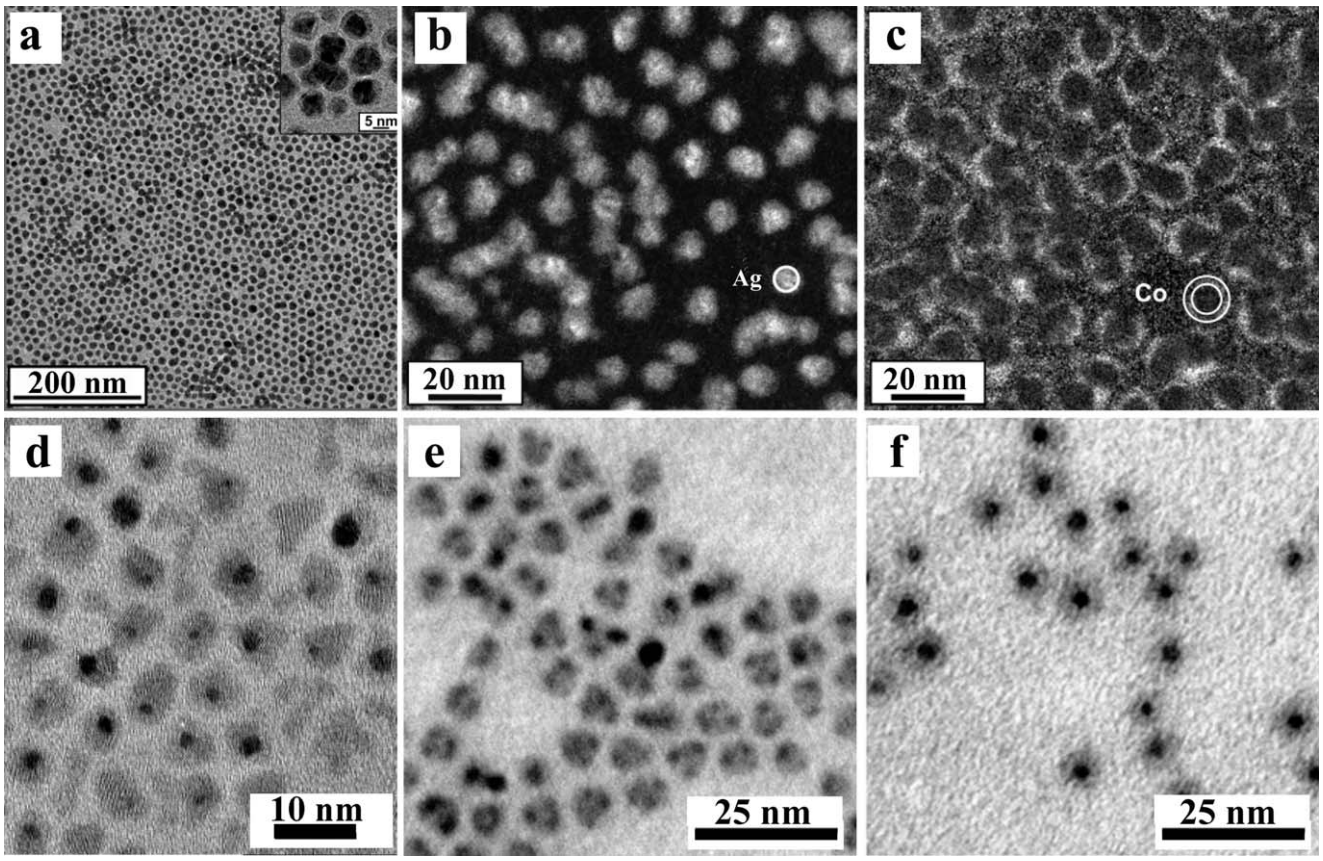

Figure 6 Gallery of TEM images showing examples of core@shell HNCs achieved by less conventional mechanisms (cf. Scheme 2h–j). (a) TEM overview and electron energy loss spectroscopy (EELS) maps of Ag (b) and Co (c) in Co@Ag HNCs obtained by self-controlled nucleation and growth (reproduced from Ref. [239] with permission, copyright American Chemical Society). (d) Au@CdSe HNCs obtained by thermal phase segregation of an alloy (reproduced from Ref. [245] with permission, copyright American Chemical Society). (e and f) Formation of Au@InAs HNCs in panel (f) upon gold diffusion within the Au-decorated InAs HNCs in panel (e) (reproduced from Ref. [246] with permission, copyright Wiley-VCH Verlag GmbH & Co. KGaA).

tion of H_2TeO_4 and Bi-LGTA complexes, while the Bi_2S_3 shell originated from slower decomposition of the latter under facet-selective adhesion of LGTA promoting anisotropic lattice development. The occasional detection of an inner Bi_2Te_2S suggested overlapping of the aforementioned pathways [242].

Finally, free-standing $Na_2Ti_3O_7$ nanosheets epitaxially decorated with Fe_3O_4 crystallites were accessed by modified route to alkali-metal titanate, involving the solvothermal treatment of TiO_2 powders, NaOH and Fe nanoparticles [243]. Notably, the resulting Fe_3O_4@$Na_2TiO_3O_7$ nanosheets were distinguished by improved Na^+ ion exchange performances and superior stability against spontaneous scrolling into tubular structures than their bare $Na_2TiO_3O_7$ counterparts. An unconventional example of chain-like magnetic Ni/Ni_3C core@shell heterostructures was generated upon $NiCl_2$ reduction and Ni-core-catalyzed organics decomposition to carbonaceous species in boiling EG [244].

(ii) *Thermally induced phase segregation and solid-state diffusion*. Au@CdSe HNCs were produced by exploiting Cd-Au alloy nanoparticles as reactants [245]. Heating the latter in the presence of Se in TOPO/TOP mixtures at 250 °C yielded CdSe, driving solid-state diffusion and coalescence of the Au atoms in the precursor alloy to a single segregated Au domain (Fig. 6d). As a result, heterostructures were obtained, in which the Au portion was almost fully surrounded by a CdSe shell (Scheme 2i). This process was likely driven by the poor miscibility of the nascent CdSe in the starting alloy as well as by the difference in CdSe and Au crystal structures and lattice parameters [245].

Other authors studied the reaction of organic-capped InAs NCs with a Au^{3+}–alkylammonium bromide complex and DDA reducing agent in toluene at room temperature [246]. At a sufficiently high Au^{3+} concentration, InAs NCs decorated with multiple Au islands were initially obtained, which then evolved to Au@InAs core@shell HNCs under inert atmosphere or into Au@In_2O_3 HNCs under air (Fig. 6e and f). Control experiments allowed the authors to conclude on the occurrence of a fast solid-state diffusion, according to which Au atoms migrated from the surface toward the interior of the semiconductor via an interstitial-substitution mechanism [247,248]. When the reaction was accomplished under inert atmosphere, the InAs NCs lost their crystalline order along the course of the Au diffusion process. The resulting amorphous-like InAs shell then became readily susceptible

to be converted to In_2O_3 once exposed to ambient oxygen (Scheme 2j). The driving force for the process can be presumed to be the elevate Au/InAs interface energy associated to the multiply-Au-decorated InAs seeds, which can be decreased upon coalescence of the Au patches into a single larger domain [246]. An analogous evolution was observed for Au—PbTe system [249].

A recent investigation deserving remark concerns the large-scale fabrication of chalcopyrite $CuInSe_2$@$CuInS_2$ core@shell nanowire bundles, which originated from solvothermal treatment of CuSe nanowires with $InCl_3$ and sublimed S in triethylene glycol at 180 °C [250]. The formation mechanism involved the interplay of competing pathways, among which simultaneous In^{3+} diffusion into the CdSe template lattice and reaction of surplus outward-diffusing lattice Cu^+ ions with S species in the solution, although ripening could also be suspected to play a role.

Oligomer-like architectures based on isotropically shaped material domains

A distinguished family of intriguing all-inorganic architectures includes HNCs with a spatially asymmetric composition, which incorporate distinct size- and shape-controlled sections of chemically and structurally dissimilar materials interconnected through one or several small bonding interfaces. Distinct from core@shell geometries, nanoheterostructures arranged in such oligomer-like topologies feature the inorganic nanocrystal analogues of complex organic molecules equipped with a number of functional moieties. While grouping the properties of different materials, they can indeed provide a diversified set of surface platforms onto which a spatially segregated distribution of functional moieties can eventually be implanted [2,5,12—15].

In seeded-growth synthesis various circumstances can lead to switching from core@shell-type to a phase-segregated development regime. Under thermodynamically controlled growth conditions, the topology will be dictated by the ultimate surface energy balance realized in the system (eq. 1), as discussed earlier. For example, materials that hardly form alloys and/or are strongly lattice-uncorrelated can develop into oligomer-type heterostructures as reducing the extension of the shared interfaces can allow minimizing the overall interfacial strain at a proportionally smaller cost of surface energy (associated to the multiple material surfaces exposed). Equally, small inorganic bonding junctions may be attained among pre-existing NCs as a means of counterbalancing the high surface energy values which would otherwise characterize colloidal mixtures of NCs of the respective materials, as, for instance, in the case of ineffective ligand stabilization. Other growth circumstances leading to non-onion-like HNCs may specifically correlate with the exploitation of seeds with a site-preferential accessibility that could arise from varying degrees of lattice-matching at different facets, or from kinetically overdriven deposition conditions associated, for example, with the inherent chemical reactivity or strength of ligand adhesion on certain surface sites [2,5,12,13,251].

Heterodimers and hetero-oligomers grouping two or more isotropically shaped (e.g., spherical, cube-like) NCs of different materials have been synthesized by seeded-growth based techniques. The available preparation schemes classified according to the relevant mechanism underlying heterostructure formation are sketched in Scheme 3: (a) direct heterogeneous nucleation; (b-c) nonepitaxial deposition followed by thermally driven coalescence-crystallization and/or solid-state atomic diffusion; (d) reactions at liquid/liquid interfaces; (e-f) self-regulated homogeneous—heterogeneous nucleation; and (g) forced attachment. Representative TEM images that illustrate the level of synthetic sophistication achievable by such mechanistic pathways can be found in Figs. 7—11.

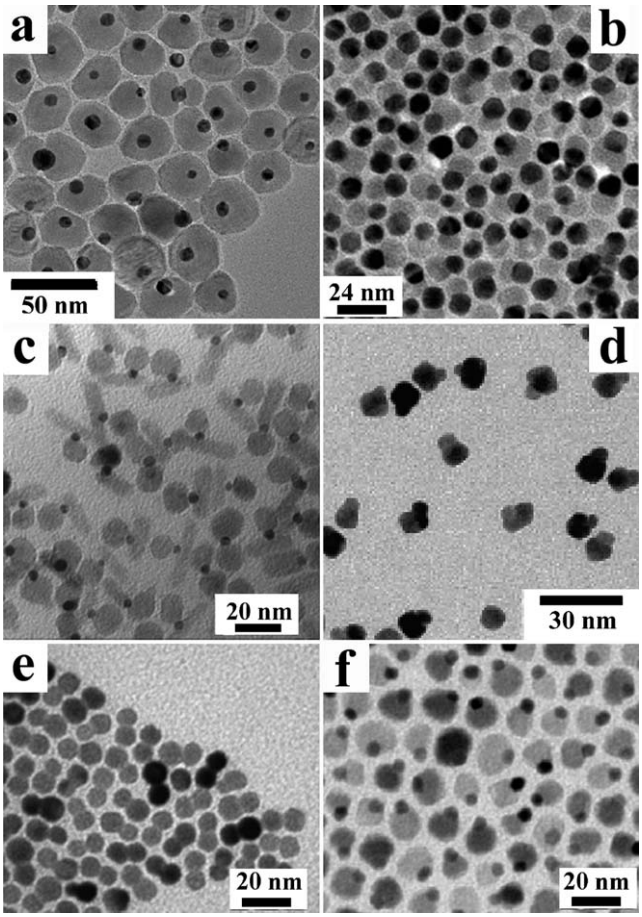

Figure 7 Gallery of TEM images showing examples of binary and ternary hetero-oligomer HNCs synthesized by direct epitaxial heterogeneous nucleation onto preformed seeds (cf. Scheme 3a). (a) Peanut-shaped Au—MnO HNCs (adapted from Ref. [252] with permission, copyright American Chemical Society). (b) Dumbbell-like Au—Fe_3O_4 HNCs (reproduced from Ref. [261] with permission, copyright American Chemical Society). (c) Au—Fe_3O_4—PbS HNCs obtained by nucleating a rod-shaped PbS section on Au—Fe_3O_4 heterodimer seeds (reproduced from Ref. [57] with permission, copyright American Chemical Society). (d) FePt—Au heterodimer HNCs with cubic-shaped FePt domains (reproduced from Ref. [80] with permission, copyright American Chemical Society). (e) Symmetric $CoPt_3$—Au heterodimer HNCs synthesized according to Ref. [269]. (f) Peanut-shaped Pt—Fe_3O_4 HNCs (adapted from Ref. [258] with permission, copyright American Chemical Society).

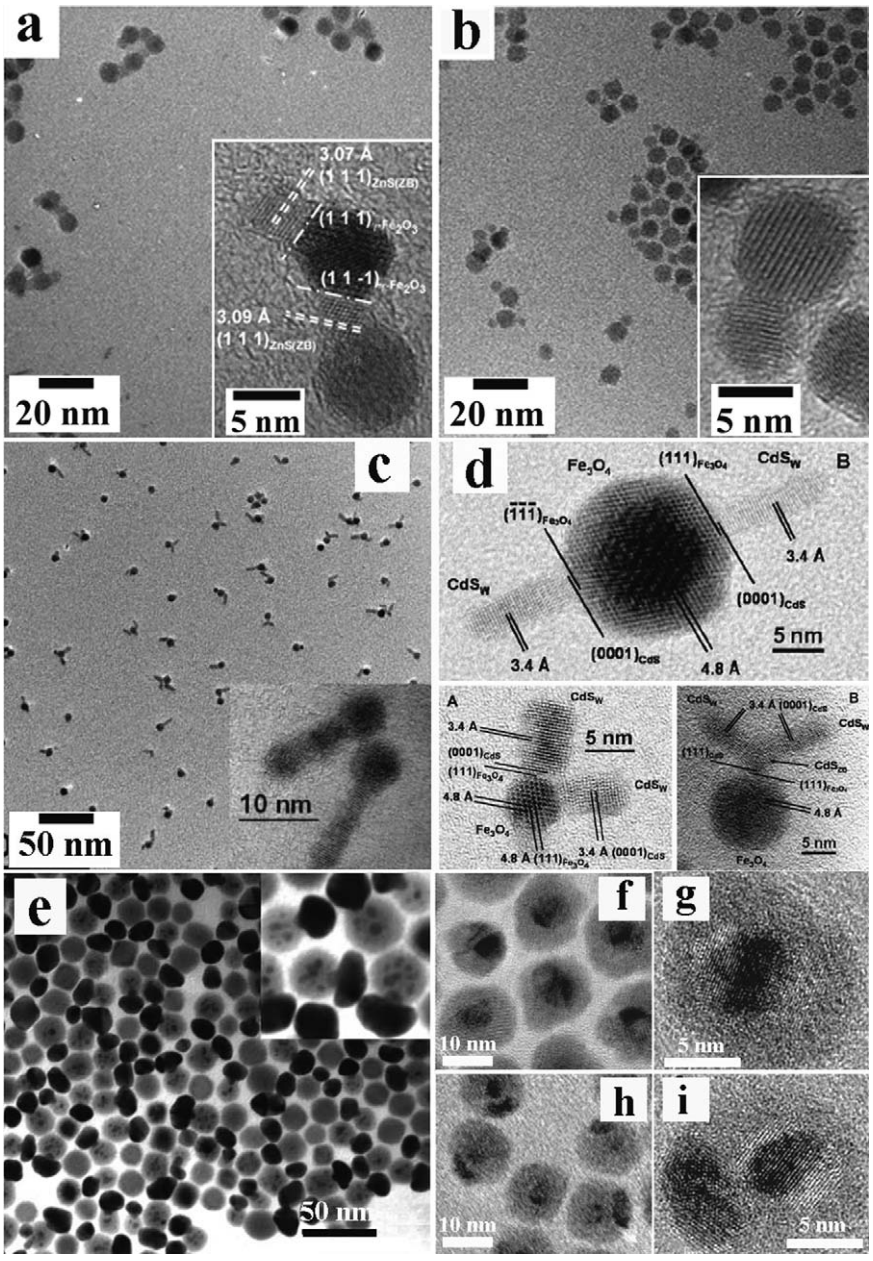

Figure 8 Gallery of TEM and HRTEM images showing examples of hetero-oligomer HNCs synthesized by post-deposition coalescence-crystallization and/or solid-state atomic diffusion (cf. Scheme 3b and c). (a and b) Binary and ternary Fe_3O_4—ZnS oligomers (adapted from Ref. [275] with permission, copyright American Chemical Society). (c and d) Fe_3O_4—CdS hetero-oligomer HNCs with one or multiple shaped CdS sections departing from a single Fe_3O_4 seed (reproduced from Ref. [277] with permission, copyright American Chemical Society). (e) Mushroom-shaped Au@PbTe—Au heterodimers HNCs (adapted from Ref. [249] with permission of the Royal Society of Chemistry). (f and g) Pt@Au@Ag_2S core@shell@shell HNCs and (h and i) Pt@Ag_2S—Au heterodimer HNCs thereof (reproduced from Ref. [279] with permission, copyright American Chemical Society).

Direct heterogeneous nucleation

This route (Scheme 3a) has been widely tacked to prepare HNCs made of various associations of magnetic, metal, and materials in the form of binary and ternary oligomers, as illustrated in Fig. 7. Such HNCs promise to deliver new technological solutions, especially in the field of sensing, imaging, and therapy in biomedicine. For example, it has been proposed that distinct material domains in a HNC can be used as platforms for the site-specific anchoring of DNA strands, proteins, and peptides, by exploiting the affinity of specific chemical moieties of such biomolecules toward inorganic surfaces [14,15]. Furthermore, while a metal or semiconductor portion can enable optical detection, a magnetic domain can be utilized for complementary purposes, such as MRI imaging and magnetic separation [14,15,80,251—254]. The importance of synergistic interactions attained by interfacing dissimilar

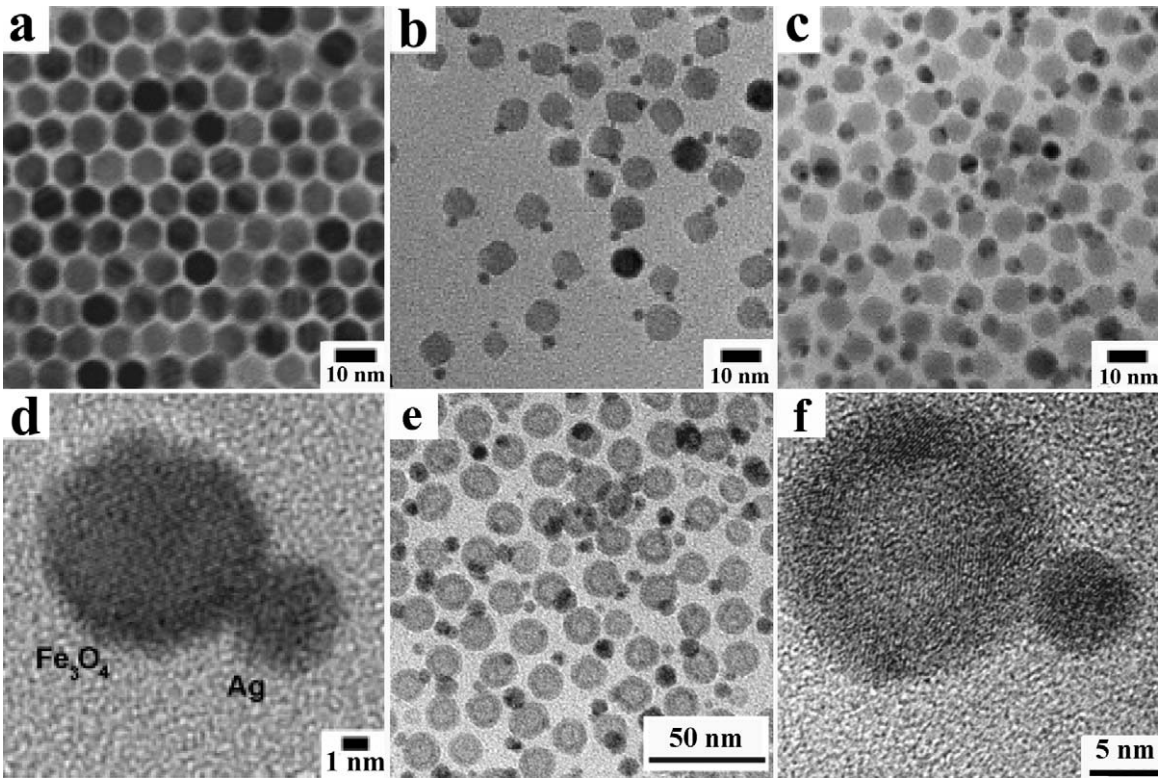

Figure 9 Gallery of TEM and HRTEM images showing examples of heterodimers synthesized at liquid/liquid interfaces (cf. Scheme 3d). (a) Starting Fe_3O_4 seeds; (b—d) Fe_3O_4—Ag heterodimers thereof with different Ag domain size (reproduced from Ref. [280] with permission, copyright American Chemical Society). (e and f) Fe_3O_4—Ag heterodimers with hollow Fe_3O_4 domain (adapted from Ref. [281] with permission, copyright American Chemical Society).

materials has clearly been recognized in catalytic studies [255—259] and prototypical optoelectronic applications [120].

Protocols based on thermal decomposition of organometallic precursors in the presence of preformed Me^1, Me^2, Me^3, Fe_3O_4 or FePt seeds in ODE or phenyl ether solvents containing OLAC, OLAM and/or TOP surfactants at 200—300 °C afforded HNCs with epitaxially joint Me^1—Fe_3O_4 (Me^1 = Au, AuAg, Pt, Ni), Me^2—CoO (Me^2 = Au, AuAg, Pt), Me^3—MnO (Me^3 = Au, Ag), Fe_3O_4—PbS, Fe_3O_4—CdSe, FePt—YZ (YZ = $CoFe_2O_4$, PbSe, CdSe) sections, respectively [57,118,120,251—253,258,260,261]. Depending on the geometric features of the two domains, these heterostructures showed a peanut-, dumbbell-, brick- or flower-like morphological profile (Fig. 7a and b). In most cases, the appreciable difference in lattice parameters of the concerned materials was presumed to be the main driving force towards heterostructure segregation into discrete domains being oriented so as to share a coherent interface over which strain could be minimized. The formation mechanism was investigated in detail for the Au—Fe_3O_4 association, for which a fundamental role of the solvent in regulating the Fe_3O_4 nucleation sites on the Au seeds was recognized [260,261]. The dumbbell-like configuration attained for reactions performed in nonpolar media was explained by invoking induction of charge polarization in proximity of the Au substrate location where Fe_3O_4 was initially deposited, which depleted the electron density elsewhere and thus inhibited further nucleation events. In contrast, in syntheses carried out in a more polar electron-donor solvent, any electron deficiency generated over the Au surface could be compensated for, thus rendering the seed a more suitable ground either for the nucleation of multiple Fe_3O_4 ''petal''-like domains or even for the achievement of uniform oxide coverage [258,260,261]. In additional mechanistic investigations on various metal/metal oxide and metal/semiconductor systems the transition from dumbbell- to flower-like geometry was achieved by increasing the temperature and/or relative precursor to seed proportions [57,118,251—253,260]. In some cases, the nature of ligands bound to the surface of the starting seeds was found to be critical to driving the preference for a heterodimer topology over a core@shell one [120], which pointed to the influence of kinetic processes on topology selection [118,251—253,260,261].

Different types of heterodimers made of Ag—Se [262], YZ—Au (YZ = ZnO, Cu_2O, FePt, CdSe, PbTe) [57,118,179,249,264—268], AuAg [106,258], $CoPt_3$—Au [268,269], Fe_3O_4—Ag [106,251,270], and Me_xS_y—Au (Me = Cu, Ag, Cd, Pb) [106,263,266,267,271,272] spherical domains were prepared via mild reduction of either SeO_3^{2-} ions, Au(I)/Au(III)— or Ag(I)—ligand complexes onto preformed Ag, YZ, $CoPt_3$, Fe_3O_4, or Me_xS_y seeds, respectively, in mild conditions (< 120 °C) (Fig. 7d—f). The properties of the attained magnetic/metal/semiconductor HNCs clearly deviated from those of the individual components alone. For example, the semiconductor luminescence was quenched due to the metal contact favouring electron migration, while the plas-

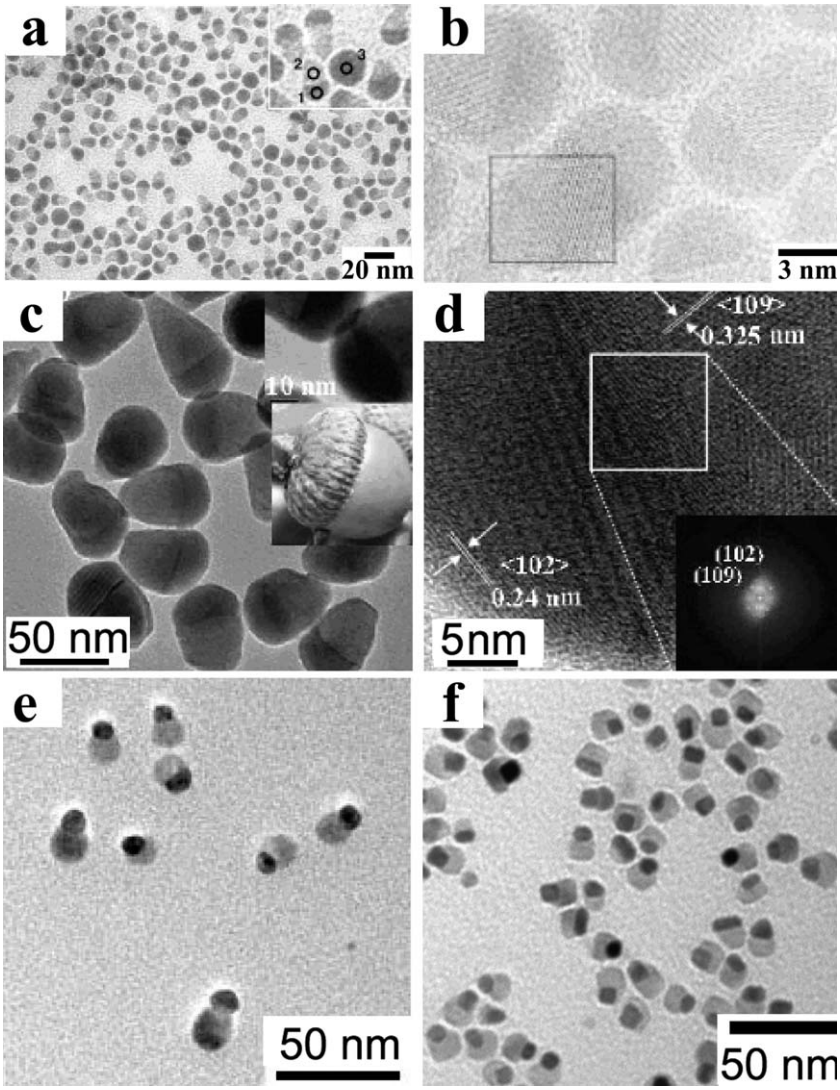

Figure 10 Gallery of TEM and HRTEM images illustrating examples of HNCs synthesized by self-controlled nucleation-growth processes (cf. Scheme 3e and f). (a and b) Co_9S_8—PdS_x (reproduced from Ref. [282] with permission, copyright American Chemical Society). (c and d) Cu_2S—In_2S_3 heterodimers (reproduced from Ref. [284] with permission, copyright American Chemical Society). (e) Ag—AgCl heterodimers (reproduced from Ref. [286] with permission, copyright Wiley-VCH Verlag GmbH & Co. KGaA). (f) FePt—Fe_3O_4 heterodimers (synthesized according to Ref. [285]).

mon resonance was largely shifted due to dielectric coating effects [57,106,118,179,249,263,265—267,271,272,268]. Also, the relevant magnetic parameters were altered following a nonmonotonic size dependence, for which an exhaustive explanation however remained elusive. These modified properties again reflected the mutual influence of interfacial electron contacting that was achieved upon formation of an inorganic heterojunction [57,106,251,263,269,270].

Among the most interesting mechanistic insights, the following findings deserve remark. The ability to tune the geometric parameters of heterodimer nanostructures was demonstrated for the Au—$CoPt_3$ and Ag—Fe_3O_4 systems, whereby $CoPt_3$ and Fe_3O_4 seeds with different sizes and shapes provided substrates with varying degrees of reactivity toward the relevant metal complex precursor, while the seed to metal-ion precursor concentration ratio and temperature regulated the size to which the Au and Ag domain could ultimately be grown (Fig. 7e) [251,269]. As a proof of concept towards development of increasingly elaborate architectures, it was shown that multicomponent hetero-oligomer could be accessed by reiteration of seeding steps (Scheme 3a). For example, ternary Fe_3O_4—Au—PbSe HNCs were synthesized by inducing heterogeneous nucleation of PbSe onto binary Fe_3O_4—Au dumbbell-shaped seeds from Pb/Se surfactant complexes [57,273]. Interestingly, PbSe nanostructures could develop anisotropically out of such Au domains (Fig. 7c) via a solution—liquid—solid (SLS) growth mechanism [2,5] and eventually detach into the solution [273]. Occasionally, heterogeneous nucleation processes were found to interplay and/or compete with red-ox replacement, cation exchange and the Kirkendall mechanism pathways, leading to creation of heterostructures that embodied an irregular topological distribution of their

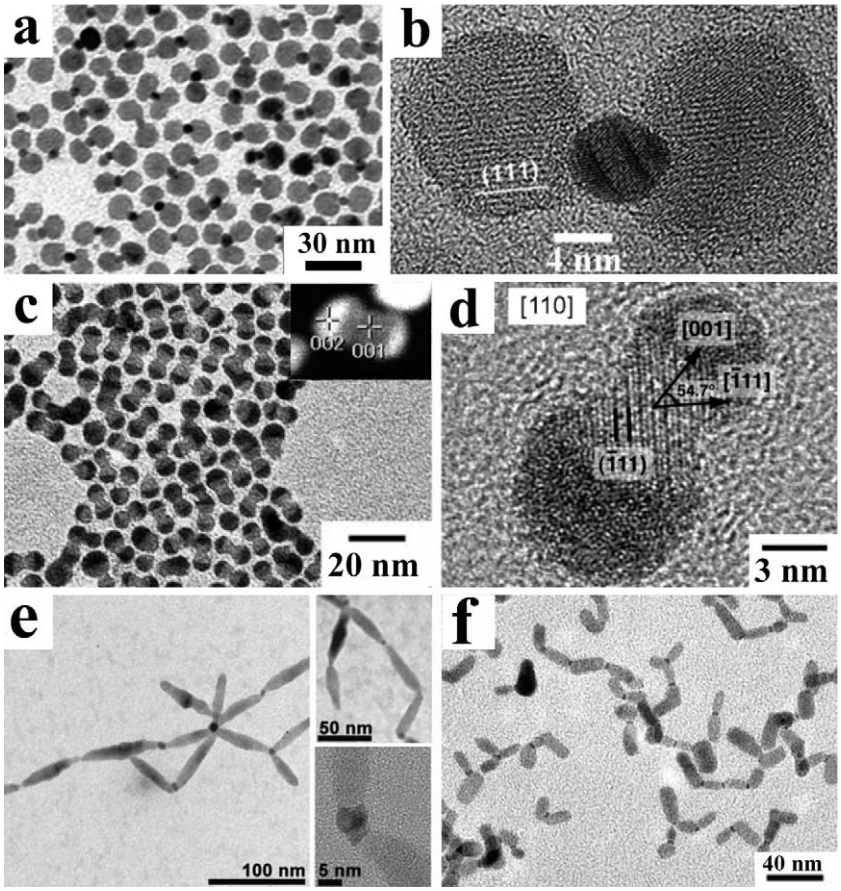

Figure 11 Gallery of TEM and HRTEM images showing examples of hetero-oligomer HNCs synthesized by induced fusion of preformed heterostructured seeds (cf. Scheme 3g). (a and b) Ternary Fe_3O_4—Au—Fe_3O_4 HNCs with a Au bridging section (reproduced from Ref. [57] with permission, copyright American Chemical Society). (c and d) Ternary PdS_x—Co_9S_8—PdS_x HNCs with an intermediate Co_9S_8 bridging portion (reproduced from Ref. [288], copyright Wiley-VCH Verlag GmbH & Co. KGaA). (e) Chain-like CdSe—Au—CdSe heterostructures (adapted from Ref. [287], copyright Wiley-VCH Verlag GmbH & Co. KGaA). (f) Chain-like CdS—PdS_x—CdS heterostructures (adapted from Ref. [289] with permission of the Royal Society of Chemistry).

chemical composition or contain void spaces in one of the component domains [263,267,274].

Post-deposition coalescence-crystallization and solid-state diffusion

A systematic investigation of how minimization of interfacial strain energy governs the topological evolution of HNCs was reported for heterostructures based on either FePt or γ-Fe_2O_3 and metal chalcogenides, MeX (Me = Cd, Zn, Hg; X = S, Se) [116—118,179,275—277]. Examples of HNCs synthesized by this mechanism are reported in Fig. 8. The synthesis of these HNCs was seeded with either γ-Fe_2O_3 or FePt seeds, onto which a highly defective and amorphous MeX layer was initially deposited upon sequential addition of standard organometallic precursors at low temperature. Upon heating at 280 °C, slow crystallization of the amorphous MeX shell gradually induced strain at the seed/MeX junction region owing to the poor lattice matching between the two materials. Over time, the shell coalesced and segregated into a discrete MeX grain aside of the γ-Fe_2O_3 seed [116—118,179,275,276] (Scheme 3b). Such evolution was explained by considering that the large junction tension in the annealed core@shell nanostructure could be greatly relieved by reduction of the interfacial area between the two materials. This energy gain could therefore be large enough to compensate for the proportionally smaller increase in the overall surface energy that eventually accompanies heterodimer formation. The topological evolution of the γ-Fe_2O_3—MeX system was accounted for on the basis of the Coincidence Site Lattice Theory (CSLT) [275—277]. The CSLT is used to explain the crystallographic relationships between two types of materials by identifying the degree of matching between points of the respective lattices, and the frequency at which this correspondence occurs along the relevant grain boundaries [278]. It was rationalized that the degree of lattice fit at a γ-Fe_2O_3/MeX interface indeed dictated the average number of MeX domains that could be accommodated on each γ-Fe_2O_3 seed, depending on the size of the latter (Fig. 8a and b) [275—277]. Adjustment of the ligand environment and of the growth kinetics regime resulted in one or multiple CdS sections that developed anisotropically out of seeds and shared similar site-coincidence relationships at the relevant CdS/γ-Fe_2O_3 interfaces (Fig. 8c and d) [277]. As for what concered their chemical—physical properties, these magnetic/semiconductor HNCs could still exhibit sufficient fluorescent emission from the MeX domains, while retaining the

typical superparamagnetic behaviour of magnetic portion [116–118,179,275,276], which suggested their utilization as bifunctional probes for dual-mode bio-imaging [15,179].

Very recently, some authors observed a transition from a Au@Ag_2S, Pt@Au@Ag_2S and Au@PbTe core@shell to corresponding Ag_2S–Au, Pt@Ag_2S–Au, and Au@PbTe–Au heterodimer arrangements upon aging at room temperature or prolonged heating at 90 °C in organic solvents, respectively (Fig. 8e–i) [249,279]. This evolution closely resembled a process inverse to that leading to Au-decorated InAs or PbTe NCs to Au@InAs and Au@PbTe core@shell HNCs, respectively [246,249], illustrated in previous paragraphs. It was proposed that electron transfer from the Au to the semiconductor domain could trigger diffusion of Au ions through the semiconductor lattice via a substitutional-interstitial mechanism [247,248] similar to that accompanying the transition from hetero-oligomer to core@shell structure observed in other heterostructured systems [246]. The overall conversion should presumably proceed on benefiting from a reduction in total free Gibbs energy (Scheme 3c).

Reactions at liquid/liquid interfaces

A technique based on performing seeded growth at a liquid/liquid interface under mild conditions was devised to synthesize heterodimers coupling a magnetic section and a noble metal domain [280,281]. Examples of HNCs synthesized by this biphasic strategy are shown in Fig. 9. In the reported procedure (Scheme 3d), an aqueous metal salt solution was brought in contact with an immiscible organic solvent (such as dichlorobenzene, dichloromethane, hexane, or DOE) in which surfactant-capped γ-Fe_2O_3/Fe_3O_4 or FePt seeds were dissolved. Upon ultrasonic irradiation under inert atmosphere, an emulsion was formed that supposedly consisted of continuous aqueous phase containing ''colloidosomes'', namely organic microdroplets stabilized by the hydrophobic seeds self-assembled at the organic/water interfaces [280]. The seeding NCs provided catalytic sites onto which the Ag^+ or $AuCl_4^-$ ions were reduced to the respective Ag or Au upon sonication, respectively. As the seeds were only partially exposed to the aqueous phase, metal deposition was spatially restricted to a small surface region and proceeded self-catalytically, thus resulting in a single metal domain on each seed (Fig. 9a–d). The ''colloidosome''–based approach was extended to the synthesis of solid Ag–hollow γ-Fe_2O_3 heterodimers starting from hollow γ-Fe_2O_3 seeds prepared by manipulating the Kirkendall effect (Fig. 9e and f) [281]. These heterodimers were proven to accommodate a site-differential surface distribution of biomolecules to enable multiple tasks in biomedicine applications [15,281].

Self-regulated homogeneous and heterogeneous nucleation

There have been also recent reports on the preparation of heterodimer HNCs by one-pot methods, in which all the reagents required to grow the heterostructures are present since the beginning of the synthesis in the same surfactant mixture. Both homogeneous and heterogeneous nucleation processes of different materials are self-governed at once, which permits simplification of overall synthetic procedure, since no separate seed preparation step is necessary. Nevertheless, identification of experimental conditions under which self-regulated nucleation/growth is established is extremely challenging, since it requires a rather delicate choice and ingenious manipulation of appropriate reaction pathways. Examples of HNCs prepared by such approaches are illustrated in Fig. 10.

When attempting to create an alloy of compounds characterized by partial miscibility and large interfacial energy, phase-segregation of two materials into separate domains may take place, leading to a dimer-like heterostructure (Scheme 3e). This was verified in the growth of Co_9S_8-PdS_x and Cu_2S-In_2S_3 heterodimers with acorn, bottle and larva-like shapes by co-decomposition of the corresponding metal carboxylate precursors in the presence of various alkylthiols [282–284] (Fig. 10a–d). During the reaction, selective homogeneous nucleation of one material was followed by growth continuation of the second one that emerged by developing an interface of graded composition. Similarly, Au–Ni HNCs were generated upon heating $HAuCl_4$ and $Ni(NO_3)_2$ in ODA at 120 °C, whereby initially generated Au seeds triggered the otherwise kinetically unviable reduction of Ni^{2+}–ODA complexes at their surface [238].

Another interesting case is represented by FePt–Fe_xO_y heterodimers with tunable geometric parameters (Fig. 10f), which were prepared by reacting $Pt(acac)_2$ and $Fe(CO)_5$ precursors in a OLAM/OLAC/octadecene environment [285]. The HNC portions were formed in two sequential steps. Initially, homogeneous nucleation and growth of FePt NCs took place at $T \leq 200$ °C, after which a thin polycrystalline Fe_xO_y shell was heterogeneously deposited onto such seeds at $T \approx 295$ °C, which soon de-wetted out (cf. Scheme 3b) and grew to larger volume as a separate domain attached aside. Since each reaction stage was selectively activated in well-defined temperature conditions, then regulation of both the temperature and the heating time guaranteed that the two material sections of the HNCs formed at distinct times of the synthesis course. As a consequence of the magnetic exchange coupling between the two soft and hard materials, the HNCs exhibited tunable single-phase-like magnetic behavior, distinct from that of their individual components, which was conveniently exploited in MRI techniques [285].

Ag–AgBr heterodimers were derived upon methanol addition to a toluene solution containing an $AgNO_3$/alkylammoium bromide complex and dodecanthiol capping ligands [286] (Fig. 10e). The alcohol here acted as both weak reducing agent for Ag^+ ions and AgBr-precipitating agent, thereby triggering simultaneous nucleation and growth of the Ag and AgBr portions of each heterodimer (Scheme 3f). This particular evolution was corroborated by statistic investigations revealing that the volume ratio of two domains maintains approximately constant over time in spite of the relatively large domain size distribution.

Reactions induced between preformed heterodimers

An original strategy was devised with the potential to access increasingly complex HNCs, in which heterodimers were regarded as small functional inorganic precursors that could

be combined with each other to form larger molecules. Examples of as-synthesized HNCs are shown in Fig. 11. It was reported that peanut-shaped ternary Fe_3O_4—Au—Fe_3O_4 HNCs, in which a Au section bridged two Fe_3O_4 domains, could be obtained by triggering welding of the Au domains that belonged to separate Au—Fe_3O_4 heterodimers in the presence of elemental sulphur [57] (Scheme 3g). Due to its high affinity to Au surfaces, it was presumed that sulphur helped to displace the capping surfactants on the Au section of the heterodimers, thereby inducing them to fuse with each other as a means of lowering their total surface energy (Fig. 11a and b). A conceptually similar activation strategy was used to create chain-like architectures by end-to-end assembly of Au-tipped metal chalcogenide NCs of various shapes (Fig. 11e) [287]. In another approach, PdS_x—Co_9S_8—PdS_x peanut-shaped HNCs, in which a central Co_9S_8 portion connects two PdS_x domains (Fig. 11c and d), were synthesized by seeding Co_9S_8 phase with PdS_x NCs using cobalt acetate and n-octadecanthiol as precursor in DOE at 230 °C [283,288]. As demonstrated by time-dependent growth investigation, the ternary PdS_x—Co_9S_8—PdS_x HNCs resulted from crystal-oriented coalescence of the acorn-shaped PdS_x—Co_9S_8 heterodimers that were formed at intermediate reaction stages. The driving force of this process appeared to be the weak organic passivation of the Co_9S_8 domains, which rendered them particularly reactive and, hence, prone to fuse with each other in the absence of extra surfactants. An analogous mechanism was exploited in the synthesis of CdS—PdS_x—CdS nanodumbbells or small chains starting from CdS—PdS_x heterostructured precursors (Fig. 11f) [289]. A crystal-oriented attachment route has been employed in the preparation of binary chain-like —$(TiO_2$—$SnO_2)_n$— heterostructures [290]. In this case, a mixture of rutile TiO_2 nanorods and cassiterite SnO_2 NCs was thermally activated under hydrothermal conditions, yielding heterostructures characterized by a ''pearl necklace'' distribution of SnO_2 and TiO_2 domains.

Heterostructures based on anisotropically shaped material sections

HNCs with a spatially asymmetric arrangement of their component domains have been obtained by programming heterogeneous growth reactions onto anisotropically shaped seeds, such as nanorods, nanowires and branched NCs, which commonly occur in noncentrosymmetric crystal phases [2,5,8,12]. This ultimately transcribes into a pronounced facet-dependent reactivity. Apart from exhibiting shape-dependent properties, anisotropic templates represent alternative intriguing platforms over which chemical pathways to spatially selective allocation of a secondary nanosized domain can be understood. On a thermodynamic basis, the preference for secondary material deposition to take place at selected location of asymmetrically shaped seeds should correspond to the topological configuration that allows minimizing the overall surface and interfacial energy of the system [2,5,12]. For example, selective heterogeneous nucleation can be regarded as a process that advantageously eliminates unstable facets of the seeds (e.g., the apexes of nanorods) at the proportionally smaller cost of strain energy associated with the attainment of lattice-mismatched heterojunctions. However, the interplay of kinetic processes associated, for example, with solution supersaturation, reactant diffusion, and/or the inherent chemical reactivity of the seeds and/or the particular molecular precursor selected, may complicate mechanistic understanding [2,5,12,292—297].

For the sake of clarity, heterojunction-based multicomponent nanomaterials discussed in the following paragraphs will be categorized according to the nature of the individual material components, namely: semiconductor—semiconductor, semiconductor—metal and

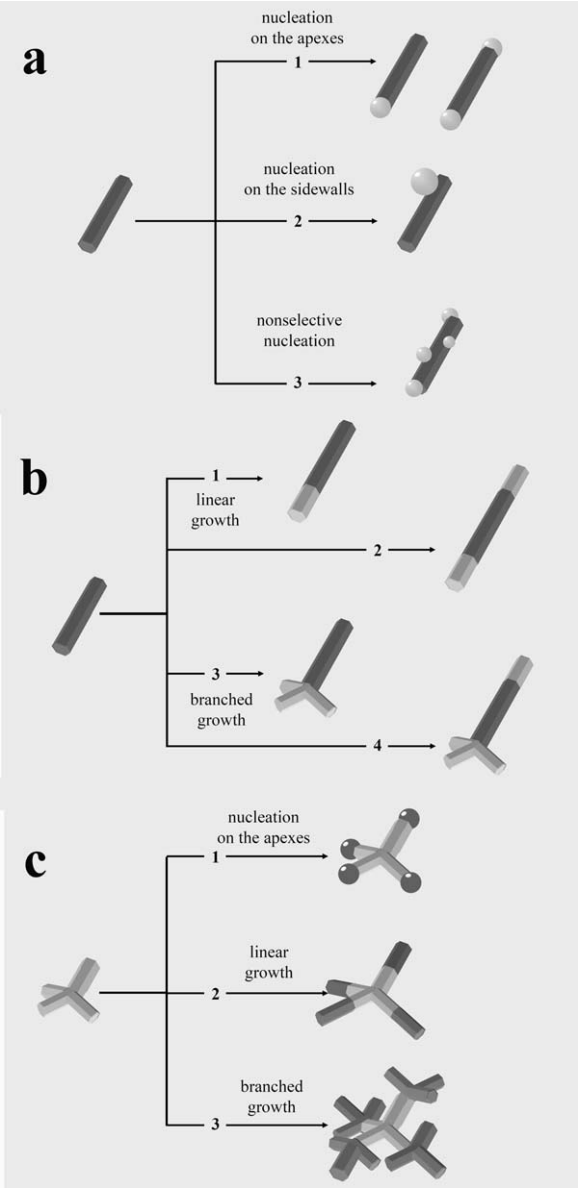

Scheme 4 Sketch of pathways leading to nanocrystal heterostructure grown from anisotropically shaped seeds: (a) functionalization of a nanorod with spherical domains of a different material at selected locations; (b) apex-selective growth continuation of a nanorod into either a linear or a branched manner; (c) growth of either spherical, linear or branched sections out of the tips of tetrapods (adapted from Ref. [11] with permission, copyright 2007 Bentham Science Publisher).

metal—metal. The following paragraphs keep a focus on nanoarchitectures made of at least one spatially anisotropic (linear or branched) section and purposely omits wire-shaped nucleated materials that are not synthesized by wet-chemistry approaches. Synthetic protocols, all generally based on the seeded-growth techniques, take advantage of mechanisms as diverse as: (i) site-specific heterogeneous nucleation; (ii) light-assisted growth; (iii) surfactant-controlled site-selective deposition; (iv) heterogeneous nucleation followed by ripening or coalescence; (v) red-ox or cation exchange reaction; and (vi) strain-driven heteroepitaxial growth. These pathways are sketched in Schemes 4—9, respectively. Representative TEM images that demonstrate the degree of synthetic control achievable by exploitation of such pathways can be found in Figs. 12—17.

Site-selective heterogeneous nucleation

Non-oxide semiconductors

The first prototypes of asymmetric HNCs have been based on metal chalcogenide nanostructures, for which a high level of size and shape control is achievable [90,299—301]. Nanorods or tetrapods of these materials commonly comprise one-dimensional sections made of *c*-axis elongated hexagonal wurtzite (*wz*) lattice, whose apex facets exhibit atomic arrangement (hence, surface energy) distinct from those of their longitudinal sidewalls, which is consistent with the mechanism of their anisotropic growth [277,292,301—303]. An additional peculiarity of the *wz* structure is that its C_{3v} symmetry does not allow a plane of symmetry perpendicular to the *c*-axis, which renders the two basal sides of a *wz* nanorod chemically nonequivalent [304,305]. One can therefore expect the longitudinal sidewalls as well as two apexes of rod-shaped NCs to exhibit significantly different propensity to accommodate deposition of secondary material portions (Scheme 4a, path 1). Furthermore, depending on the specific material (ZnO, MgS, CdSe) there may be crystallographic deviations from the ideal structure, which can result in a permanent intrinsic dipole moment [306] that may further influence their behaviour in heterogeneous deposition synthesis [307,308]. Demonstrations are given in Fig. 12. An interesting proof-of-concept was provided by the fabrication of matchstick-like or dumbbell-like architectures made of spherical PbSe or CdTe sections grown on either one or both tips of CdS or CdSe nanorod seeds [292,301,302]. The possibility of switching the heterostructure topology from a PbSe—CdS—PbSe dumbbell-like to a PbSe—CdS matchstick-like profile was an indirect striking evidence for the non-equivalence of two basal planes of the wurtzite CdS nanorods that were exploited as seeds for PbSe (Fig. 12a). Access to either growth modes was facilitated

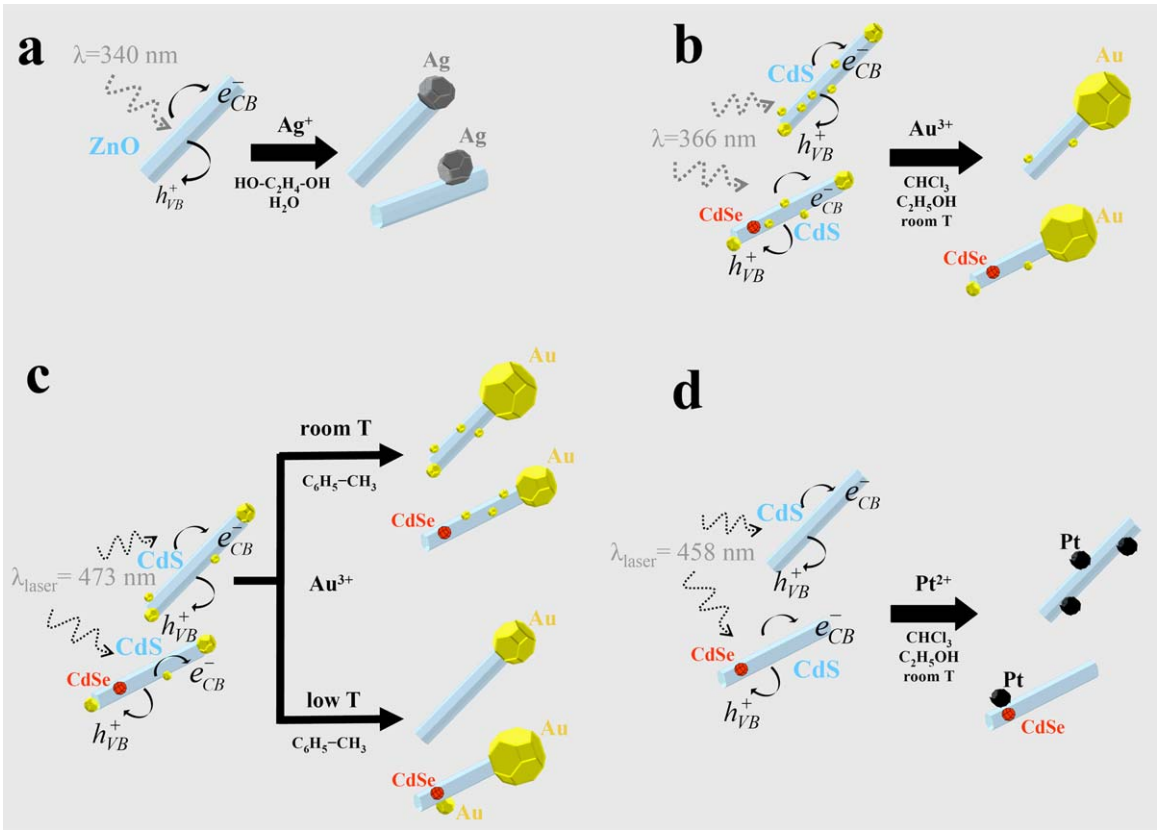

Scheme 5 Sketch of light-assisted pathways leading to semiconductor—metal HNCs with varying topologies: (a) site-preferential photocatalytic deposition of Ag onto ZnO nanorods; (b and c) transition of multiple Au-decorated CdS and eccentric CdSe@CdS nanorod heterostructures to corresponding quasi matchstick-like HNCs that carry one larger Au head and residual Au patches along the longitudinal sidewalls, triggered by different irradiation conditions; (d) photocatalytic reduction of Pt on CdS and eccentric CdSe@CdS nanorods.

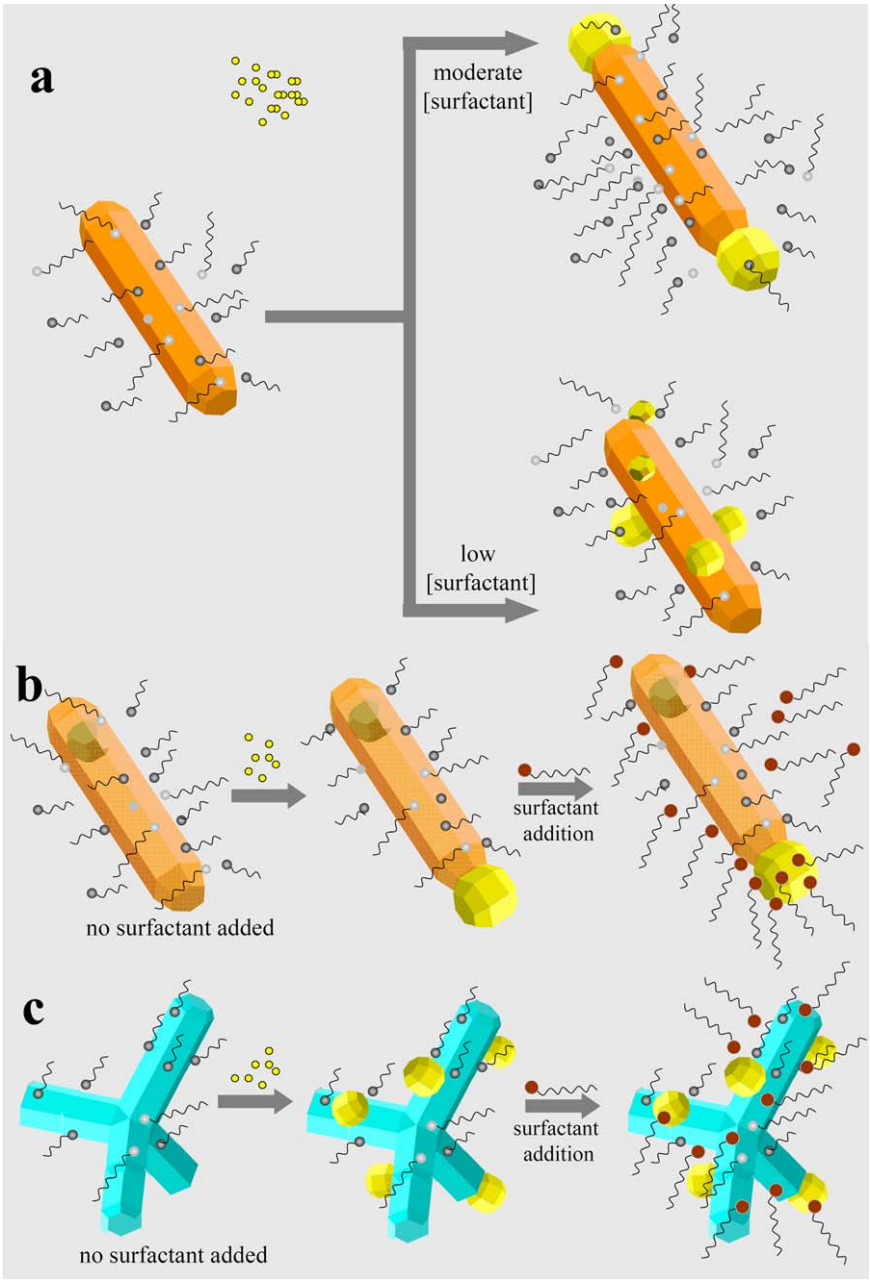

Scheme 6 Sketch of surfactant-controlled pathways leading to site-preferential heterogeneous nucleation of secondary material domains onto anisotropically shaped seeds: (a) nanorod seeds in the presence of varying surfactant concentration prior to heterogeneous nucleation reaction; (b and c) nanorod and tetrapod seeds to which extra surfactants are added after the heterogeneous nucleation and growth processes have almost reached completion.

by careful adjustment of the seed to Pb/Se precursor ratio and their absolute concentration [292], as done for other systems [293–297].

As done for their core@shell counterparts, in anisotropic hetero-oligomer associations of dissimilar crystalline semiconductors the energy level structure across the interface can be engineered so as to realize either a type-I [19,20,44,45] or a type-II band configuration [19,20,46,309], whereby confinement or spatial separation of the photogenerated charge carriers can be achieved, respectively. Such hybrid nanoarchitectures have attracted appreciable interest for the realization of photoemitting [29,310,311] and photovoltaic/photoconductive devices [24,311,312]. At the relevant bonding heterointerfaces the mismatched lattice arrangement can break the crystal periodicity to a varying extent, giving rise to noticleable interfacial strain, which may, in turn, affect the band-gap alignment [40,313]. Misfit strain may be alleviated: (i) through induced interfacial defects, such as dislocations, stacking faults or interfacial lattice adaptation (coherency strain) [40] that may be easily activated under the typical high-temperature conditions in which synthesis is performed; and/or (ii) through gradual change of the chemical composition of the heterojunction regions, across which constituent atoms can inter-diffuse

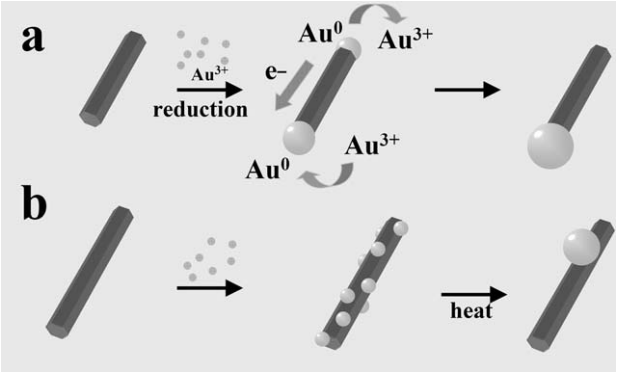

Scheme 7 Sketch of pathways leading to topology evolution in HNCs based on decorated nanorods: (a) conversion of dumbbells to matchsticks by intra-particle metal ripening; (b) conversion of multiple- to single-domain functionalized nanorods by thermal coalescence.

[314,315]. In this regard, recent experimental results [314] and thermodynamic modeling [316,317] indicated that in the case of one-dimensional segmented CdTe—CdSe—CdTe HNCs the temperature was decisive in determining the attainment of either alloyed or abrupt interfaces.

An exceptionally high versatility was achieved in the manipulation of the formation kinetics of HNCs based on metal chalcogenides. By exploiting well-established organometallic chemistry principles known for the individual semiconductors and adjusting the reaction conditions, it was possible to decide on which locations as well as in which manner the growth of an additional material should occur. The synthesis of complex HNCs based on mixtures of spherical (*s*), linear (*l*) and branched (*b*) portions was reported [298]. For various binary and ternary combinations of semiconductors, such as *s*PbSe—*l*CdSe—*s*PbSe, *s*PbSe—*l*CdS [292], *l*CdS—*l*CdSe, *l*CdSe—*b*CdTe, *b*CdSe—*l*CdTe, *b*CdSe—*b*CdTe [298], *l*CdSe—*l*CdTe [31], *l*CdTe—*l*CdSe—*l*CdTe [300,301], binary *l*CdSe—*b*CdTe, *s*CdSe—*l*CdS, *s*ZnSe—*l*CdS—*s*ZnSe [318,319], *l*CdS—*l*CdTe—*l*CdS [299,314,320], *s*Cu_2S—*l*In_2S_3 [321] and multiblock *l*CdTe—*l*CdSe—*l*CdTe-*l*CdSe—*l*CdTe [303], it was demonstrated that by means of sequential reactant injections the tips of nanorod (or tetrapod) seeds could be epitaxially continued by the introduction of either a linear (Scheme 4b, paths 1—2; Scheme 4c, paths 1—2) or a branched sections (Scheme 4b, path 3; Scheme 4c, path 3), respectively. Barbell-shaped multisegmented *s*CdTe—*l*CdSe—*s*CdTe heterostructures were found to convert to lower aspect-ratio CdSeTe alloyed nanostructures upon aging their growth solution at 300 °C, during which the *s*CdTe apexes thermally coalesced and reshaped along with interdiffusion of Te and Se species [314].

One attractive aspect that discloses the technological potential of semiconductor heterostructures organized in a collinear type-II geometry is represented by their capability of enhancing charge carrier delocalization [19,300,322,323], the exploitation of which can be envisaged in the field of solar energy conversion [76]. Upon visible light absorption, photogenerated electrons and holes can spatially separate over distances as large as ~30 nm [298] with electron transfer occurring on the time scale of several hundreds of femtoseconds [324]. For example, in the case of *l*CdSe—*l*CdTe HNCs the timescale of intra-particle carrier transfer competed with that of ultrafast relaxation dynamics [19,325,324]. These values could eventually be tuned by either changing the geometric parameters

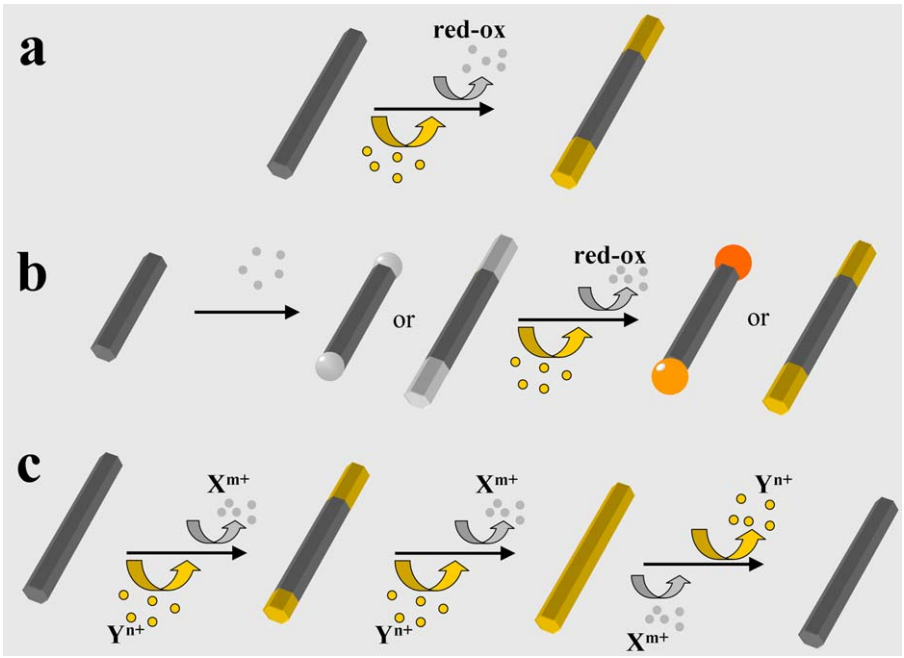

Scheme 8 Sketch of mechanisms of HNC formation via selective red-ox replacement and cation exchange reactions: (a) sacrificial red-ox conversion of the apexes of single-material nanorod seeds; (b) sacrificial red-ox conversion of the foreign apexes of dumbbell-shaped nanorod heterostructures; (c) forward and backward facet-selective $Y^{n+} \rightarrow X^{n+}$ and $X^{n+} \rightarrow Y^{n+}$ cation exchange reactions leading to interconversion of metal sulfide nanorods.

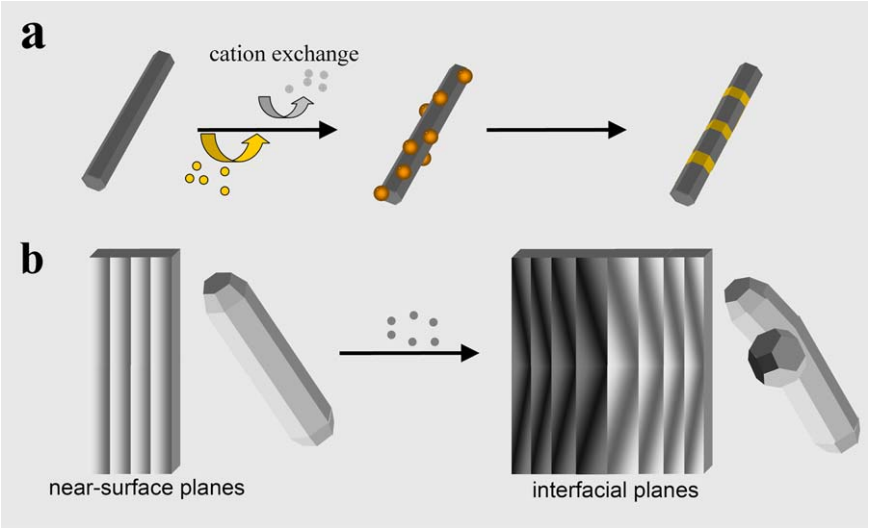

Scheme 9 Sketch of pathways leading to HNC via involvement of lattice strain fields: (a) intra-particle ripening assisted by solid-state cation diffusion; (b) bending of near-surface planes at the interface (adapted from Ref. [12] with permission, copyright Wiley-VCH Verlag GmbH & Co. KGaA).

of the heteroarchitectures or manipulating the surrounding medium (temperature and solvent) [309]. Further evidence for ultrafast photoinduced charge separation was provided in type-II barbell-shaped *s*ZnSe—*l*CdS—*s*ZnSe [319], *s*ZnSe-*l*CdS-*s*ZnSe [318], *s*CdTe—*l*CdSe—*s*CdTe [300,301], and *s*PbSe—*l*CdSe—*s*PbSe HNCs [292].

Transition-metal oxides

Various example of semiconductor HNCs incorporating metal oxides have been reported.

Tip-preferential deposition of TiO_2 was observed onto acetate-coated ZnO nanorods [305]. In this case, a hydrothermal treatment of the ZnO nanorods with amorphous TiO_2 powders was used to synthesize binary oxide heterostructures, in which a single amorphous TiO_2 head cap was ultimately attached to either nanorod apexes and eventually annealed to crystalline anatase. The TiO_2-decorated apex was identified as the Zn-terminated polar basal plane of *c*-axis elongated ZnO wurtzite lattice, which was regarded as more chemically reactive owing to its inherent atomic arrangement [305].

Nonselective heterostructures based on CdS nanowires epitaxially decorated with multiple nanometer-size α-Fe_2O_3 (hematite) or sub-micrometer-size Fe_3O_4 (magnetite) domains were achieved by solvothermal treatment of Fe(III) salts in the presence of polymer stabilizers dissolved in DMF or EG, respectively [325]. The resulting HNCs not only retained fluorescence emission, but also showed enhanced photocatalitic reactivity in organics degradation and weak ferromagnetic-like behavior at room temperature.

Intriguing branched α-Fe_2O_3—SnO_2 HNCs were built from crystallographic-oriented epitaxial SnO_2 growth on shaped α-Fe_2O_3 seeds upon hydrothermal dehydratation of $Sn(OH)_6^{2-}$ species [326,327]. For instance, when 6-fold symmetrical spindle-shaped α-Fe_2O_3 seeds were used, SnO_2 nucleated onto each (1 1 0) template facet, developing into small adjacent rods that progressively merged together laterally to decrease the overall surface energy. When, on the other hand, SnO_2 overgrowth took place on cubic-shaped seeds, the secondary oxide nucleated on the α-Fe_2O_3 facets slantwise at fixed angle of 65°, a geometry that minimized interfacial lattice mismatch down to 1% and reduced the generation of misfit dislocations. A similar tendency toward branching was observed on employing hexahedron-shaped α-Fe_2O_3 seeds [326]. Compared to pure α-Fe_2O_3 particles, branched α-Fe_2O_3—SnO_2 HNCs showed prominent photocatalytic activity towards organic dye degradation under both visible and UV light irradiation [327].

Finally, a nonaqueous approach to magnetic-semiconductor γ-Fe_2O_3—TiO_2 HNCs with switchable hetero-oligomer to heterodimer topologies and tunable geometric parameters was demonstrated (Fig. 12e—h) [297,328]. The key concept relied on exploitation of brookite TiO_2 nanorod seeds with specifically shape-tailored profiles and facet distribution at their apexes [329] as substrate seeds for γ-Fe_2O_3 overgrowth upon decomposition of $Fe(CO)_5$ in OLAM/OLAC/hexadecan-1,2-diol mixtures at 280 °C. The TiO_2 seeds exhibited size- and shape-dependent anisotropic reactivity, which allowed producing HNCs individually made of a single TiO_2 section functionalized with either one or multiple spherical γ-Fe_2O_3 domains at distinctive locations (Scheme 4a). The surface-interface energy balance associated with the formation of the different architectures was discussed on the basis of comparative experimental strain analysis and CSLT interpretation [278]. Topology selection was rationalized on the basis of a diffusion-limited mechanism, according to which γ-Fe_2O_3 deposition on the TiO_2 seeds switched in between a thermodynamically controlled and a kinetically overdriven regime, depending on the modality of precursor delivery and seed structure. The anisotropic reactivity offered by the uniquely structured seeds could be accentuated at high precursor to seed ratios because of spatial inhomogeneity of inward monomer fluxes under diffusion-controlled growth conditions [297]. The as-synthesized γ-Fe_2O_3—TiO_2 offered a rich scenario of photocatalytic properties or modified

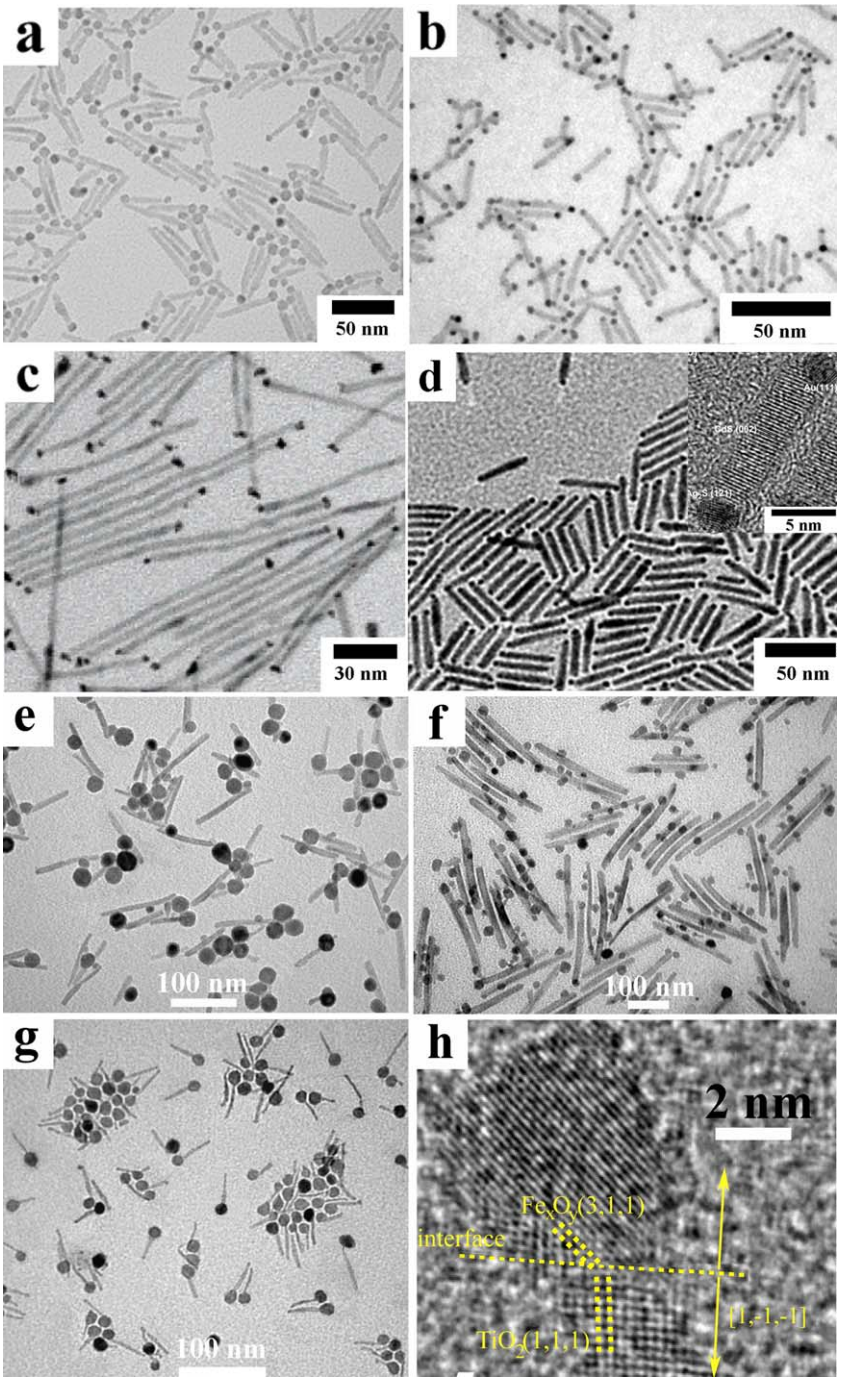

Figure 12 Gallery of TEM and HRTEM images showing examples of anisotropic HNCs synthesized by site-selective heterogeneous deposition on preformed nanorods seeds (cf. Scheme 4a). (a) Nanomatchsticks of single-PbSe-tipped CdS-nanorods (reproduced from Ref. [292] with permission, copyright American Chemical Society). (b) Nanodumbbells of double-Au-tipped CdSe nanorods (reproduced from Ref. [330] with permission, copyright AAAS); (c) Nanodumbbells of double-Pt-tipped CdS nanorods (reproduced from Ref. [339] with permission, copyright American Chemical Society). (d) Asymmetric nanodumbbells of Au- and Ag-tipped CdSe@CdS nanorods (adapted from Ref. [296] with permission, copyright Wiley-VCH Verlag GmbH & Co. KGaA). (e and f) Hetero-oligomers made of multiply γ-Fe_2O_3-decorated brookite TiO_2 nanorods (adapted from Ref. [328] with permission of the PCCP Owner Societies). (g and h) Nanomatchsticks made of sigle-γ-Fe_2O_3-tipped brookite TiO_2 nanorods (reproduced from Ref. [297] with permission, copyright American Chemical Society).

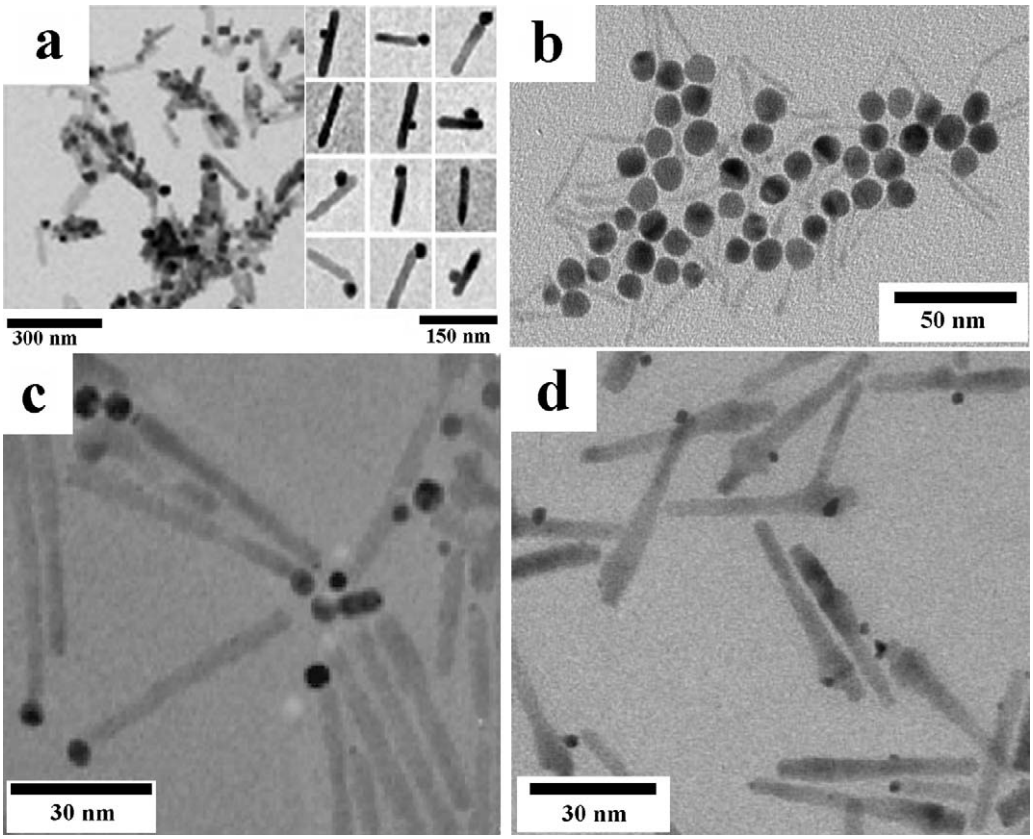

Figure 13 Gallery of TEM images showing examples of anisotropic HNCs synthesized under light assistance (cf. Scheme 5). (a) Heterodimer HNCs made of Ag-decorated ZnO nanorods (reproduced from Ref. [308] copyright Wiley-VCH Verlag GmbH & Co. KGaA). (b) Matchstick-shaped HNCs made of Au-tipped eccentric CdSe@CdS core@shell nanorods synthesized according to Ref. [352] under 366-nm lamp irradiation. (c) Matchstick-shaped HNCs made of Au-tipped eccentric CdSe@CdS core@shell nanorods stimulated under 473-nm laser irradiation (adapted from Ref. [334] with permission, copyright American Chemical Society). (d) Heterodimer HNCs made of Pt-tipped eccentric CdSe@CdS nanorods, whereby the Au domain is located in correspondence of the CdS-buried CdSe core (adapted from Ref. [91] with permission, copyright Wiley-VCH Verlag GmbH & Co. KGaA).

magnetic responses, which clearly diverged from those exhibited by their individual components and physical mixture counterparts [297,328].

Non-oxide semicondutors/transition-metals

Other relevant HNC prototypes obtained by the heterogeneous nucleation/growth mechanism are represented by semiconductor-metal heterostructures, whereby semiconductor NCs have served as templates for the metal growth [330—335]. As an example (Scheme 4a, path 1 and Scheme 4c, path 1), CdX (X = S, Se,Te) nanorods or tetrapods were equipped with small Au domains (<3—4 nm) at selected locations generated by reducing an Au(III)—alkylammonium bromide complex with DDA at room temperature [330—335] (Fig. 12b). When the protocol was applied to CdS nanorod seeds, a remarkably different topological evolution was observed, depending on whether Au formation was accomplished in aerobic or anaerobic growth conditions [331]. In the presence of atmospheric O_2, Au domains nucleated only at one end of the starting seeds, whereas in the absence of O_2 they formed at both tips, followed by deposition of extra metal patches on the longitudinal nanorod sidewalls at defect sites presumably induced by slight DDA etching [331,336,337]. Lowering the temperature (down to 0 °C) played a critical role in deactivating such defect-triggered Au deposition, which was attributed to a progressive transition of the stabilizing alkyl chains of surface-bound DDA to a rigid phase preventing the Au(III)-surfactant complexes from approaching the nanorod seed body [334]. Generally, because of the pencil-shaped profile of the nanorod tips, Au domains predominantly resulted in being off-centred relative to the long rod axis as the metal nucleated on the 45°-oriented (1 0 1)-type terminal facets [335]. On the other hand, starting from nanowire seeds, which likely offered a high surface density of catalytic defects or high-energy edge regions, heterostructures made of evenly Ag-decorated sidewalls according to a *Volmer—Weber* deposition regime were exclusively obtained [87,338].

Moderate to high temperature pyrolysis routes were exploited to access CdX—Me heterostructructures based on CdX (X = Se, S) nanorods functionalized with Me (Me = Pt, PtNi, PtCo, Co, Ni) domains [295,338—340]. For these systems a high degree of selectivity for metal nucleation at both seed apexes could generally be guaranteed (Scheme 4a, path 1), unless nanowires were used as deposition templates instead of nanorods (Scheme 4a, path 3) [338,341]. However, when delicate organometallic chemistry was manipulated, the choice of coordinating ligands and adjustment of their

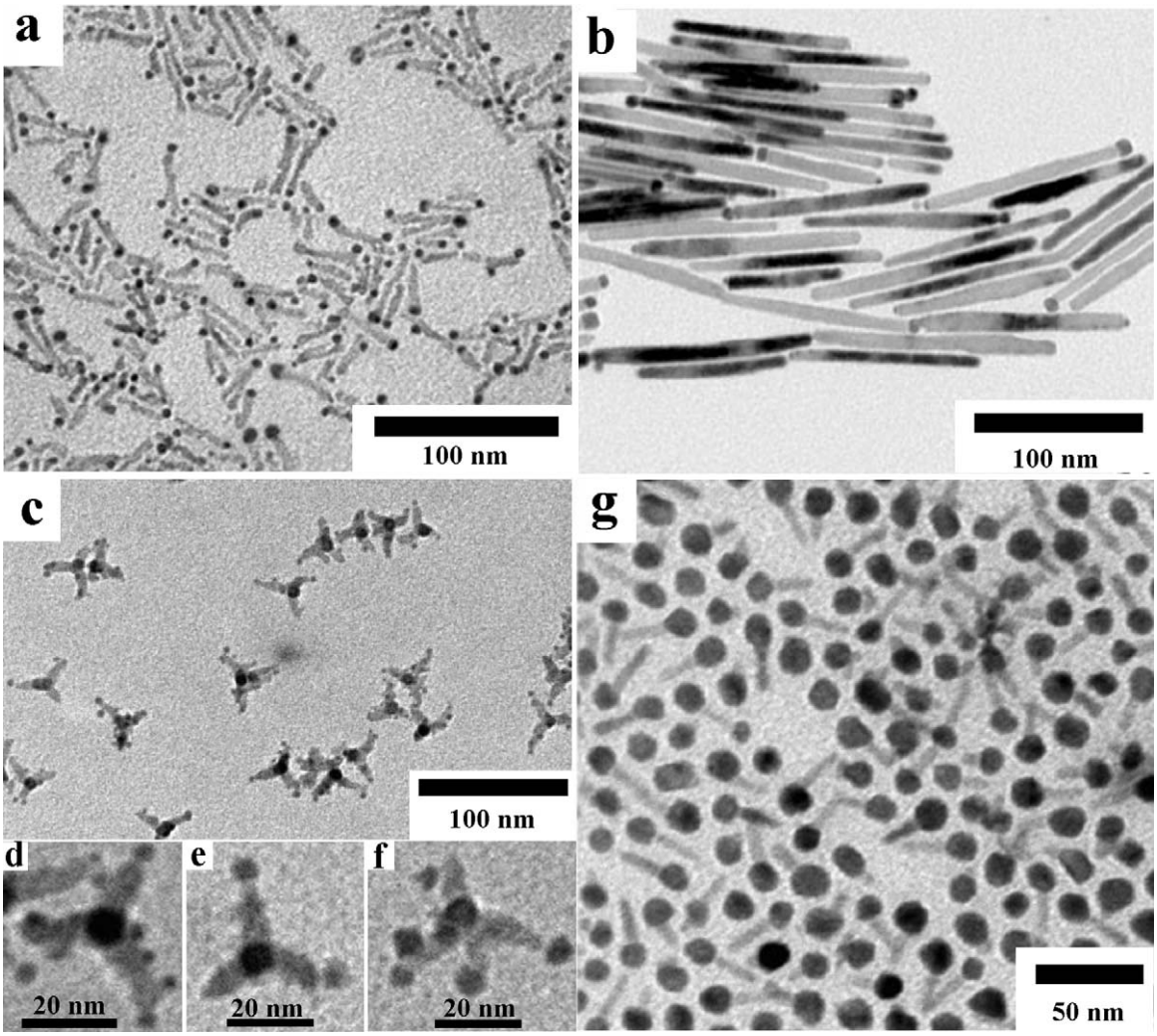

Figure 14 Gallery of TEM images showing examples of anisotropic HNCs synthesized by surfactant-controlled selective heterogeneous nucleation mechanism (cf. Scheme 6). (a) HNCs made of Co-tipped anatase TiO_2 nanorods (reproduced from Ref. [293] with permission, copyright American Chemical Society). (b) Dumbbell-like HNCs made of Au-tipped Co nanorods (reproduced from Ref. [294] with permission, copyright Wiley-VCH Verlag GmbH & Co. KGaA). (c—f) Oligomer-type HNCs made of Co-decorated γ-Fe_2O_3 tetrapods (reproduced with permission from Ref. [356], copyright American Chemical Society). (g) Matchstick-like HNCs made of eccentric CdSe@CdS nanorods tipped with a single Co head (synthesized according to Ref. [307]).

concentration in the synthesis media appeared to be critical in ensuring topological selectivity, which pointed to the interplay of kinetic processes [295]. In all of the aforementioned cases, the strong electronic band coupling between the semiconductor and the metal sections was corroborated by a significant luminescence quenching, reflecting increased charge-carrier separating properties [342]. However, localized surface states at the relevant interfaces were also expected to affect the ultimate optical behavior of such HNCs [338,342,343]. Depending on the reaction medium (e.g., presence of hole scavengers) and the irradiation conditions, the metal section could either act a sink for the electrons photogenerated in the semiconductor or help shuttling them to the solution, which transcribed, for instance, in efficient charge retention [342] or enhanced photocatalytic reduction yield [332,342,344,345]. The magnetic properties were also found to be modified upon heterojunction attainment [295,338].

Recently, access to Janus-type Ag—CdSe@CdS—Au HNCs made of asymmetrically Au- and Ag-tipped CdSe@CdS nanorods has been demonstrated by a smart strategy that relies on delicately accentuating differences in the free energy barrier for heterogeneous nucleation at the two heads of the seeds by judicious regulation of the metal ion supersaturation level [292—297]. Thus, upon consecutive addition of calibrated amounts of Au(III)- and Ag(I)-surfactant complexes to the seed solution, CdSe@CdS—Au matchsticks and asymmetric Ag—CdSe@CdS—Au dumbbells were obtained (Fig. 12d). The technique was extendible to the preparation of single- and double-Ag_2S-tipped CdSe@CdS nanorod HNCs [296].

Transition-metal oxides/transition-metals

The impact of semiconductor/metal interfacing was clearly verified for HNCs based on Ag-decorated ZnO nanorods prepared by a one-pot surfactant-free ethanol-mediated

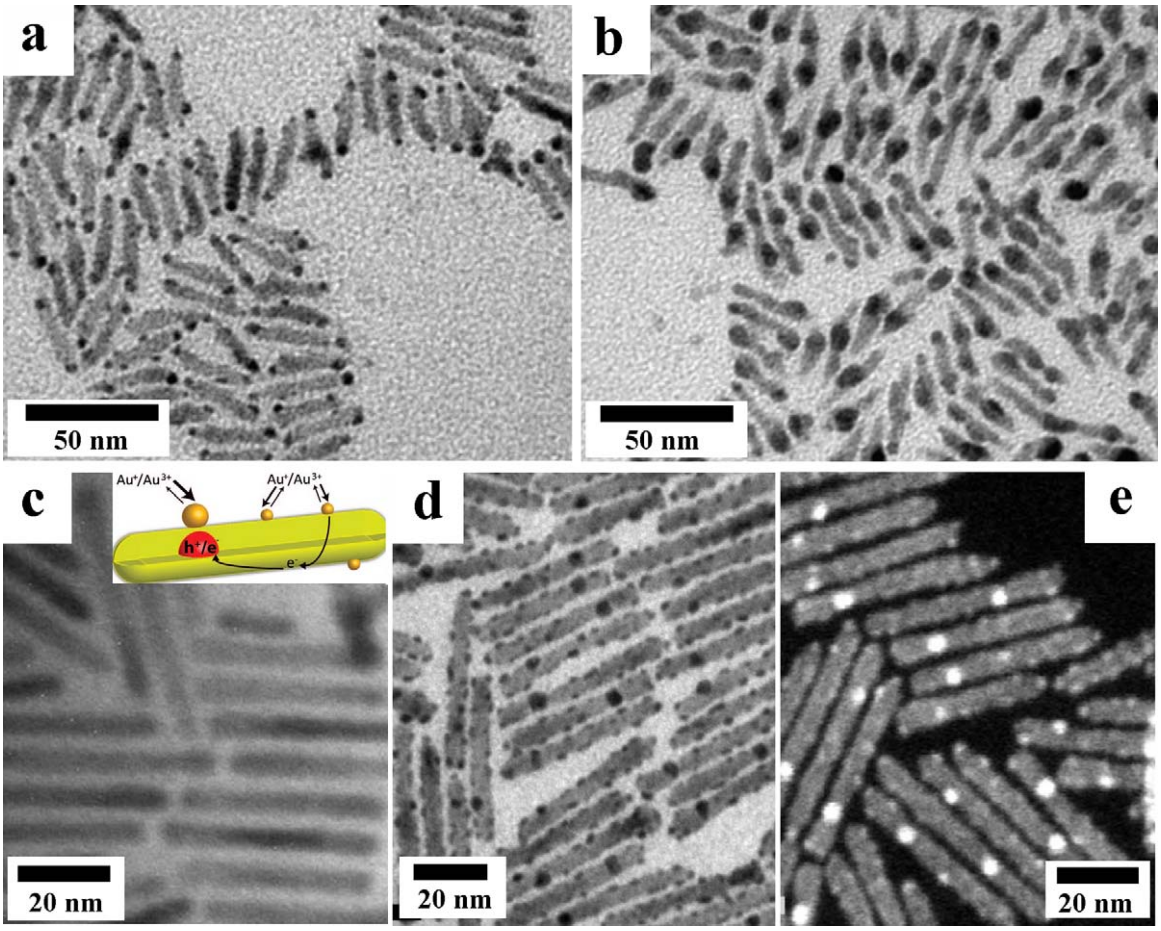

Figure 15 Gallery of TEM images showing examples of HNC topological changes driven by intraparticle electrochemical ripening (cf. Scheme 7). (a and b) Evolution from Au—CdSe—Au nanodumbbells to Au—CdSe nanomatchsticks, respectively (synthesized according to Ref. [265]). (c) CdSe@CdS core@shell nanorod seeds and (d and e) corresponding Au-decorated CdSe@CdS nanorod heterostructures thereof. The HAADF image in panel *e* shows that a larger Au domain is located in correspondence of the CdS-buried CdSe core (adapted from Ref. [357] with permission, copyright American Chemical Society).

solvothermal approach involving alkaline hydrolysis of zinc acetate and reduction of silver acetate at 160 °C [346]. The as-synthesized binary Ag—ZnO HNCs exhibited enhanced photocatalytic performances, compared to pure ZnO, which were ascribable to Ag-promoted interfacial charge carrier separation under UV stimulation. Similar properties were assessed for densely Au-decorated ZnO nanorods prepared by Cu-foil-driven reduction of $HAuCl_4$ in the presence of $CoCl_2$ as homogeneous nucleation inhibitor [347]. In the case of binary Ag-functionalized $Zn_{0.9}Co_{0.1}O$ nanorods prepared by a one-pot solvothermal route magnetization analyses indicated that the synergistic effect of Ag/Co codoping changed their behaviour from paramagnetic to ferromagnetic at room temperature [348,349]. In another interesting report, seed-facet accessibility selectively governed by the poly(vinyl pyrrolidone) (PVP) polymer stabilizer was determined to be the shape-determining driving force for epitaxial overgrowth of ZnO nanorod sections out of the (1 1 1)-type facets of truncated nanocube Ag seeds in alkaline media, leading to multipod heterostructures [350].

Recently, a set of photocatalytically active TiO_2—Me heterostructures (Me = Ag, Pt, Ru, PtRu) nanorods has been synthesized in one-pot protocol involving hydrolysis of $TiCl_3$ and its conversion to intermediate Ti(III)-oxide nanostructures capable to reduce metal salts at their surface [351]. The resulting HNCs consisted of rutile TiO_2 nanorods densely covered with ultrasmall metallic particles, which are in great demand for disparate catalytic applications.

Light-assisted heterogeneous nucleation

A set of binary metal-semiconductor HNCs has been derived upon seeding with semiconductor nanorods under light-irradiation assistance at room temperature (Scheme 5). Examples are shown in Fig. 13. Under photocatalytic activation of metal ion reduction, one single metal domain with upper size larger than that otherwise achievable by other routes can be nucleated in proximity of either nanorod terminations [308,331,334,352,353]. This tendency may tentatively be considered as arising from internal-dipole-driven redistribution of photogenerated conduction electrons, although some favourable lattice-matching conditions at those regions may be a prerequisite to realizing such growth regime. For example, a UV-driven photocat-

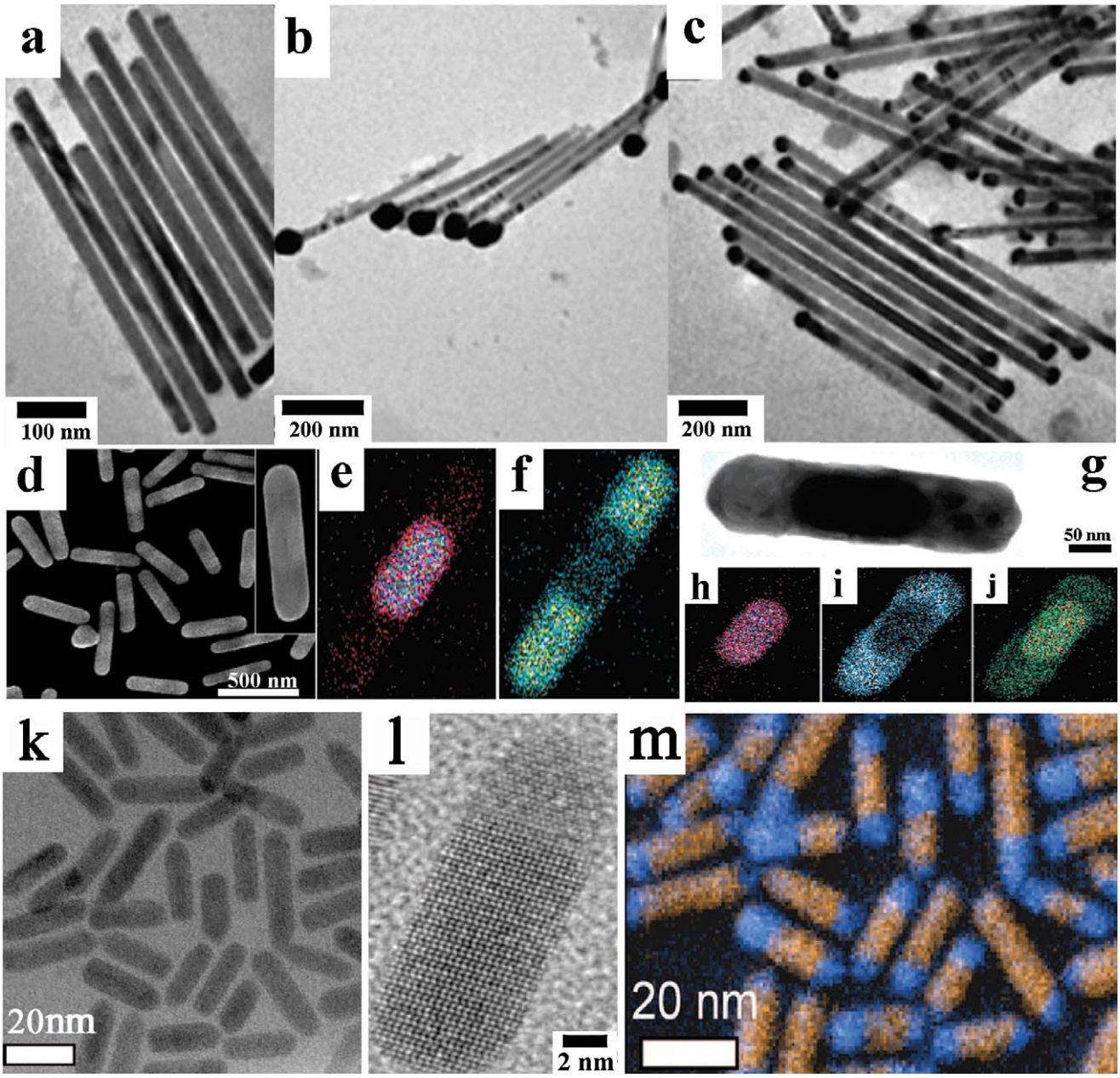

Figure 16 Gallery of TEM, HRTEM and SEM images showing examples of HNCs synthesized by galvanic replacement and cation exchange reactions (cf. Scheme 8). (a) Te nanorod seeds and (b—c) single- and double-Au-tipped Te nanorods thereof obtained by selective tip oxidation (reproduced from Ref. [354] with permission of the Royal Society of Chemistry). (d) Segmented Ag—Au—Ag nanorods along with (e and f) corresponding EDS elemental maps of Au and Ag, respectively. (g) Segmented Ag_2S—Au—Ag_2S nanorods derived from the heterostructures in panel (d) upon a red-ox reaction, along with (h—j) corresponding EDS elemental maps of Au, Ag and Au + S, respectively (adapted from Ref. [361] with permission, copyright American Chemical Society). (k and l) Binary heterostructures made of Cu_2S-tipped CdS nanorods, synthesized by partial Cu^+ for Cd^{2+} cation exchange, along with (m) corresponding color-composite Cd (orange) and Cu (blue) energy-filtered TEM map (adapted from Ref. [363] with permission, copyright American Chemical Society).

alytic $AgNO_3$ reduction approach was exploited for preparing Ag-functionalized ZnO nanorods (Fig. 13a) [308]. Due to the labile acetate capping on ZnO seeds employed, metallic Ag embryos are allowed to deposit on the rods and then catalyze further Ag^+ ion reduction at their surface, thus circumventing undesired homogenous nucleation in the bulk solution (Scheme 5a).

Similarly, recent reports showed the formation of matchstick-like HNCs, individually composed of a single large Au domain attached to one side of CdS and eccentric CdSe@CdS nanorod seeds, by assisting the known Au(III)/alkylammonium/DDA reduction route with UV light [334,352]. Plausibly, upon addition of the Au(III)-surfactant complex precursor to the seed solution, DDA-driven nucle-

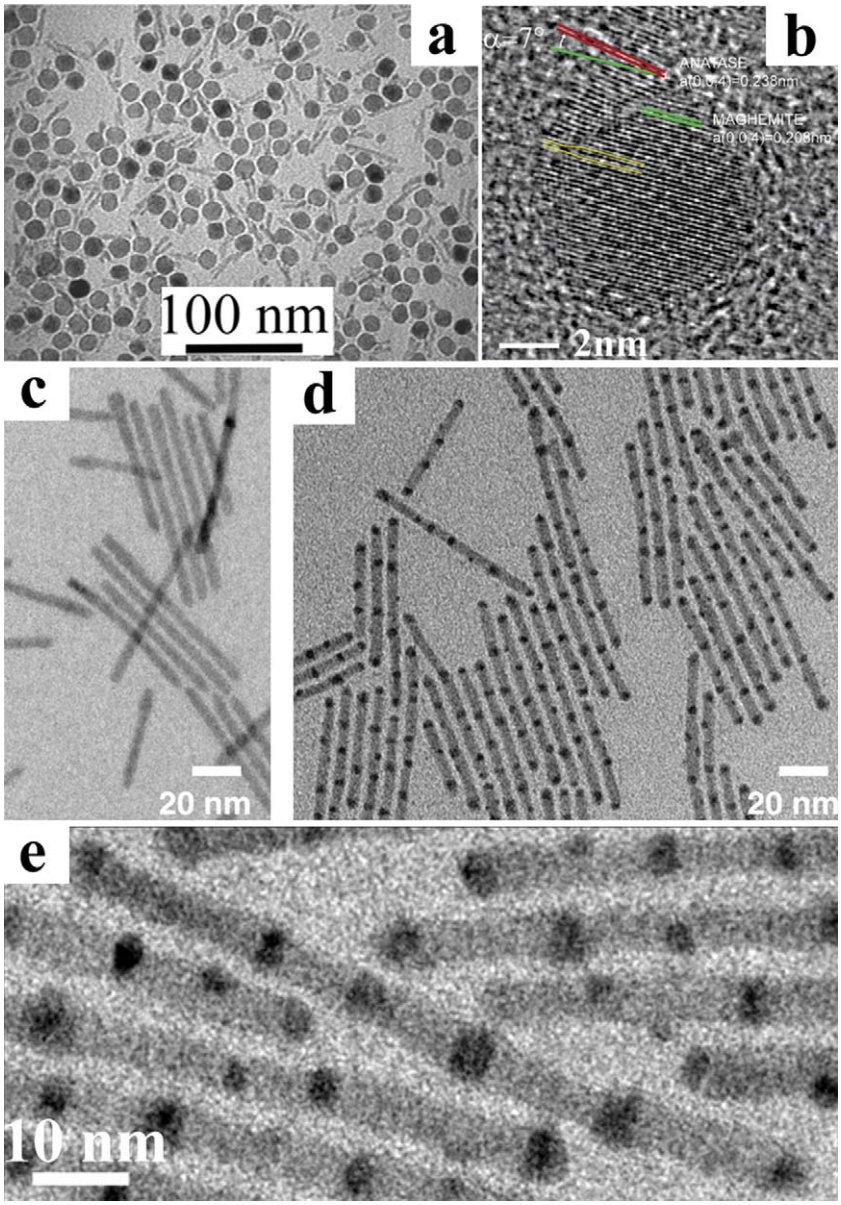

Figure 17 TEM and HRTEM examples of HNCs achieved by strain-driven heteroepitaxial growth (cf. Scheme 9). (a and b) Heterodimers made of single-γ-Fe_2O_3-functionalized anatase TiO_2 nanorods (reproduced with permission from Ref. [368], copyright American Chemical Society). (c) CdS nanorods before and (d and e) after development of a periodic array of Ag_2S domains within their body (reproduced from Ref. [365] with permission, copyright AAAS).

ation of tiny Au clusters instantaneously took place on the sulphur-rich facets of CdS [331,353], after which under weak lamp photoexcitation (λ = 366 nm) electrons generated in the semiconductor section were readily transferred to metal clusters where they could propel further metal reduction (Scheme 5b), leading to extra-large Au heads (Fig. 13b). Although concomitant thermally activated nucleation of small Au patches along the nanorod body could occasionally accompany such selective one-tipped Au growth regime, such drawback was suppressed on decreasing the temperature or increasing the CdS shell thickness [334]. On the other hand, laser irradiation (λ = 473 nm) at low temperature (Scheme 5c) promoted formation of a second Au domain at the buried CdSe core location (Fig. 13c) [334]. In the case of Pt photodeposition on either on CdSe, CdS or CdSe@CdS seeds, the steric hindrance of the alkylamine coating on the seeds was critical in governing their accessibility to the metal species (Fig. 13d) [91]. Interestingly, while Pt nucleation occurred nonselectively on CdSe- and CdS-only nanorod seeds, their CdSe@CdS core@shell counterparts preferentially accommodated a single Pt domain along the longitudinal sidewall in correspondence of the inner CdSe core [91,345] (Scheme 5d). While deeper a mechanistic insight into the formation of these heterostructures has yet to be gained, these results highlight that both seed structure and irradiation conditions are delicate factors on which the topology of such metal-semiconductor HNCs critically depend.

Surfactant-controlled selective heterogeneous nucleation

For several material associations investigation of the conditions underlying heterostructure formation has allowed inferring facet-preferential adhesion of surfactants or ligands as the main mechanism responsible for regulating both accessibility and site-dependent reactivity of selected shaped seeds (Scheme 6). Examples are reported in Fig. 14.

Among the available prototypes, appealing sets of heterometallic HNCs have been reported. A clear influence of the growing environment on the ultimate location of secondary material domains was found in the synthesis of Au-decorated Co nanorods from AuCl(tht) (tht = tetrahydrothiophene) precursors in the presence of lauric acid (LA) and HDA (Fig. 14b). In this system, the Co seeds triggered the otherwise kinetically prohibited Au(I) reduction to Au(0), while surface-adsorbed LA and HDA conferred a robust protective coating to the longitudinal sidewalls of the nanorods, which explained why the deposition of Au remained mainly confined to their tips instead [294]. A similar role was assigned to CTAB during the formation of Au—Te matchstick-shaped heterostructures [354,355].

In yet another case, Pt-tipped Au nanorods were prepared by careful manipulation of $PtCl_4^{2-}$ reduction with ascorbic acid in the presence of CTAB surfactant and of Ag^+ ions [104]. Concomitant underpotential deposition of an Ag wetting layer and CTAB adhesion along the longitudinal facets of Au nanorod seeds dictated the Pt deposition mode thereon. Overall, depending on the detailed Au seed morphology and/or Pt/Au molar ratio, a topological evolution from dumbbell-shaped Pt—Au—Pt heterostructures with Pt entirely deposited on the apex regions [108] to finely Pt-decorated Au nanorods with varying degree of Pt coverage [111,112] could be driven. These bimetallic hybrid systems showed red-shifted longitudinal plasmon resonance [104,108,111,112] and electrocatalytic activity for O_2 reduction [111].

Magnetic/semiconductor Co-decorated TiO_2 nanorods were synthesized by thermal decomposition of $Co_2(CO)_8$ under assistance of octanoic acid (OCAC) and OLAM at 250—280 °C (Fig. 14a) [293]. A calibrated temporal variation of the OCAC/OLAM concentration along the synthesis course was conveniently used to switch heterogeneous Co nucleation from a tip-preferential to a nonselective deposition regime, in which the metal grew also onto the longitudinal sidewalls of the NRs (Scheme 6a). Both types of TiO_2/Co heterojunction configurations were favourable in terms of interfacial lattice strain, according to the CSLT arguments [278]. Hence, site-preferential Co overgrowth was rationalized as being a process that compensated for the increase in the overall surface tension caused by progressive weakening of organic passivation on the respective seed facets at controllably low surfactant concentration. As the two materials communicated through rather extended interfaces, proximity effects at the interface unusually influenced the magnetic anisotropy of the Co domains [293]. In a similar way, an OLAC-controlled heterogeneous deposition dynamics was involved in the formation of visible-photoresponsive HNCs made of PbS-decorated TiO_2 nanorods in OLAC/OLAM mixtures at 180 °C [291].

To achieve Co deposition on eccentric CdSe@CdS nanorods and γ-Fe_2O_3 tetrapods by $Co_2(CO)_8$ decomposition, noncoordinating ODE was selected as reaction medium [307,356]. The seeds became activated toward heterogeneous nucleation due to partial displacement of their tightly bound capping agents. A technique based on slow $Co_2(CO)_8$ addition and delayed delivery of excess OLAC surfactant to a stage at which Co growth was approaching completion guaranteed heterostructure formation in high yield and colloidal stability (Scheme 6b and c).

In the first case, matchstick-like HNCs made of single-Co-head tipped CdSe@CdS nanorods were obtained, whereby the Co domain was found on the apex that was diametrically opposed to the CdS region embedding the CdSe core (Fig. 14g) [307]. This was consistent with the mechanism of unidirectional CdS shell development (Scheme 6b) [44]. According to control syntheses with CdS-only nanorods, the inner core@shell structure of the seeds appeared to be responsible for the observed anisotropic reactivity, which was tentatively attributed to a modified inner dipole moment. Interestingly, the CdSe@CdS—Co HNCs retained appreciable fluorescent emission in spite of photoexcited charge transfer from the semiconductor to the metal domain and exhibited anomalous ferromagnetic-like behavior at room temperature.

In the second case, HNCs made of a γ-Fe_2O_3 tetrapod skeleton randomly decorated with multiple Co domains (Fig. 14c—f) were generated (Scheme 6c), across which FiM—FM exchange coupling was established, leading to a rich scenario of unique magnetic properties among which exchange bias fields, higher saturation magnetization, coercitivity, and improved thermal stability of the magnetization [356].

Heterogeneous nucleation followed by ripening or coalescence

It has been verified that certain heterostructures may be unstable under selected conditions, evolving to a different (i.e., nonequivalent) topological configuration presumably characterized by higher thermodynamic stability [330,331,265,357,358]. The most remarkable case concerned the transformation of Au—CdX—Au (X = Se, S) nanodumbbells into matchstick-like architectures with a single Au tip via an intraparticle Ostwald-ripening promoted by high Au(III) precursor concentrations [330,331,265]. Examples are shown in Fig. 15. The driving forces for this evolution arise from the surface energy and the size dependence of the red-ox potential (Scheme 7a). Indeed, Au—CdSe—Au nanodumbbells inevitably possessed Au domains with slightly dissimilar sizes, with the smaller Au tip being less stable due to its higher surface energy and stronger susceptibility to oxidation compared to the larger one [265]. For growth or ripening to occur, the smaller Au tip had to be oxidized to Au^{3+} ions that should consequently be released to the solution. An excess of free ammonium bromide ligands in solution could catalyze Au^{3+} resolubilization and renewed deposition onto the bigger Au head [265]. When this occurred, electrons shuttled all the way across the dumbbell by hopping through surface states and reaching the opposite bigger Au tip, where they were used to reduce gold ions and make that tip grow further. The pro-

cess stopped when the smaller Au gold tip disappeared completely (Fig. 15a and b). Interestingly, this evolution was not observed when electrons could not travel through the CdSe section, as in the case of a nano-tetrapod. The central section of the tetrapods contained several defects that acted as a barrier for the free movement of electrons. Therefore, only simultaneous growth of four gold tips took place in tetrapods without any ripening being induced. This mechanism was also observed in the transformation of multiply-Au-decorated CdS nanorods into Au—CdS matchstick-like structures [331].

More recently, Au deposition by means of the mild Au(III)/alkyl ammonium bromide/DDA route has been attempted on the surface of seeded-grown bicomponent seeds with an inner core@shell geometry, such as asymmetric CdSe@CdS or ZnSe@CdS core@shell nanorods embedding a spherical CdSe or ZnSe core eccentrically located within a rod-shaped CdS shell [357]. In the former cases, multiple Au patches were detected along the nanorod seeds, among which the one that had grown the largest was preferentially located in proximity of the region whether the inner CdSe core was buried (Fig. 15c—e). Such evolution was again considered to occur via an intraparticle ripening process that led to dissolution of the smaller Au patches and preferential reduction of the as-released Au^{3+} species on the domain at which to electrons are more localized because of type-I band alignment. This hypothesis was indirectly supported by the all-unselective Au deposition regime observed when their type-II ZnSe@CdS counterparts were involved as seeds [357].

It is remarkable that metal-tipped semiconductor HNCs can be utilized as a set of functional building blocks. For example, Au terminations were functionalized with molecules capable of bio-recognition, thereby permitting tracing of biologically relevant events [330,359]. In addition, Au tips could be forced to weld together with the aid of suitable additives (e.g., iodine) [287] opening new perspectives in the deliberate assembly of complex chain-like nanostructures to be exploitable (e.g., as electrical contacts) in miniaturized devices.

In another report, a synthesis of PbSe—TiO_2 HNCs in OLAM/OLAC-rich environment was described, where TiO_2 nanorods, initially grown at 300 °C, were subsequently reacted with Pb/Se precursors at 100 °C [358]. The heterogeneous nucleation of multiple small (~2 nm) PbSe islands took place, whose size and density per seed kept on increasing proportionally to the precursor concentration. Prolonged thermal annealing of the heterostructures drove coalescence of the tiny PbSe patches into one single domain attached at one side of the TiO_2 nanorod seed (Scheme 7b). Compared to molecularly bridged donor—acceptor counterparts, in this case the epitaxial contact and the type-II conduction band offset enabled a quick and efficient electron transfer from photoexcited PbSe into the TiO_2 nanorod, reducing the probability of carrier trapping at the interface [358].

Galvanic replacement reaction

On a few occasions galvanic replacement reactions have purposely been employed to prepare heterostructured HNCs that can hardly be synthesized by other means. Due to the strong size-dependence of red-ox potentials of nanomaterials, these pathways may be suspected to be operative also during application of other protocols based on other heterogeneous nucleation mechanisms. Examples are shown in Fig. 16. In one report (Scheme 8a), matchstick-shaped Au—Te nanowires were obtained by selective oxidation of Te nanowires with aqueous $AuCl_4^-$ at sufficiently high concentration of CTAB preferentially adhering onto the longitudinal sidewalls of the seeds (Fig. 16a—c) [354,355]. By applying a similar strategy localized oxidation of Pd nanorods was accomplished with aqueous $AuCl_4^-$ ions [360], leading to either Au—Pd—Au nanodumbbells or to Pd—Au tadpole-like heterostructures (in which one Au head is attached to a Pd tail) via an Ostwald ripening process similar to that previously reported for the CdSe(S)—Au system [265].

In another study, the growth of Au-tipped semiconductor nanorods was performed through reduction of a Au(III)—alkylammonium bromide complex by the Te^{2-} and Se^{2-} anions of CdTe or PbSe sacrificial domains initially nucleated on the apexes of CdX (X = S, Se) nanorods [303] (Scheme 8b). This resulted in the substitution of the CdTe/PbSe material for Au, thus leading to Au—CdX—Au nanodumbells. The process of Au decoration of hyperbranched CdTe nanostructures involved similar pathways [333].

Another report demonstrated the preparation of segmented Ag_2S—Au—Ag_2S rod-like HNCs via two seeding steps (Fig. 16d—j) [361]. First, segmented Ag—Au—Ag heterostructures were produced by performing $AgNO_3$ reduction in diethylene glycol at 260 °C in the presence of multiply twinned dodecahedral Au seeds and of PVP as shape-directing agent. Under such conditions, Ag selectively nucleated on Au, developing into two rod-shaped sections that departed at opposite directions out of each seed. The outer Ag sections could be stoichiometrically converted to Ag_2S upon reaction with Na_2S, yielding corresponding Ag_2S—Au—Ag_2S HNCs that retained the morphology of their parent Ag—Au—Ag heterostructures (Scheme 8b) [361].

Cation exchange

A flexible route to manipulate both the composition and crystal-phase distribution of inorganic nanostructures is represented by reversible transformation mediated by solid-state cation exchange (Scheme 8c) [362]. Several metal chalcogenides nanocrystals have proven to be interconvertible by such a mechanism ($CdX \rightarrow Me_xE_y$, where E = S, Se, Te; Me = Pd, Pt, Cu, Pb), the driving force of which depends on the solvation energies of the entering and leaving cations as well as on the presence of suitable metal-coordinating species [362—364]. In particular, anisotropically shaped nanostructures offer an interesting set of templates over which spatially selective atomic exchange reactions leading to partial compositional changes can result in the formation of asymmetric heterostructures where two metal cations share a common anion along the same lattice framework. For example, various topologically controlled CdS—Cu_2S heterostructures were derived from preformed CdS nanorods upon reaction with Cu(I)-salt in methanol/toluene solution [363]. Depending on the Cu^+ to Cd^{2+} molar ratio realized in the solution, Cu_2S nucleated on either one or both nanorod terminations and grew with the heterointerface frontline

spanning the seed diameter and moving inwards at different rates along the opposite directions of longitudinal axis. As a result, segmented Ag_2S—CdS—Ag_2S HNCs were obtained, in which the opposite Ag_2S sections possessed dissimilar volumes (Fig. 16k—m). On the basis of theoretical modelling and calculations, it was concluded that the formation energies of epitaxial CdS/Ag_2S heterointerfaces should be determined by a generally positive chemical contribution and by a facet-dependent elastic energy contribution, which ultimately rendered the CdS/Ag_2S interfaces formed at the CdS seed apexes more stable [363]. Further synthetic developments in this direction demonstrated that judicious manipulation of consecutive cation exchange reactions could afford nanostructures with tailored composition, which can hardly be achieved by conventional routes. This was shown, for example, in the case of the interconversion between wurtzite CdS, chalcocite Cu_2S and rock salt (cubic) PbS nanocrystals, which was accomplished along preservation of the original nanostructure shapes [364].

Strain-driven heterostructure formation

Interesting NC heterostructures have been engineered by taking advantage of the generation of strain fields during heteroepitaxial growth (Scheme 9). Examples are reported in Fig. 17. One case that illustrates strain manipulation as a means of engineering complex colloidal heterostructures is represented by the spontaneous creation of linear arrays of quantum-confined domains within a rod-shaped ionic semiconductor section of a different material. The synthetic method relied on the partial Cd^{2+} exchange for Ag^+ ions that took place when a toluene suspension of CdS nanorods was reacted with a methanol solution of $AgNO_3$ at −66 °C under substoichiometric conditions [365]. In the early advancement stages, Ag^+ replacement reaction produced tiny Ag_2S islands randomly distributed on the CdS nanorods, which then evolved into periodically spaced Ag_2S segments (Fig. 17c—e) via an intra-particle Ostwald ripening process sustained by fast diffusion across the CdS (Scheme 9a). Two factors were determined to drive CdS—$(Ag_2S—CdS)_n$—CdS nanorod superlattice formation, unlike found for their CdS—Cu_2S analogue [363]. First, owing to the high energy cost for CdS/Ag_2S interface formation, the coalescence of small Ag_2S patches into larger domains was energetically convenient, and indeed an Ostwald ripening process occurred. Second, because of the hexagonal-CdS/monoclinic-Ag_2S lattice misfit at the epitaxial junctions, adjacent Ag_2S segments experienced elastic repulsions that arose from strain fields in the intervening CdS regions. These forces could prevent further ripening after the Ag_2S domains had reached a size spanning the nanorod diameter [363,365,366]. The obtained CdS—$(Ag_2S—CdS)_n$—CdS striped nanorods displayed characteristic optical properties, such as quenching of visible CdS luminescence and retention of near-infrared Ag_2S fluorescence, which were actually expected for linear arrays of Ag_2S quantum dots electronically coupled to confining regions of CdS in a type-I band arrangement [20]. Transient absorption spectroscopy measurements proved that the Ag_2S domains embedded within CdS introduced relaxation pathways that accelerated the decay dynamics of trapped electrons on the picosecond time scale. This suggested strong electronic coupling held between the two materials [367]. Eventually, striped CdS—$(Ag_2S—CdS)_n$—CdS HNCs could be fully converted to Ag_2S nanorods and back-transformed to CdS—$(Ag_2S—CdS)_n$—CdS HNCs via a reverse Cd^{2+} for Ag^+ exchange reaction, along which the distinctive optical properties of the respective systems could be observed [367].

Another case that illustrates the role of strain is represented by the synthesis of asymmetric binary HNCs, each made of one rod-shaped TiO_2 section and one size-tunable γ-Fe_2O_3 spherical domain attached longitudinally, which were obtained by decomposing $Fe(CO)_5$ in a ternary mixture of OLAC, OLAM and 1,2-hexadecandiol in the presence of anatase TiO_2 nanorods at 240—300 °C [368] (Fig. 17a and b). The γ-Fe_2O_3 deposition proceeded as a means of selectively eliminating high-energy edges on the longitudinal stepped sidewalls of the TiO_2 seeds (Scheme 4a, path 2). However, constraints imposed by the huge interfacial strain (8—11%) limited ''wetting'' of the (0 1 1)/(1 0 1) facets underneath the edges, causing the TiO_2 section to be deformed and bowed toward the γ-Fe_2O_3 sphere. The TiO_2 and γ-Fe_2O_3 lattices were coherently connected via a rather limited junction area at which the near-surface planes of the respective materials were locally curved. This allowed the strain accumulated at the interface to be accommodated to a great extent, paying only a proportionally smaller cost of additional surface energy (Scheme 9b). These factors jointly accounted for the inhibition of reiterated deposition events, on one side, and for the ultimate size (15 nm) to which the γ-Fe_2O_3 domains could be enlarged. Owing to the limited contact area shared with TiO_2, the magnetic properties of the HNCs essentially resembled those of unbound γ-Fe_2O_3 particles [368].

Conclusions

The chemical synthesis of multimaterial nanocrystal heterostructures combining sections of oxide, metal and semiconductor materials in a single multifunctional nanoscale object represents a challenging research direction along which nanochemistry research is investing substantial efforts.

The wet-chemical preparation of HNCs is a rather demanding task, as the ability to tailor specific nanosized materials must be integrated with the understanding of the thermodynamic parameters and kinetic processes which govern heteroepitaxial growth in liquid media. Current synthetic achievements suggest that an increased level of synthetic sophistication and topological selectivity in HNC preparation should ultimately be reachable by means of seeded-growth techniques that exploit seeds with suitably engineered compositional and structural parameters, while profiting from a deeper knowledge of solid-state and liquid-phase mechanisms responsible for compositional, structural, and topological evolution of nanoheterostructures.

Presently, full realization of the technological perspectives of HNCs remains yet hindered by the limited degree of synthetic perfection and property control with which heterostructures can be engineered. These issues are especially significant for associations of nonhomologous and/or

structurally uncorrelated materials, for which the search for multifunctionality may conflict with partial degradation of some native properties of any of the concerned material components due, for example, to unfavourable changes in electronic structure and/or to formation of defective interfaces. In some cases, it yet remains difficult to decouple mere proximity effects from unambiguous emergence of new or abnormal chemical—physical phenomena as a result of heterojunction formation.

On the long term, it can be envisioned that innovative design and improved synthetic capabilities in the development of elaborate HNCs with defined topologies will deliver exciting opportunities in both fundamental understanding and practical exploitation of unconventional properties and functionalities stemming from properly engineered heterostructures with tailored interfaces and structural features. It can be expected that future progress along these directions will disclose fascinating horizons in disparate optoelectronic, magnetic, biomedical, photovoltaic and catalytic applications, boosting each of them to an unprecedented level of performance.

Acknowledgment

The authors acknowlege financial support by the Italian Ministry of Education, University and Research through the project AEROCOMP (contract MIUR no. DM48391).

References

[1] C. Burda, X.B. Chen, R. Narayanan, M.A. El-Sayed, Chem. Rev. 105 (2005) 1025.
[2] P.D. Cozzoli (Ed.), Advanced Wet-Chemical Synthetic Approaches to Inorganic Nanostructures;, Transworld Research Network, Kerala, India, 2008.
[3] M. Niederberger, N. Pinna, Metal Oxide Nanoparticles in Organic Solvents-Synthesis, Formation, Assembly and Application, Springer-Verlag, London, UK, 2009.
[4] D.V. Talapin, J.-S. Lee, M.V. Kovalenko, E.V. Shevchenko, Chem. Rev. 110 (2010) 389.
[5] P.D. Cozzoli, T. Pellegrino, L. Manna, Chem. Soc. Rev. 35 (2006) 1195.
[6] A.L. Rogach (Ed.), Semiconductor Nanocrystal Quantum Dots: Synthesis, Assembly, Spectroscopy and Applications, Springer-Verlag, Wien, Austria, 2008.
[7] W.C.W. Chan (Ed.), Bio-Applications of Nanoparticles — Experimental Medicine and Biology, vol. 620, Landes Bioscience and Springer Science + Business Media, New York, USA, 2007.
[8] Y.-W. Jun, J.-S. Choi, J. Cheon, Angew. Chem. Int. Ed. 45 (2006) 3414.
[9] J. Park, E. Lee, N.-M. Hwang, M. Kang, S.C. Kim, Y. Hwang, et al., Angew. Chem. Int. Ed. 44 (2005) 2872.
[10] S.G. Kwon, T. Hyeon, Acc. Chem. Res. 41 (2008) 1696.
[11] R. Buonsanti, M. Casavola, G. Caputo, P.D. Cozzoli, Recent Pat. Nanotechnol. 1 (2007) 224.
[12] M. Casavola, R. Buonsanti, G. Caputo, P.D. Cozzoli, Eur. J. Inorg. Chem. (6) (2008) 837.
[13] R. Costi, A.E. Saunders, U. Banin, Angew. Chem. Int. Ed. 49 (2010) 4878.
[14] Y.-W. Jun, J.-S. Choi, J. Cheon, Chem. Commun. (12) (2007) 1203.
[15] J. Gao, H. Gu, B. Xu, Acc. Chem. Res. 42 (2009) 1097.
[16] P. Reiss, M. Protière, L. Li, Small 5 (2009) 154.
[17] J. Park, J. Joo, S.G. Kwon, Y. Jang, T. Hyeon, Angew. Chem. Int. Ed. 46 (2007) 4630.
[18] C. de Mello-Donegà, P. Liljeroth, D. Vanmaekelbergh, Small 1 (2005) 1152.
[19] I.V. Markov, Crystal Growth for Beginners: Fundamentals of Nucleation, Crystal Growth, and Epitaxy, World Scientific, Singapore, 2003.
[20] G.D. Scholes, Adv. Funct. Mater. 18 (2008) 1157.
[21] J.T. Hu, L.S. Li, W.D. Yang, L. Manna, L.-W. Wang, A.P. Alivisatos, Science 292 (2001) 2060.
[22] M. Bruchez, M. Moronne, P. Gin, S. Weiss, A.P. Alivisatos, Science 281 (1998) 2013.
[23] W.U. Huynh, J.J. Dittmer, A.P. Alivisatos, Science 295 (2002) 2425.
[24] I. Gur, N.A. Fromer, M.L. Geier, A.P. Alivisatos, Science 310 (2005) 462.
[25] J. Müller, J.M. Lupton, A.L. Rogach, J. Feldmann, D.V. Talapin, H. Weller, Phys. Rev. Lett. 93 (2004) 167402.
[26] J. Müller, J.M. Lupton, A.L. Rogach, J. Feldmann, D.V. Talapin, H. Weller, Phys. Rev. B 72 (2005) 205339.
[27] K. Becker, J.M. Lupton, J. Müller, A.L. Rogach, D.V. Talapin, H. Weller, J. Feldmann, Nat. Mater. 5 (2006) 777.
[28] R.A.M. Hikmet, P.T.K. Chin, D.V. Talapin, H. Weller, Adv. Mater. 17 (2005) 1436.
[29] A. Rizzo, C. Nobile, M. Mazzeo, M. De Giorgi, A. Fiore, L. Carbone, et al., ACS Nano 3 (2009) 1506.
[30] S. Deka, A. Quarta, M.G. Lupo, A. Falqui, S. Boninelli, C. Giannini, et al., J. Am. Chem. Soc. 131 (2009) 2948.
[31] A. Persano, M. De Giorgi, A. Fiore, R. Cingolani, L. Manna, A. Cola, et al., ACS Nano 4 (2010) 1646.
[32] M. Zavelani-Rossi, M.G. Lupo, R. Krahne, L. Manna, G. Lanzani, Nanoscale 2 (2010) 931.
[33] A. Quarta, A. Ragusa, S. Deka, C. Tortiglione, A. Tino, R. Cingolani, et al., Langmuir 25 (2009) 12614.
[34] C. Tortiglione, A. Quarta, M.A. Malvindi, A. Tino, T. Pellegrino, PLOS One 4 (2009) e7698.
[35] M.A. Malvindi, L. Carbone, A. Quarta, A. Tino, L. Manna, T. Pellegrino, et al., Small 4 (2008) 1747.
[36] P. Reiss, J. Bleuse, A. Pron, Nano Lett. 2 (2002) 781.
[37] B.O. Dabbousi, J. Rodriguez-Viejo, F.V. Mikulec, J.R. Heine, H. Mattoussi, R. Ober, et al., J. Phys. Chem. B 101 (1997) 9463.
[38] X.G. Peng, M.C. Schlamp, A.V. Kadavanich, A.P. Alivisatos, J. Am. Chem. Soc. 119 (1997) 7019.
[39] J.J. Li, Y.A. Wang, W.Z. Guo, J.C. Keay, T.D. Mishima, M.B. Johnson, et al., J. Am. Chem. Soc. 125 (2003) 12567.
[40] X.B. Chen, Y.B. Lou, A.C. Samia, C. Burda, Nano Lett. 3 (2003) 799.
[41] J.S. Steckel, J.P. Zimmer, S. Coe-Sullivan, N.E. Stott, V. Bulovic, M.G. Bawendi, Angew. Chem. Int. Ed. 43 (2004) 2154.
[42] D.C. Pan, Q. Wang, S.C. Jiang, X.L. Ji, L.J. An, Adv. Mater. 17 (2005) 176.
[43] T. Mokari, U. Banin, Chem. Mater. 15 (2003) 3955.
[44] L. Carbone, C. Nobile, M. De Giorgi, F. Della Sala, G. Morello, P. Pompa, et al., Nano Lett. 7 (2007) 2942.
[45] D.V. Talapin, J.H. Nelson, E.V. Shevchenko, S. Aloni, B. Sadtler, A.P. Alivisatos, Nano Lett. 7 (2007) 2951.
[46] A. Fiore, R. Mastria, M.G. Lupo, G. Lanzani, C. Giannini, E. Carlino, et al., J. Am. Chem. Soc. 131 (2009) 2274.
[47] J.A. Goebl, R.W. Black, J. Puthussery, J. Giblin, T.H. Kosel, M. Kuno, J. Am. Chem. Soc. 130 (2008) 14822.
[48] L. Wang, H.W. Wei, Y.J. Fan, X.Z. Liu, J.H. Zhan, Nanoscale Res. Lett. 4 (2009) 558.
[49] M.R. Kim, Y.M. Kang, D.J. Jang, J. Phys. Chem. C 111 (2007) 18507.
[50] M. Protière, P. Reiss, Small 3 (2007) 399.
[51] R. Xie, X. Peng, Angew. Chem. Int. Ed. 47 (2008) 7677.

[52] Y. Chen, J. Vela, H. Htoon, J.L. Casson, D.J. Werder, D.A. Bussian, et al., J. Am. Chem. Soc. 130 (2008) 5026.
[53] B. Mahler, P. Spinicelli, S. Buil, X. Quelin, J.-P. Hermier, B. Dubertret, Nat. Mater. 7 (2008) 659.
[54] A.M. Smith, A.M. Mohs, S. Nie, Nat. Nanotechnol. 4 (2009) 56.
[55] B. Mahler, N. Lequeux, B. Dubertret, J. Am. Chem. Soc. 132 (2010) 953.
[56] E. Lifshitz, M. Brumer, A. Kigel, A. Sashchiuk, M. Bashouti, M. Sirota, et al., J. Phys. Chem. B 110 (2006) 25356.
[57] W. Shi, H. Zeng, Y. Sahoo, T.Y. Ohulchanskyy, Y. Ding, Z.L. Wang, et al., Nano Lett. 6 (2006) 875.
[58] D.V. Talapin, R. Koeppe, S. Gotzinger, A. Kornowski, J.M. Lupton, A.L. Rogach, et al., Nano Lett. 3 (2003) 1677.
[59] D. Steiner, D. Dorfs, U. Banin, F. Della Sala, L. Manna, O. Millo, Nano Lett. 8 (2008) 2954.
[60] A. Sitt, F. Della Sala, G. Menagen, U. Banin, Nano Lett. 9 (2009) 3470.
[61] R.M. Kraus, P.G. Lagoudakis, A.L. Rogach, D.V. Talapin, H. Weller, J.M. Lupton, J. Feldmann, Phys. Rev. Lett. 98 (2007) 017401.
[62] G. Morello, F. Della Sala, L. Carbone, L. Manna, G. Maruccio, R. Cingolani, et al., Phys. Rev. B 78 (2008) 195313.
[63] G. Morello, F. Della Sala, L. Carbone, L. Manna, R. Cingolani, M. De Giorgi, Superlattice Microst. 47 (2010) 174.
[64] C.L. Choi, K.J. Koski, S. Sivasankar, A.P. Alivisatos, Nano Lett. 9 (2009) 3544.
[65] V.I. Klimov, S.A. Ivanov, J. Nanda, M. Achermann, I. Bezel, J.A. McGuire, et al., Nature 447 (2007) 441.
[66] S.A. Ivanov, A. Piryatinski, J. Nanda, S. Tretiak, K.R. Zavadil, W.O. Wallace, et al., J. Am. Chem. Soc. 129 (2007) 11708.
[67] K. Yu, B. Zaman, S. Romanova, D.S. Wang, J.A. Ripmeester, Small 1 (2005) 332.
[68] R. Xie, X. Zhong, T. Basché, Adv. Mater. 17 (2005) 2741.
[69] S. Kim, B. Fisher, H.J. Eisler, M.G. Bawendi, J. Am. Chem. Soc. 125 (2003) 11466.
[70] B. Blackman, D.M. Battaglia, T.D. Mishima, M.B. Johnson, X. Peng, Chem. Mater. 19 (2007) 3815.
[71] D. Dorfs, A. Salant, I. Popov, U. Banin, Small 4 (2008) 1319.
[72] N.N. Hewa-Kasakarage, M. Kirsanova, A. Nemchinov, N. Schmall, P.Z. El-Khoury, A.N. Tarnovsky, et al., J. Am. Chem. Soc. 131 (2009) 1328.
[73] H. Zhong, G.D. Scholes, J. Am. Chem. Soc. 131 (2009) 9170.
[74] R.B. Vasiliev, D.N. Dirin, M.S. Sokolikova, S.G. Dorofeev, A.G. Vitukhnovsky, A.M. Gaskov, Mendeleev Commun. 19 (2009) 128.
[75] X. Li, H. Shen, S. Li, J.-Z. Niu, H. Wang, L.-S. Li, J. Mater. Chem. 20 (2010) 923.
[76] S. Kumar, G.D. Scholes, Microchim. Acta 160 (2008) 315.
[77] A.L. Rogach, A. Eychmüller, S.G. Hickey, S.V. Kershaw, Small 3 (2007) 536.
[78] A.G. Vitukhnovsky, A.S. Shul'ga, S.A. Ambrozevich, E.M. Khokhlov, R.B. Vasiliev, D.N. Dirin, et al., Phys. Lett. A 373 (2009) 2287.
[79] H. Bao, Y. Gong, Z. Li, M. Gao, Chem. Mater. 16 (2004) 3853.
[80] J.-S. Choi, Y.-W. Jun, S.-I. Yeon, H.C. Kim, J.-S. Shin, J. Cheon, J. Am. Chem. Soc. 128 (2006) 15982.
[81] L. Manna, E.C. Scher, L.S. Li, A.P. Alivisatos, J. Am. Chem. Soc. 124 (2002) 7136.
[82] D.V. Talapin, I. Mekis, S. Gotzinger, A. Kornowski, O. Benson, H. Weller, J. Phys. Chem. B 108 (2004) 18826.
[83] A.M. Aharoni, I. Popov, U. Banin, J. Am. Chem. Soc. 128 (2006) 257.
[84] A. Eychmüller, A. Mews, H. Weller, Chem. Phys. Lett. 208 (1993) 59.
[85] D. Schooss, A. Mews, A. Eychmüller, H. Weller, Phys. Rev. B-Conden. Matter 49 (1994) 17072.
[86] A. Mews, A. Eychmüller, Ber. Bunsen Phys. Chem. 102 (1998) 1343.
[87] D.V. Talapin, H. Yu, E.V. Shevchenko, A. Lobo, C.B. Murray, J. Phys. Chem. C 111 (2007) 14049.
[88] T. Mokari, S.E. Habas, M. Zhang, P. Yang, Angew. Chem. Int. Ed. 47 (2008) 5605.
[89] D. Baranov, A. Fiore, M. van Huis, C. Giannini, A. Falqui, U. Lafont, et al., Nano Lett. 10 (2010) 743.
[90] H. Zhong, Y. Zhou, Y. Yang, C. Yang, Y. Li, J. Phys. Chem. C 111 (2007) 6538.
[91] G. Dukovic, M.G. Merkle, J.H. Nelson, S.M. Hughes, A.P. Alivisatos, Adv. Mater. 20 (2008) 4306.
[92] Y. Li, R. Mastria, A. Fiore, C. Nobile, Y. Lunxiang, M. Biasucci, et al., Adv. Mater. 21 (2009) 4461.
[93] S.E. Habas, H. Lee, V. Radmilovic, G.A. Somorjai, P. Yang, Nat. Mater. 6 (2007) 692.
[94] Z. Peng, H. Yang, J. Am. Chem. Soc. 131 (2009) 7542.
[95] B. Lim, M. Jiang, P.H.C. Camargo, E.C. Cho, J. Tao, X. Lu, et al., Science 324 (2009) 1302.
[96] Y.W. Cao, R. Jin, C.A. Mirkin, J. Am. Chem. Soc. 123 (2001) 7961.
[97] I. Srnova-Sloufova, B. Vlckova, Z. Bastl, T.L. Hasslett, Langmuir 20 (2004) 3407.
[98] M. Liu, P. Guyot-Sionnest, J. Phys. Chem. B 108 (2005) 5882.
[99] B. Rodríguez-González, A. Burrows, M. Watanabe, C.J. Kiely, L.M. Liz-Marzán, J. Mater. Chem. 15 (2005) 1755.
[100] Y. Bao, H. Calderon, K.M. Krishnan, J. Phys. Chem. C 111 (2007) 1941.
[101] F. Bao, J.-F. Li, B. Ren, J.-L. Yao, R.-A. Gu, Z.-Q. Tian, Phys. Chem. C 112 (2008) 345.
[102] D. Ferrer, A. Torres-Castro, X. Gao, S. Sepulveda-Guzman, U. Ortiz-Mendez, M. Jose-Yacaman, Nano Lett. 7 (2007) 1701.
[103] Y. Borodko, S.E. Habas, M. Koebel, P. Yang, H. Frei, G.A. Somorjai, J. Phys. Chem. B 110 (2006) 23052.
[104] M. Grzelczak, J. Pérez-Juste, B. Rodríguez-González, L.M. Liz-Marzán, J. Mater. Chem. 16 (2006) 3946.
[105] Y. Xiang, X. Wu, D. Liu, X. Jiang, W. Chu, Z. Li, et al., Nano Lett. 6 (2006) 2290.
[106] J. Yang, J.Y. Ying, Nat. Mater. 8 (2009) 683.
[107] M. Grzelczak, B. Rodríguez-González, J. Pérez-Juste, L.M. Liz-Marzán, Adv. Mater. 19 (2007) 2262.
[108] B.P. Khanal, E.R. Zubarev, Angew. Chem. Int. Ed. 48 (2009) 6888.
[109] B. Lim, H. Kobayashi, T. Yu, J. Wang, M.J. Kim, Z.-Y. Li, et al., J. Am. Chem. Soc. 132 (2010) 2506.
[110] E.C. Cho, P.H.C. Camargo, Y. Xia, Adv. Mater. 22 (2010) 744.
[111] S.J. Guo, L. Wang, W. Wang, Y.X. Fang, E.K. Wang, J. Colloid Interf. Sci. 315 (2007) 363.
[112] L. Feng, X. Wu, L. Ren, Y. Xiang, W. He, K. Zhang, J. Xie, et al., Chem. Eur. J. 14 (2008) 9764.
[113] J. Zhang, Y. Tang, L. Weng, M. Ouyang, Nano Lett. 9 (2009) 4061.
[114] H. Kim, M. Achermann, L.P. Balet, J.A. Hollingsworth, V.I. Klimov, J. Am. Chem. Soc. 127 (2005) 544.
[115] J. Gao, B. Zhang, Y. Gao, Y. Pan, X. Zhang, B. Xu, J. Am. Chem. Soc. 129 (2007) 11928.
[116] M. Zanella, A. Falqui, S. Kudera, L. Manna, M.F. Casula, W.J. Parak, J. Mater. Chem. 18 (2008) 4311.
[117] H.W. Gu, R.K. Zheng, X.X. Zhang, B. Xu, J. Am. Chem. Soc. 126 (2004) 5664.
[118] S. He, H. Zhang, S. Delikanli, Y. Qin, M.T. Swihart, H. Zeng, J. Phys. Chem. C 113 (2009) 87.
[119] J.-S. Lee, E.V. Shevchenko, D.V. Talapin, J. Am. Chem. Soc. 130 (2008) 9673.
[120] J.-S. Lee, M.I. Bodnarchuk, E.V. Shevchenko, D.V. Talapin, J. Am. Chem. Soc. 132 (2010) 6382.
[121] Z. Sun, Z. Yang, J. Zhou, M.H. Yeung, W. Ni, H. Wu, et al., Angew. Chem. Int. Ed. 48 (2009) 2881.
[122] J. Zhang, Y. Tang, K. Lee, M. Ouyang, Science 327 (2010) 1634.
[123] J. Yang, J.Y. Ying, Chem. Commun. (22) (2009) 3187.

[124] H. Huang, S. Huang, X. Liu, Y. Zeng, X. Yu, B. Liao, et al., Biosens. Bioelectron. 24 (2009) 3025.
[125] H. Huang, X. Liu, Y. Zeng, X. Yu, B. Liao, P. Yi, et al., Biomaterials 30 (2009) 5622.
[126] G. Oldfield, T. Ung, P. Mulvaney, Adv. Mater. 12 (2000) 1519.
[127] J. Li, H.C. Zeng, Angew. Chem. Int. Ed. 44 (2005) 4342.
[128] H. Sakai, T. Kanda, H. Shibata, T. Ohkubo, M. Abe, J. Am. Chem. Soc. 128 (2006) 4944.
[129] C.-H. Kuo, T.-E. Hua, M.H. Huang, J. Am. Chem. Soc. 131 (2009) 17871.
[130] V. Subramanian, E.E. Wolf, P.V. Kamat, J. Phys. Chem. B 107 (2003) 7479.
[131] V. Subramanian, E.E. Wolf, P.V. Kamat, Langmuir 19 (2003) 469.
[132] A. Dawson, P.V. Kamat, J. Phys. Chem. B 105 (2001) 960.
[133] P.V. Kamat, M. Flumiani, A. Dawson, Colloid Surf. A 202 (2002) 269.
[134] A. Wood, M. Giersig, P. Mulvaney, J. Phys. Chem. B 105 (2001) 8810.
[135] T. Hikov, M.-K. Schroeter, L. Khodeir, A. Chemseddine, M. Muhler, R.A. Fischer, Phys. Chem. Chem. Phys. 8 (2006) 1550.
[136] S.F. Chen, J.P. Li, K. Qian, W.P. Xu, Y. Lu, W.X. Huang, et al., Nano Res. 3 (2010) 244.
[137] P.V. Kamat, J. Phys. Chem. C 111 (2007) 2834.
[138] T. Gao, Q. Li, T. Wang, Chem. Mater. 17 (2005) 887.
[139] G.K. Shan, X. Wang, Y. Liu, Surf. Sci. 582 (2005) 61.
[140] T. Gao, T. Wang, Chem. Commun. (22) (2004) 2558.
[141] J. Cao, J.-Z. Sun, H.-Y. Li, J. Hong, M. Wang, J. Mater. Chem. 14 (2004) 1203.
[142] K. Das, S.K. De, J. Phys. Chem. C 113 (2009) 3494.
[143] J. Schrier, D.O. Demchenko, L.-W. Wang, A.P. Alivisatos, Nano Lett. 7 (2007) 2377.
[144] W. Qin, D. Zhang, D. Zhao, L. Wang, K. Zheng, Chem. Commun. 46 (2010) 2304.
[145] F. Aldeek, L. Balan, G. Medjahdi, T. Roques-Carmes, J.-P. Malval, C. Mustin, et al., J. Phys. Chem. C 113 (2009) 19458.
[146] A. Kar, A. Datta, A. Patra, J. Mater. Chem. 20 (2010) 916.
[147] L.Y. Wang, J. Luo, Q. Fan, M. Suzuki, I.S. Suzuki, M.H. Engelhard, Y.H. Lin, et al., J. Phys. Chem. B 109 (2005) 21593.
[148] H.Y. Park, M.J. Schadt, L. Wang, I-Im S. Lim, P.N. Njoki, S.H. Kim, et al., Langmuir 23 (2007) 9050.
[149] J.L. Lyon, D.A. Fleming, M.B. Stone, P. Schiffer, M.E. Williams, Nano Lett. 4 (2004) 719.
[150] P. Gong, H. Li, X. He, K. Wang, J. Hu, W. Tan, et al., Nanotechnology 18 (2007) 285604.
[151] K. Yano, V. Nandwana, G.S. Chaubey, N. Poudyal, S. Kang, H. Arami, et al., J. Phys. Chem. C 113 (2009) 13088.
[152] B. Chudasama, A. Vala, N. Andhariya, R. Upadhyay, R. Mehta, Nano Res. 2 (2009) 955.
[153] Z. Xu, Y. Hou, S. Sun, J. Am. Chem. Soc. 129 (2007) 8698.
[154] C. Xu, K. Xu, H. Gu, R. Zheng, H. Liu, X. Zhang, et al., Am. Chem. Soc. 126 (2004) 9938.
[155] J. Li, H. Zeng, S. Sun, J.P. Liu, Z.L. Wang, J. Phys. Chem. B 108 (2004) 14005.
[156] Y. Hou, Z. Xu, S. Peng, C. Rong, J.P. Liu, S. Sun, Adv. Mater. 19 (2007) 3349.
[157] T. Zhou, M. Lu, Z. Zhang, H. Gong, W.S. Chin, B. Liu, Adv. Mater. 22 (2010) 403.
[158] X.W. Teng, D. Black, N.J. Watkins, Y.L. Gao, H. Yang, Nano Lett. 3 (2003) 261.
[159] H. Zeng, J. Li, Z.L. Wang, J.P. Liu, S.H. Sun, Nano Lett. 4 (2004) 187.
[160] H. Zeng, S.H. Sun, J. Li, Z.L. Wang, J.P. Liu, Appl. Phys. Lett. 85 (2004) 792.
[161] X. Teng, H. Yang, Nanotechnology 16 (2005) S554.
[162] W. Chiu, P. Khiew, M. Cloke, D. Isa, H. Lim, T. Tan, et al., J. Phys. Chem. C 114 (2010) 8212.
[163] O. Masala, R. Seshadri, J. Am. Chem. Soc. 127 (2005) 9354.
[164] M. Verelst, T.O. Ely, C. Amiens, E. Snoeck, P. Lecante, A. Mosset, et al., Chem. Mater. 11 (1999) 2702.
[165] P. Miltenyi, M. Gierlings, M. Bamming, U. May, G. Guntherodt, J. Nogués, et al., Appl. Phys. Lett. 75 (1999) 2304.
[166] J. Nogués, J. Sort, V. Langlais, V. Skumryevù, S. Suriñach, J.S. Muñoz, et al., Phys. Rep. 422 (2005) 65.
[167] K.B. Li, Z.B. Guo, Y.K. Zheng, G.C. Han, J.J. Qiu, P. Lu, et al., J. Nanosci. Nanotechnol. 7 (2007) 1.
[168] V. Skumryevù, S. Stoyanov, Y. Zhang, G. Hadjipanayis, D. Givord, J. Nogués, Nature 423 (2003) 850.
[169] R.Y. Hong, S.Z. Zhang, G.Q. Di, H.Z. Li, Y. Zheng, J. Ding, et al., Mater. Res. Bull. 43 (2008) 2457.
[170] Y.J. Chen, P. Gao, C.L. Zhu, R.X. Wang, L.J. Wang, M.S. Cao, et al., J. Appl. Phys. 106 (2009) 054303.
[171] Y.-J. Chen, P. Gao, R.-X. Wang, C.-L. Zhu, L.-J. Wang, M.-S. Cao, et al., J. Phys. Chem. C 113 (2009) 10061.
[172] Y.-J. Chen, F. Zhang, G.-G. Zhao, X.-Y. Fang, H.-B. Jin, P. Gao, et al., J. Phys. Chem. C 114 (2010) 9239.
[173] Q. Zhang, W. Fun, L. Gao, Appl. Catal. B: Environ. 76 (2007) 6.
[174] V.N. Girija, S. Chaubey, N. Poudyal, C.-B. Rong, J.P. Liu, Chem. Mater. 20 (2008) 475.
[175] D. Yang, H. Liu, Z. Zheng, Y. Yuan, J.-C. Zhao, E.R. Waclawik, et al., J. Am. Chem. Soc. 131 (2009) 17885.
[176] M.G. Ma, J.F. Zhu, S.W. Cao, F. Chen, R.C. Sun, J. Alloys Compd. 492 (2010) 559.
[177] A. Guerrero-Martínez, J. Pérez-Juste, L.M. Liz-Marzán, Adv. Mater. 22 (2010) 1182.
[178] Z. Zhelev, H. Ohba, R. Bakalova, J. Am. Chem. Soc. 128 (2006) 6324.
[179] S.T. Selvan, P.K. Patra, C.Y. Ang, J.Y. Ying, Angew. Chem. Int. Ed. 46 (2007) 2448.
[180] A. Burns, H. Ow, U. Wiesner, Chem. Soc. Rev. 35 (2006) 1028.
[181] A. Wolcott, D. Gerion, M. Visconte, J. Sun, A. Schwartzberg, S. Chen, et al., J. Phys. Chem. B 110 (2006) 5779.
[182] M.L. Darbandi, W. Lu, J. Fang, T. Nann, Langmuir 22 (2006) 4371.
[183] S.H. Liu, M.Y. Han, Adv. Funct. Mater. 15 (2005) 961.
[184] V. Salgueirino-Maceira, M.A. Correa-Duarte, M. Farle, A. Lopez-Quintela, K. Sieradzki, R. Diaz, Chem. Mater. 18 (2006) 2701.
[185] R. He, X. You, J. Shao, F. Gao, B. Pan, D. Cui, Nanotechnology 18 (2007) 315601.
[186] S.H. Joo, J.Y. Park, C.-K. Tsung, Y. Yamada, P. Yang, G.A. Somorjai, Nat. Mater. 8 (2009) 126.
[187] P.M. Arnal, M. Comotti, F. Schüth, Angew. Chem. Int. Ed. 45 (2006) 8224.
[188] X. Huang, C. Guo, J. Zuo, N. Zheng, G.D. Stucky, Small 5 (2009) 361.
[189] R. Guttel, M. Paul, F. Schuth, Chem. Commun. 46 (2010) 895.
[190] A.T. Heitsch, D.K. Smith, R.N. Patel, D. Ress, B.A. Korgel, J. Solid State Chem. 181 (2008) 1590.
[191] L.M. Liz-Marzán, M. Giersig, P. Mulvaney, Langmuir 12 (1996) 4329.
[192] Y. Kobayashi, H. Katakami, E. Mine, D. Nagao, M. Konno, L.M. Liz-Marzán, J. Colloid Interf. Sci. 283 (2005) 392.
[193] I. Pastoriza-Santos, J. Pérez-Juste, L.M. Liz-Marzán, Chem. Mater. 18 (2006) 2465.
[194] Y. Kobayashi, M. Horie, M. Konno, B. Rodríguez-González, L.M. Liz-Marzán, J. Phys. Chem. B 107 (2003) 7420.
[195] T.-J. Yoon, K.N. Yu, E. Kim, J.S. Kim, B.G. Kim, S.-H. Yu, et al., Small 2 (2006) 209.
[196] D.C. Lee, F.V. Mikulec, J.M. Pelaez, B. Koo, B.A. Korgel, J. Phys. Chem. B 110 (2006) 11160.
[197] L.M. Liz-Marzán, P. Mulvaney, J. Phys. Chem. B 107 (2003) 7312.

[198] L.M. Liz-Marzán, Langmuir 22 (2006) 32.
[199] D. Yang, J. Hu, S. Fu, J. Phys. Chem. C 113 (2009) 7646.
[200] Y. Deng, D. Qi, C. Deng, Z. Zhang, D. Zhao, J. Am. Chem. Soc. 130 (2008) 28.
[201] J. Zhou, L. Meng, Q. Lu, J. Fu, X. Huang, Chem. Commun. (42) (2009) 6370.
[202] H. Chen, C. Deng, X. Zhang, Angew. Chem. Int. Ed. 49 (2010) 607.
[203] C. Cannas, A. Musinu, A. Ardu, F. Orrù, D. Peddis, M. Casu, et al., Chem. Mater. 22 (2010) 3353.
[204] Y. Wang, Z. Tang, X. Liang, L.M. Liz-Marzán, N.A. Kotov, Nano Lett. 4 (2004) 225.
[205] Z. Jan, S. Xu, E. Kucur, F. Meister, M. Batentschuk, F. Gindele, et al., Adv. Mater. 20 (2008) 4068.
[206] V. Salgueirino-Maceira, F. Caruso, L.M. Liz-Marzán, J. Phys. Chem. B 107 (2003) 10990.
[207] J. Lee, J.C. Park, H. Song, Adv. Mater. 20 (2008) 1523.
[208] J.C. Park, J.U. Bang, J. Lee, C.H. Ko, H. Song, J. Mater. Chem. 20 (2010) 1239.
[209] V. Salgueirino-Maceira, M.A. Correa-Duarte, M. Spasova, L.M. Liz-Marzán, M. Farle, Adv. Funct. Mater. 16 (2006) 509.
[210] Y. Song, X. Cao, Y. Guo, P. Chen, Q. Zhao, G. Shen, Chem. Mater. 21 (2009) 68.
[211] F. Zhang, G.B. Braun, Y. Shi, Y. Zhang, X. Sun, N.O. Reich, et al., J. Am. Chem. Soc. 132 (2010) 2850.
[212] T. Ung, L.M. Liz-Marzán, P. Mulvaney, J. Phys. Chem. B 103 (1999) 6770.
[213] Y. Piao, J. Kim, H.B. Na, D. Kim, J.S. Baek, M.K. Ko, J.H. Lee, M. Shokouhimehr, T. Hyeon, Nat. Mater. 7 (2008) 242.
[214] J. Shin, H. Kim, I.S. Lee, Chem. Commun. (43) (2008) 5553.
[215] J.I. Park, J. Cheon, J. Am. Chem. Soc. 123 (2001) 5743.
[216] W.R. Lee, M.G. Kim, J.R. Choi, J.I. Park, S.J. Ko, S.J. Oh, et al., J. Am. Chem. Soc. 127 (2005) 16090.
[217] S.-J. Cho, J.-C. Idrobo, J. Olamit, K. Liu, N.D. Browning, S.M. Kauzlarich, Chem. Mater. 17 (2005) 3181.
[218] J. Yang, J.Y. Lee, H.P. Too, J. Phys. Chem. B 109 (2005) 19208.
[219] J.B. Tracy, D.N. Weiss, D.P. Dinega, M.G. Bawendi, Phys. Rev. B 72 (2005) 064404.
[220] I.S. Lee, N. Lee, J. Park, B.H. Kim, Y.-W. Yi, T. Kim, et al., J. Am. Chem. Soc. 128 (2006) 10658.
[221] G. Salazar-Alvarez, J. Sort, S. Suriñach, M.D. Baró, J. Nogués, J. Am. Chem. Soc. 129 (2007) 9102.
[222] S. Peng, C. Wang, J. Xie, S. Sun, J. Am. Chem. Soc. 128 (2006) 10676.
[223] S.S. Sheng Peng, Angew. Chem. Int. Ed. 46 (2007) 4155.
[224] A. Cabot, V.F. Puntes, E. Shevchenko, Y. Yin, L. Balcells, M.A. Marcus, et al., J. Am. Chem. Soc. 129 (2007) 10358.
[225] K. An, T. Hyeon, Nano Today 4 (2009) 359.
[226] A.E. Berkowitz, G.F. Rodriguez, J.I. Hong, K. An, T. Hyeon, N. Agarwal, et al., J. Phys. D-Appl. Phys. 41 (2008) 134007.
[227] A.E. Berkowitz, G.F. Rodriguez, J.I. Hong, K. An, T. Hyeon, N. Agarwal, et al., Phys. Rev. B 77 (2008) 024403.
[228] J. Gao, G. Liang, J.S. Cheung, Y. Pan, Y. Kuang, F. Zhao, et al., J. Am. Chem. Soc. 130 (2008) 11828.
[229] Y. Yin, R.M. Rioux, C.K. Erdonmez, S. Hughes, G.A. Somorjai, A.P. Alivisatos, Science 304 (2004) 711.
[230] J. Gao, G. Liang, B. Zhang, Y. Kuang, X. Zhang, B. Xu, J. Am. Chem. Soc. 129 (2007) 1428.
[231] E.V. Shevchenko, M.I. Bodnarchuk, M.V. Kovalenko, D.V. Talapin, R.K. Smith, S. Aloni, et al., Adv. Mater. 20 (2008) 4323.
[232] S.H. Kim, Y.D. Yin, A.P. Alivisatos, G.A. Somorjai, J.T. Yates, J. Am. Chem. Soc. 129 (2007) 9510.
[233] X. Peng, J. Wickham, A.P. Alivisatos, J. Am. Chem. Soc. 120 (1998) 5343.
[234] I. Pastoriza-Santos, D.S. Koktysh, A.A. Mamedov, M. Giersig, N.A. Kotov, L.M. Liz-Marzán, Langmuir 16 (2000) 2731.
[235] R.T. Tom, A.S. Nair, N. Singh, M. Aslam, C.L. Nagendra, R. Philip, et al., Langmuir 19 (2003) 3439.
[236] T. Hirakawa, P.V. Kamat, Langmuir 20 (2004) 5645.
[237] T. Hirakawa, P.V. Kamat, J. Am. Chem. Soc. 127 (2005) 3928.
[238] D. Wang, Y. Li, J. Am. Chem. Soc. 132 (2010) 6280.
[239] N.S. Sobal, M. Hilgendorff, H. Mohwald, M. Giersig, M. Spasova, T. Radetic, et al., Nano Lett. 2 (2002) 621.
[240] K.J. Carroll, S. Calvin, T.F. Ekiert, K.M. Unruh, E.E. Carpenter, Chem. Mater. 22 (2010) 2175.
[241] J. Lai, K.V.P.M. Shafi, A. Ulman, K. Loos, R. Popovitz-Biro, Y. Lee, et al., J. Am. Chem. Soc. 127 (2005) 5730.
[242] A. Purkayastha, Q. Yan, M.S. Raghuveer, D.D. Gandhi, H. Li, Z.W. Liu, R.V. Ramanujan, T. Borca-Tasciuc, G. Ramanath, Adv. Mater. 20 (2008) 2679.
[243] X.B. Cao, X.D. Xue, L.W. Zhu, P. Chen, Y.Y. Song, M. Chen, J. Mater. Chem. 20 (2010) 2322.
[244] W. Zhou, K. Zheng, L. He, R. Wang, L. Guo, C. Chen, et al., Nano Lett. 8 (2008) 1147.
[245] W. Lu, B. Wang, J. Zeng, X.P. Wang, S.Y. Zhang, J.G. Hou, Langmuir 21 (2005) 3684.
[246] T. Mokari, A. Aharoni, I. Popov, U. Banin, Angew. Chem. Int. Ed. 45 (2006) 8001.
[247] D. Turnbull, F.C. Frank, Phys. Rev. 104 (1956) 617.
[248] U. Gösele, F. Morehead, W. Frank, A. Seeger, Appl. Phys. Lett. 38 (1981) 157.
[249] I.R. Franchini, G. Bertoni, A. Falqui, C. Giannini, L.W. Wang, L. Manna, J. Mater. Chem. 20 (2010) 1357.
[250] J. Xu, C.-S. Lee, Y.-B. Tang, X. Chen, Z.-H. Chen, W.-J. Zhang, et al., ACS Nano 4 (2010) 1845.
[251] J. Jiang, H. Gu, H. Shao, E. Devlin, G.C. Papaefthymiou, J.Y. Ying, Adv. Mater. 20 (2008) 4403.
[252] S.-H. Choi, H.B. Na, Y.I. Park, K. An, S.G. Kwon, Y. Jang, et al., J. Am. Chem. Soc. 130 (2008) 15573.
[253] T.D. Schladt, M.I. Shukoor, K. Schneider, M.N. Tahir, F. Natalio, I. Ament, et al., Angew. Chem. Int. Ed. 49 (2010) 3976.
[254] C. Xu, J. Xie, D. Ho, C. Wang, N. Kohler, E.G. Walsh, et al., Angew. Chem. Int. Ed. 47 (2008) 173.
[255] H. Yin, C. Wang, H. Zhu, S.H. Overbury, S. Sun, S. Dai, Chem. Commun. (36) (2008) 4357.
[256] B. Wu, H. Zhang, C. Chen, S. Lin, N. Zheng, Nano Res. 2 (2009) 975.
[257] C. Wang, H. Daimon, S. Sun, Nano Lett. 9 (2009) 1493.
[258] C. Wang, H. Yin, S. Dai, S. Sun, Chem. Mater. 22 (2010) 3277.
[259] Y. Lee, M.A. Garcia, N.A. Frey Huls, S. Sun, Angew. Chem. Int. Ed. 49 (2010) 1271.
[260] Y. Wei, R. Klajn, A.O. Pinchuk, B.A. Grzybowski, Small 4 (2008) 1635.
[261] H. Yu, M. Chen, P.M. Rice, S.X. Wang, R.L. White, S. Sun, Nano Lett. 5 (2005) 379.
[262] X. Gao, L. Yu, R. MacCuspie, H. Matsui, Adv. Mater. 17 (2005) 426.
[263] J. Yang, J. Peng, Q. Zhang, F. Peng, H. Wang, H. Yu, Angew. Chem. Int. Ed. 48 (2009) 3991.
[264] X.K. Wang, Y. Yu, H. Zhang, J. Phys. Chem. C 111 (2007) 3836.
[265] T. Mokari, C.G. Sztrum, A. Salant, E. Rabani, U. Banin, Nat. Mater. 4 (2005) 855.
[266] J. Zeng, H. Jianliu, C. Liu, C.H. Wu, Y. Lin, X. Wang, et al., Adv. Mater. 22 (2010) 1936.
[267] S.E. Wark, C.-H. Hsia, D.H. Son, J. Am. Chem. Soc. 130 (2008) 9550.
[268] N. Pazos-Perez, Y. Gao, M. Hilgendorff, S. Irsen, J. Pérez-Juste, M. Spasova, et al., Chem. Mater. 19 (2007) 4415.
[269] T. Pellegrino, A. Fiore, E. Carlino, C. Giannini, P.D. Cozzoli, G. Ciccarella, et al., J. Am. Chem. Soc. 128 (2006) 6690.
[270] L. Zhang, Y.-H. Dou, H.-C. Gu, J. Colloid Interf. Sci. 297 (2006) 660.
[271] J. Yang, L. Levina, E.H. Sargent, S.O. Kelley, J. Mater. Chem. 16 (2006) 4025.

[272] J. Yang, H.I. Elim, Q. Zhang, J.Y. Lee, W. Ji, J. Am. Chem. Soc. 128 (2006) 11921.
[273] W. Shi, Y. Sahoo, H. Zeng, Y. Ding, M.T. Swihart, P.N. Prasad, Adv. Mater. 18 (2006) 1889.
[274] Y.L. Liu, A.R.H. Walker, J. Phys. Chem. C 114 (2010) 4264.
[275] K.W. Kwon, M. Shim, J. Am. Chem. Soc. 127 (2005) 10269.
[276] K.-W. Kwon, B.H. Lee, M. Shim, Chem. Mater. 18 (2006) 6357.
[277] H. McDaniel, M. Shim, ACS Nano 3 (2009) 434.
[278] V. Randle, The Role of the Coincidence Site Lattice in Grain Boundary Engineering, Woodhead Publishing Limited, Cambridge, England, 1997.
[279] J. Yang, J.Y. Ying, J. Am. Chem. Soc. 132 (2010) 2114.
[280] H.W. Gu, Z.M. Yang, J.H. Gao, C.K. Chang, B. Xu, J. Am. Chem. Soc. 127 (2005) 34.
[281] Y. Pan, J.H. Gao, B. Zhang, X.X. Zhang, B. Xu, Langmuir 26 (2010) 4184.
[282] T. Teranishi, Y. Inoue, M. Nakaya, Y. Oumi, T. Sano, J. Am. Chem. Soc. 126 (2004) 9914.
[283] T. Teranishi, Y. Inoue, M. Saruyama, M. Nakaya, M. Kanehara, Chem. Lett. 36 (2007) 490.
[284] S.H. Choi, E.G. Kim, T. Hyeon, J. Am. Chem. Soc. 128 (2006) 2520.
[285] A. Figuerola, A. Fiore, R. Di Corato, A. Falqui, C. Giannini, E. Micotti, et al., J. Am. Chem. Soc. 130 (2008) 1477.
[286] A.E. Saunders, I. Popov, U. Banin, Z. Anorg. Allg. Chem. 633 (2007) 2414.
[287] A. Figuerola, I.R. Franchini, A. Fiore, R. Mastria, A. Falqui, G. Bertoni, et al., Adv. Mater. 21 (2009) 550.
[288] T. Teranishi, M. Saruyama, M. Nakaya, M. Kanehara, Angew. Chem. Int. Ed. 46 (2007) 1713.
[289] M. Saruyama, M. Kanehara, T. Teranishi, Chem. Commun. (19) (2009) 2724.
[290] C. Ribeiro, E. Longo, E.R. Leite, Appl. Phys. Lett. 91 (2007) 103105.
[291] K.P. Acharya, N.N. Hewa-Kasakarage, T.R. Alabi, I. Nemitz, E. Khon, B. Ullrich, et al., J. Phys. Chem. C 114 (2010) 12496.
[292] S. Kudera, L. Carbone, M.F. Casula, R. Cingolani, A. Falqui, E. Snoeck, et al., Nano Lett. 5 (2005) 445.
[293] M. Casavola, V. Grillo, E. Carlino, C. Giannini, F. Gozzo, E. Fernandez Pinel, et al., Nano Lett. 7 (2007) 1386.
[294] F. Wetz, K. Soulantica, A. Falqui, M. Respaud, E. Snoeck, B. Chaudret, Angew. Chem. Int. Ed. 46 (2007) 7079.
[295] J. Maynadiè, A. Salant, A. Falqui, M. Respaud, E. Shaviv, U. Banin, et al., Angew. Chem. Int. Ed. 48 (2009) 1814.
[296] S. Chakrabortty, J.A. Yang, Y.M. Tan, N. Mishra, Y. Chan, Angew. Chem. Int. Ed. 49 (2010) 2888.
[297] R. Buonsanti, V. Grillo, E. Carlino, C. Giannini, F. Gozzo, M. Garcia-Hernandez, et al., J. Am. Chem. Soc. 132 (2010) 2437.
[298] D.J. Milliron, S.M. Hughes, Y. Cui, L. Manna, J. Li, L.-W. Wang, et al., Nature 430 (2004) 190.
[299] F. Shieh, A.E. Saunders, B.A. Korgel, J. Phys. Chem. B 109 (2005) 8538.
[300] S. Kumar, M. Jones, S.S. Lo, G.D. Scholes, Small 3 (2007) 1633.
[301] J.E. Halpert, V.J. Porter, J.P. Zimmer, M.G. Bawendi, J. Am. Chem. Soc. 128 (2006) 12590.
[302] L. Carbone, S. Kudera, C. Giannini, G. Ciccarella, R. Cingolani, P.D. Cozzoli, et al., J. Mater. Chem. 16 (2006) 3952.
[303] L. Xi, C. Boothroyd, Y.M. Lam, Chem. Mater. 21 (2009) 1465.
[304] J.J. Shiang, A.V. Kadavanich, R.K. Grubbs, A.P. Alivisatos, J. Phys. Chem. 99 (1995) 17417.
[305] C. Cheng, K.F. Yu, Y. Cai, K.K. Fung, N. Wang, J. Phys. Chem. C 111 (2007) 16712.
[306] T. Nann, J. Schneider, Chem. Phys. Lett. 384 (2004) 150.
[307] S. Deka, A. Falqui, G. Bertoni, C. Sangregorio, G. Poneti, G. Morello, et al., J. Am. Chem. Soc. 131 (2009) 12817.
[308] C. Pacholski, A. Kornowski, H. Weller, Angew. Chem. Int. Ed. 43 (2004) 4774.
[309] S.S. Lo, Y. Khan, M. Jones, G.D. Scholes, J. Chem. Phys. 131 (2009) 084714.
[310] P.O. Anikeeva, J.E. Halpert, M.G. Bawendi, V. Bulovic, Nano Lett. 9 (2009) 2532.
[311] W. Ma, J.M. Luther, H. Zheng, Y. Wu, A.P. Alivisatos, Nano Lett. 9 (2009) 1699.
[312] B. Tian, X. Zheng, T.J. Kempa, Y. Fang, N. Yu, G. Yu, et al., Nature 449 (2007) 885.
[313] Y. Luo, L.-W. Wang, ACS Nano 4 (2010) 91.
[314] B. Koo, B.A. Korgel, Nano Lett. 8 (2008) 2490.
[315] Z. Peng, H. You, H. Yang, ACS Nano 4 (2010) 1501.
[316] T. Sadowski, R. Ramprasad, Appl. Phys. Lett. 96 (2010) 101906.
[317] T. Sadowski, R. Ramprasad, J. Phys. Chem. C 114 (2010) 1773.
[318] M. Kirsanova, A. Nemchinov, N.N. Hewa-Kasakarage, N. Schmall, M. Zamkov, Chem. Mater. 21 (2009) 4305.
[319] N.N. Hewa-Kasakarage, P.Z. El-Khoury, A.N. Tarnovsky, M. Kirsanova, I. Nemitz, A. Nemchinov, et al., ACS Nano 4 (2010) 1837.
[320] A.E. Saunders, B. Koo, X. Wang, C.-K. Shih, B.A. Korgel, ChemPhysChem 9 (2008) 1158.
[321] W. Han, L. Yi, N. Zhao, A. Tang, M. Gao, Z. Tang, J. Am. Chem. Soc. 130 (2008) 13152.
[322] J. He, S.S. Lo, J. Kim, G.D. Scholes, Nano Lett. 8 (2008) 4007.
[323] C.J. Dooley, S.D. Dimitrov, T. Fiebig, J. Phys. Chem. C 112 (2008) 12074.
[324] M. Jones, S. Kumar, S.S. Lo, G.D. Scholes, J. Phys. Chem. C 112 (2008) 5423.
[325] L. Wang, H. Wei, Y. Fan, X. Gu, J. Zhan, J. Phys. Chem. C 113 (2009) 14119.
[326] M. Niu, Y. Cheng, Y. Wang, L. Cui, F. Bao, L. Zhou, Cryst. Growth Des. 8 (2008) 1727.
[327] M. Niu, F. Huang, L. Cui, P. Huang, Y. Yu, Y. Wang, ACS Nano 4 (2010) 681.
[328] R. Buonsanti, E. Snoeck, C. Giannini, F. Gozzo, M. Garcia-Hernandez, M.A. Garcia, et al., Phys. Chem. Chem. Phys. 11 (2009) 3680.
[329] R. Buonsanti, V. Grillo, E. Carlino, C. Giannini, T. Kipp, R. Cingolani, et al., J. Am. Chem. Soc. 130 (2008) 11223.
[330] T. Mokari, E. Rothenberg, I. Popov, R. Costi, U. Banin, Science 304 (2004) 1787.
[331] A.E. Saunders, I. Popov, U. Banin, J. Phys. Chem. B 110 (2006) 25421.
[332] H. Yang, Met. Mater. Int. 12 (2006) 351.
[333] Y. Khalavka, C. Sönnichsen, Adv. Mater. 20 (2008) 588.
[334] G. Menagen, J.E. Macdonald, Y. Shemesh, I. Popov, U. Banin, J. Am. Chem. Soc. 131 (2009) 17406.
[335] C. O'Sullivan, S. Ahmed, K.M. Ryan, J. Mater. Chem. 18 (2008) 5218.
[336] G. Pilania, T. Sadowski, R. Ramprasad, J. Phys. Chem. C 113 (2009) 1863.
[337] M. Saruyama, M. Kanehara, T. Teranishi, J. Am. Chem. Soc. 132 (2010) 3280.
[338] I. Jen-La Plante, S.E. Habas, B.D. Yuhas, D.J. Gargas, T. Mokari, Chem. Mater. 21 (2009) 3662.
[339] S.E. Habas, P. Yang, T. Mokari, J. Am. Chem. Soc. 130 (2008) 3294.
[340] B.D. Yuhas, S.E. Habas, S.C. Fakra, T. Mokari, ACS Nano 3 (2009) 3369.
[341] L. Wang, X. Liu, M. Yang, Y. Fan, J. Zhan, Eur. J. Inorg. Chem. 2009 (2009) 897.
[342] R. Costi, A.E. Saunders, E. Elmalem, A. Salant, U. Banin, Nano Lett. 8 (2008) 637.
[343] D. Steiner, T. Mokari, U. Banin, O. Millo, Phys. Rev. Lett. 95 (2005) 056805.
[344] L. Amirav, A.P. Alivisatos, J. Phys. Chem. Lett. 1 (2010) 1051.

[345] E. Elmalem, A.E. Saunders, R. Costi, A. Salant, U. Banin, Adv. Mater. 20 (2008) 4312.
[346] Y. Zheng, L. Zheng, Y. Zhan, X. Lin, Q. Zheng, K. Wei, Inorg. Chem. 46 (2007) 6980.
[347] Q. Wang, B. Geng, S. Wang, Environ. Sci. Technol. 43 (2009) 8968.
[348] T. Yao, W. Yan, Z. Sun, Z. Pan, B. He, Y. Jiang, et al., J. Phys. Chem. C 113 (2009) 3581.
[349] X. Qiu, L. Li, C. Tang, G. Li, J. Am. Chem. Soc. 129 (2007) 11908.
[350] F.-R. Fan, Y. Ding, D.-Y. Liu, Z.-Q. Tian, Z.L. Wang, J. Am. Chem. Soc. 131 (2009) 12036.
[351] Y. Xie, K. Ding, Z. Liu, R. Tao, Z. Sun, H. Zhang, et al., J. Am. Chem. Soc. 131 (2009) 6648.
[352] L. Carbone, A. Jakab, Y. Khalavka, C. Sönnichsen, Nano Lett. 9 (2009) 3710.
[353] J. McBride, J. Treadway, L.C. Feldman, S.J. Pennycook, S.J. Rosenthal, Nano Lett. 6 (2006) 1496.
[354] Z.-H. Lin, Y.-W. Lin, K.-H. Lee, H.-T. Chang, J. Mater. Chem. 18 (2008) 2569.
[355] T.P. Vinod, M. Yang, J. Kim, N.A. Kotov, Langmuir 25 (2009) 13545.
[356] M. Casavola, A. Falqui, M.A. Garcia, M. Garcia-Hernandez, C. Giannini, R. Cingolani, P.D. Cozzoli, Nano Lett. 9 (2009) 366.
[357] G. Menagen, D. Mocatta, A. Salant, I. Popov, D. Dorfs, U. Banin, Chem. Mater. 20 (2008) 6900.
[358] K.P. Acharya, T.R. Alabi, N. Schmall, N.N. Hewa-Kasakarage, M. Kirsanova, A. Nemchinov, E. Khon, M. Zamkov, J. Phys. Chem. C 113 (2009) 19531.
[359] A. Salant, E. Amitay-Sadowsky, U. Banin, J. Am. Chem. Soc. 128 (2006) 10006.
[360] P.H.C. Camargo, Y. Xiong, L. Ji, J.M. Zuo, Y. Xia, J. Am. Chem. Soc. 129 (2007) 15452.
[361] D. Seo, C.I. Yoo, J. Jung, H. Song, J. Am. Chem. Soc. 130 (2008) 2940.
[362] D.H. Son, S.M. Hughes, Y. Yin, A.P. Alivisatos, Science 306 (2004) 1009.
[363] B. Sadtler, D.O. Demchenko, H. Zheng, S.M. Hughes, M.G. Merkle, U. Dahmen, L.-W. Wang, A.P. Alivisatos, J. Am. Chem. Soc. 131 (2009) 5285.
[364] J.M. Luther, H. Zheng, B. Sadtler, A.P. Alivisatos, J. Am. Chem. Soc. 131 (2009) 16851.
[365] R.D. Robinson, B. Sadtler, D.O. Demchenko, C.K. Erdonmez, L.-W. Wang, A.P. Alivisatos, Science 317 (2007) 355.
[366] D.O. Demchenko, R.D. Robinson, B. Sadtler, C.K. Erdonmez, A.P. Alivisatos, L.-W. Wang, ACS Nano 2 (2008) 627.
[367] P. Peng, B. Sadtler, A.P. Alivisatos, R.J. Saykally, J. Phys. Chem. C 114 (2010) 5879.
[368] R. Buonsanti, V. Grillo, E. Carlino, C. Giannini, M.L. Curri, C. Innocenti, C. Sangregorio, K. Achterhold, F.G. Parak, A. Agostiano, P.D. Cozzoli, J. Am. Chem. Soc. 128 (2006) 16953.

Luigi Carbone received his MSc degree in Chemistry from the University of Bari, Italy, in 2003, and his PhD in ''Materials and Innovative Technologies'' from the University of Salento, Lecce, Italy, in 2007. His PhD activities had been carried out at the National Nanotechnology Laboratory (NNL) — Nanoscience Institute of CNR, Lecce (Italy), focusing on the development of synthetic approaches to colloidal semiconductor nanocrystal structures. From 2007 to 2009 he has worked as a postdoctoral fellow at the Institut für Physikalische Chemie, University of Mainz, Germany, dealing with the synthesis of hybrid nanocrystals combining plasmonic metals and quantum-confined semiconductors. Presently, he is working as Junior Researcher at NNL-CNR. His research interests relate to the colloidal synthesis and the optical properties of visible to near-infrared emitting metal chalcogenide nanostructures.

P. Davide Cozzoli received his MSc degree in Chemistry in 1999 and his PhD Award in Chemical Sciences in 2004 from the University of Bari, Italy. His PhD research activities, partially carried out at the University of Hamburg, Germany, had been focused on the synthesis and photocatalytic applications of oxide nanocrystals. From 2004 to 2005 he has worked as post-doctoral fellow at the University of Bari. From 2005 to 2007 he has been Junior Researcher at the National Nanotechnology Laboratory (NNL) - Nanoscience Institute of CNR, Lecce, Italy. Currently, he holds a permanent position as Senior Staff Researcher at the Faculty of Industrial Engineering of the University of Salento, Lecce, Italy, and leads the Nanochemistry Division of NNL-CNR serving as Researcher Associate of CNR. He also serves as Associated Editor for ''Science of Advanced Materials''. His research interests involve the chemical synthesis, characterization and multipurpose applications of advanced nanocrystal heterostructures.